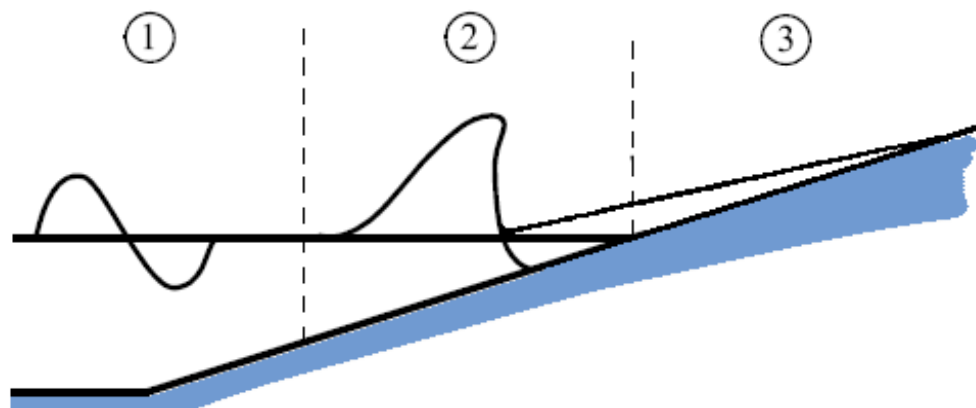


Numerical modeling of wave run-up on a dike

Simulations with the VOF-model ComFLOW



I.C. van den Bosch
December, 2010

Title

Numerical modeling of wave run-up on a dike

Delft University of Technology
Faculty of Civil Engineering and
Geosciences
Section of Fluid Mechanics

Project
1202229-008

Pages
85

Keywords

Numerical modelling, Navier-Stokes, VOF-modelling, ComFLOW, Run-up, Wave-structure interaction, Run-down, Wave breaking.

Supervising committee:

Prof.dr.ir. W.S.J. Uijtewaal
Dr. ir. R.J. Labeur
Dr. ir. I. Wenneker
Ir. H.J. Verhagen
Dr. ir. M.R.A. van Gent

A thesis submitted in partial fulfilment of the requirements for the degree of
Master of Science in Hydraulic Engineering.

Date	Author	Review	Approved by
Dec. 2010	I.C. van den Bosch	I. Wenneker	M.R.A. van Gent

State
Final

Summary

Wave fields in the close vicinity of a coastal structure can be very complex, this is especially the case during extreme storm conditions and for complex geometries. There is a growing interest for numerical simulation tools capable of predicting in detail the complex hydrodynamic loads due to waves and currents and its effect at structures. In this context the model ComFLOW will be used in this thesis to study wave run-up on dikes. The code is a (3D) hydrodynamic flow model based on the incompressible Navier-Stokes equations. The evolution of the free water surface is described by the Volume-of-Fluid method (VOF). The model is capable of calculating velocities, pressures and water levels in a detailed level, while geometries are easily adjustable.

The objective of this study is to analyze numerical simulation of wave run-up and other relevant wave-structure interaction processes on smooth and impermeable coastal structures with perpendicular wave attack and to investigate whether the Volume of Fluid (VOF) model ComFLOW is able to accurately represent these processes with 2DV simulations. A related aim is to determine whether the model is robust and which model settings are preferred.

To investigate whether the numerical model different mathematical aspects properly solves for relevant processes, simulation results are compared with analytical solutions. Its performance with respect to accuracy of shoreline movement, velocities along geometries, flooding of the domain at high speed and similarity to the analytical solution is investigated. Three analytical test cases are considered: the dam break test with a horizontal bed and with an upward sloping bed and test of Carrier and Greenspan of a standing wave on a sloping structure. The maximum run-up and run-down values of the analytical solution are well reproduced by the model. General performance of the model for the analytical solutions is well. The study of the analytical solutions led to the following observation: numerical diffusion can lead to a decrease of run-up and run-down heights. Numerical dissipation factors that are indicate as influential on the results:

- The discretization of the geometry
- The algorithm of flooding of dry cells
- Artificial viscosity

An analysis of the different wave-structure interaction processes is performed, by studying not only wave run-up, but also wave run-down, reflection and visual inspection of the type of wave breaking. Simulations are performed with regular waves, three different slopes are used (of 1:3, 1:4 and 1:6). In combination with seven different wave conditions, this gives a wide range of breaker parameters. The results are compared with data from experimental model tests of Schüttrumpf and Bruun and Günbak. During these simulations different model settings are investigated, including grid refinement, different methods to prescribe incident waves and refinement of the discretization of the geometry. The number of integration points define in the discretization a dimension for the smoothness of the geometry, in this study a number of 4 and 8 integration points is used.

To test the performance of the model qualitatively, the numerical results are compared with video recordings of breaking wave on a slope of a physical experiment. This is intended to be illustrative to give a general idea how well the breaking or non-breaking of waves for different breaker parameters is represented. Visual inspection showed that the model represents the wave motion along the slope well.

The results with respect to wave run-up are convincing, having very good resemblance with data of physical experiments. Especially for lower values of the breaker parameter ($\xi < 2$), which are breaking waves, the run-up results do not show a significant deviation compared to the experimental results. Nevertheless, for wave with higher breaker parameters ($\xi > 2$), the computed wave run-up values are in the lower regions of the experimental data. For these non-breaking waves, the (relative) numerical dissipation is too high during structure-wave interaction and hold responsible for the underestimation of relative wave run-up (Ru/H) of approximately 0.3 compared to the experimental data of Schüttrumpf.

The numerical dissipation due to the discretization of the geometry is indicated as the main cause of the lower wave run-up heights as compared with experimental data. By means of the stair-case boundaries, numerical roughness is created at the slope. Artificial viscosity and the restriction in the flooding algorithm are other processes that are indicated as cause for numerical dissipation, but it is assumed that they have a small influence on the wave run-up.

The results concerning wave run-down are less convincing than the run-up results. The relative wave run-down is overestimated (hence the lowest water level reached in the simulations is lower than in the experiments) compared to experimental data, especially in the region of $\xi < 3$. An overestimation for relative run down (Rd/H) of approximately 0.6 compared to the data of Schüttrumpf and 1 to Bruun and Günbak is observed. For values of $\xi > 3$ the run-down results and are in the same range as the data of Schüttrumpf. It is observed that the numerical model simulates the retreating of the wave too fast, but no clear explanation is found for this. The answer may lay in the different physical characteristics of wave run-up and run-down or the difference in handling of flooding and drying of cells by the numerical model.

Both run-up and run-down results show, for a given value of the breaker parameter, dependency on the slope, which already should have been accounted for in the breaker parameter. Steeper slopes have a smaller vertical amplitude at the slope, resulting in lower run-up and run-down values. A clear explanation is not found for the observed dependency in this study, but two hypothesis are formulated: the number of grid cells the wave runs through at the slope or the difference in numerical roughness that is formed for different slopes due to discretization of the geometry.

Reflection is analyzed by separating the incoming and reflected waves from simulated wave signals. The calculated reflection coefficients show good resemblance with data from physical experiments, showing that the right amount of wave energy is reflected at the structure. Nevertheless, the same trend is observed for the non-breaking waves as for the run-up results. Results for waves that give lower run-up values also show lower reflection, as this energy is dissipated at the slope.

Concerning model settings the following settings are preferred:

- When simulating smooth bodies it is advised is to set the number of integration points as high as possible to obtain the smoothest geometry.
- The number of grid cells per wave length and wave height give guidance for the choice of the grid size in terms of relevant physical parameters. In horizontal direction 170-200 grid cells per wave length and 4-6 cells per wave height in vertical direction are concerned sufficient for these type of simulations.
- The robust settings for the generating and absorbing boundary conditions (GABC) perform very well and handle the generation and absorption of wave satisfying.

Overall it can be stated that the model is well able to accurately represent different wave-interaction processes including wave run-up and the model proved to be robust for this type of simulations.

Acknowledgements

This research is undertaken in order to obtain the degree of Master of Science at Delft University of Technology at the faculty of Civil Engineering and Geosciences. This study has been carried out at Deltares under the guidance of the section of Environmental Fluid Mechanics. This report is aimed at everyone involved in coastal engineering with special interest in numerical modeling and coastal protection.

I would like to thank Ivo Wenneker, my supervisor at Deltares, for all his help and guidance during my research, during the weekly meetings and all the times I came by with questions. I would like to thank Robert Jan Labeur for all his help, especially his help with the analytical solutions. And the fact that this study made him not to sleep for over a week. Furthermore, I want to thank the other members of my committee. My fellow students at Deltares for all the good times, the lunches, coffees and cookies, all the extraordinary figures and not to forget the shared problems with Matlab.

Moreover I could not have done this without the support of my friends and family. Especially the distraction that was provided by them during this graduation project.

December 2010,

Ilse van den Bosch

Table of contents

List of symbols	vi
1 Introduction	1
1.1 Motive for research	1
1.2 Problem definition	2
1.3 Objective and methodology	3
2 Wave processes	5
2.1 Breaker parameter	5
2.1.1 Wave breaker types	6
2.2 Wave run-up	6
2.3 Wave run-down	8
2.4 Reflection	10
2.5 Summary of wave processes	11
3 ComFLOW	13
3.1 Mathematical model	13
3.1.1 Governing equations	13
3.1.2 Boundary conditions	14
3.2 Numerical model	15
3.2.1 Grid and geometry definition	15
3.2.2 Free surface description	17
3.2.3 Cell labeling	17
3.2.4 Discretization of the continuity and Navier-Stokes equations	17
3.2.5 Free surface boundary conditions: velocities	18
3.3 Wave generation and boundary conditions	19
3.3.1 Description of wave generation	19
3.3.2 Generation and Absorbing Boundary Condition (GABC)	19
3.4 Numerical default settings	20
4 Analytical solutions	23
4.1 Dam break test	23
4.1.1 Horizontal channel, dry bed	23
4.1.2 Sloping channel, dry bed	29
4.2 Waves on a sloping beach	35
4.3 Discussion and concluding remarks	38
5 Run-up simulations with regular waves	41
5.1 Numerical setup	41
5.1.1 Domain, geometry and boundary conditions	41
5.1.2 Grid size	42
5.2 Simulation setup	43
5.2.1 Wave conditions	43
5.2.2 Output ComFLOW	44
5.3 Results and analysis of physical processes	44
5.3.1 General wave-structure interaction performance	44

5.3.2	Wave run-up	48
5.3.3	Wave run-down	56
5.3.4	Reflection	57
5.4	Sensitivity analysis of the use of monitoring lines	59
5.4.1	Placement of monitoring lines	59
5.4.2	Uncertainty margins in wave run-up and run-down results	62
5.5	Analysis of numerical performance	63
5.5.1	Artificial viscosity	63
5.5.2	Robustness	65
5.5.3	CPU time	66
5.6	Concluding remarks	66
6	Wave breaker types	69
6.1	Numerical and physical model setup	69
6.2	Results	70
6.2.1	Surging wave	71
6.2.2	Plunging wave	73
7	Conclusions and recommendations	77
7.1	Conclusions	77
7.2	Recommendations	78
	Bibliography	80
	List of Tables	82
	List of Figures	83
	Appendices	

List of symbols

Roman symbols

Symbol	Unit	Description
A	m	Wave amplitude (H/2)
$A^{x/y/z}$	-	Edge aperture
c	m/s	Wave celerity
F_b	-	Volume aperture
g	m/s ²	Gravitational acceleration
H	m	Wave height
h	m	Waterdepth
h_0	m	Initial waterdepth
H_i	m	Incoming wave height
H_r	m	Reflected wave height
H_s	m	Significant wave height
k	1/m	Wave number ($2\pi/L$)
k_{art}	m ² /s	Artificial viscosity
K_r	-	Reflection coefficient
L	m	Wave length
L_0	m	Deep water wave length
p	N/m ²	Pressure
p_0	N/m ²	Atmospheric pressure
q	m ² /s	Discharge
R_d	m	Wave run-down
R_u	m	Wave run-up
s		Slope ($\tan \theta$)
S_0	-	Bed slope ($\sin \theta$)
T	s	Wave period
t	s	Time
u	m/s	Velocity component in x-direction
u_n	m/s	Normal direction of the velocity
u_t	m/s	Tangential direction of the velocity
v	m/s	Velocity component in y-direction
w	m/s	Velocity component in z-direction
x_n	m	Normal direction of the free surface
x_t	m	Tangential direction of the free surface

Greek symbols

Symbol	Unit	Description
α	°	Slope angle
γ	-	Reduction factor
η	m	Surface elevation
θ	°	Bed slope

κ	-	Total curvature of free surface
μ	kg/ms	Dynamic viscosity
ξ	-	Breaker parameter
ρ	kg/m ³	Density
σ	kg/m	Kinematic surface tension
ω	rad/s	Angular wave frequency ($2\pi/T$)
Φ	s	Phase

1 Introduction

This report is written in the context of the Master of Science Thesis at Delft University of Technology, faculty Civil Engineering and Geosciences, section Hydraulic Engineering and Environmental Fluid mechanics. The research has been carried out in cooperation with Deltares and presents the results of numerical simulations with the ComFLOW model for wave run-up on a dike.

1.1 Motive for research

The Netherlands has a long tradition in protecting the low-lying country against the sea. Dikes and seawalls along the coast have been constructed to protect the hinterland from flooding. Waves and currents can induce large forces and loading on these structures, which have to be designed to withstand these forces. Due to climate change, stronger storms are expected, leading to more severe wave loading in the future. Understanding changes in flood risk, due to increasing wave loading on seawalls, is a key requirement for the effective management of coastal defenses and essential as the risk of loss of life and economic damage is getting higher. Creating the need for a very detailed (and still increasing) level of knowledge on the prediction and predictability of hydrodynamic loading.

Analyses of dike breaching events in The Netherlands and Germany show that most of them were initiated by the failure of inner slopes of dikes. Overtopping waves cause erosion on the inner slope and crest, slip failure of the inner slope or a combination of both, this phenomenon is one of the most important causes of failure of sea dikes (Van Gent, 2002).

Overtopping discharges occur because of waves running up the face of a seawall. If these wave run-up levels are high enough water will reach and pass over the crest of the wall. This causes a discontinuous sheet of water passing over the crest. Foregoing implicates that wave overtopping and run-up heights are interrelated and these are the main parameters in determining the crest height of a dike. Good insight in these phenomena is needed for the design, assessment and management of coastal structures. In order to obtain better understanding, these complex phenomena are subjected to a growing interest for research. An example is the investigation of the Dutch government on existing statutory criteria for overtopping (RWS, 2007).

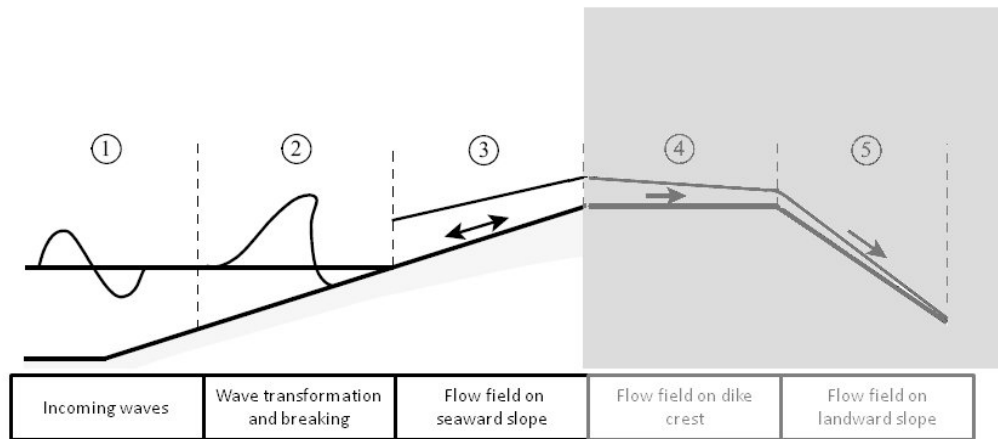


Figure 1.1: Flow domain of wave overtopping on a dike, subdivided in five sub-flow domains. This study focuses on sub-domain 1,2 and 3. (Schüttrumpf, 2001: figure 2.8)

Analyzing the flow domain of wave overtopping on a dike (see Figure 1.1) it can be subdivided this into five sub-domains. The first three sub-domains are selected for this research, which includes all processes at seaward slope of the dike. Wave overtopping is dependent on the processes associated to wave breaking and wave run-up on the seaward slope of the dike. Run-up is the basic input parameters for calculation of number of overtopping wave over a dike, which is required to calculate overtopping volumes, velocities and flow depths. Therefore it is advisable to first investigate the processes in the first three sub-domains before going into the last two sub-domains.

1.2 Problem definition

Wave fields in the close vicinity of a coastal structure can be very complex, this is especially the case during extreme storm conditions and for complex geometries. In shallow areas the wave field is subjected to significant transformations, for example due to wave breaking, shoaling and refraction. These transformations lead to highly non-linear and complex wave dynamics. For the study of hydrodynamic processes such as wave run-up in this environment three different basic methods are available: analytical, experimental and numerical.

Analytical models have proven to be inadequate and inaccurate for these predictions. For a long time experimental methods were the only way most topics in the coastal engineering field could be studied. Experimental methods comprise usually physical model tests in which a scale model is tested in a flume or basin with correctly scaled wave conditions. However, model testing is known to have some disadvantages, such as scale and model effects, limited reproducibility and high costs.

There is a growing interest for numerical simulation tools capable of predicting in detail the hydrodynamic loads due to waves and currents and its effect at structures, see for example Veldman and Huijismans (2008) and references therein. A numerical model can quickly be adapted to small changes in geometry or conditions, scaling effects can be avoided, and detailed insight in the hydrodynamic processes can be obtained. Not until recently, numerical models could not predict the complex and non-linear wave situations that occur in heavy seas and shallow areas. Research among others by (Kleefsman, 2005, Kleefsman et al., 2002) has shown that new hydrodynamic models based on the Navier-Stokes equations, in combination with a Volume Of

Fluid (VOF) based method for the description of the free-surface dynamics, are able to predict such effects. The (3D) VOF-based ComFLOW code developed at the University of Groningen (RUG) has shown potential for the modeling of detailed wave simulations. An ongoing research program has the objective to improve, develop and validate the model for complex free-surface flow at off-shore and coastal structures (Veldman and Huijsmans, 2008). In this context the program ComFLOW will be used in this thesis to study wave run-up on dikes and could be extended to wave overtopping.

1.3 Objective and methodology

The objective of this research is twofold. In the first place it will contribute to the application of ComFLOW to coastal engineering problems and to gain better insight in the capabilities and limitations of the model in this matter. In second place if the model is capable of accurate simulations of wave run-up, it could be used in future research and potentially assist and/or contribute to the design and assessment of sea dikes. The model is capable of calculating velocities, pressures and water levels in a detailed level and geometries are easy adjustable. Therefore, it can be used as a numerical flume. The objective of the research presented in this thesis can be phrased as:

To thoroughly analyze numerical simulations of wave run-up and other relevant wave-structure interaction processes on smooth and impermeable coastal structures with perpendicular wave attack and to verify the ability of the Volume of Fluid (VOF) model ComFLOW to represent these processes.

A smooth structure like a dike or embankment is mostly impermeable for water or waves and the slope has no, or almost no roughness. A type of dike typically seen at the Dutch coast, examples are embankments covered with a placed block revetment, asphalt or concrete slope. In ComFLOW it is (at the start of this study) only possible to simulate solid, impermeable structures without surface roughness. Sub-questions related to the objective are formulated to structure the research:

- Which physical processes are important for proper numerical reproduction of wave-structure interaction at the seaward slope of the dike?
- Is ComFLOW capable of accurate predictions with 2DV simulations of these relevant physical processes?
- Does the model show robustness during simulations? And which model settings are preferred?

In order to reach the formulated goal, the model should extensively be tested using a wide range of examples. Therefore the following methodology is adapted:

- To investigate whether the numerical model different mathematical aspects properly solves for relevant processes, simulation results will be compared with analytical solutions known from literature. Its performance with respect to accuracy of shoreline movement, velocities along geometries, flooding of the domain at high speed and similarity to the analytical solution will be investigated. These tests should give more insight in the cause of the differences and resemblances that occur during the wave run-up simulations in the next step and the overall performance of the model.
- Regular waves will be simulated on three different slopes (1:6, 1:4, and 1:3) in combination with 7 different wave conditions. The general performance with respect to wave interaction

with the structure will be analyzed. Wave run-up and other wave-structure interaction processes will be compared with experimental data.

- The last step in this study is meant to be illustrative. For two different breaker types of waves on the slope ComFLOW simulations will be visually compared with video recordings of a physical model test with regular waves. Differences and agreement in outcome are analyzed in a qualitatively way.

The flow-diagram of the methodology, see Figure 1.2, gives an overview of the steps taken, the relevant processes and the corresponding chapters. Therefore it also acts as the outline of the report.

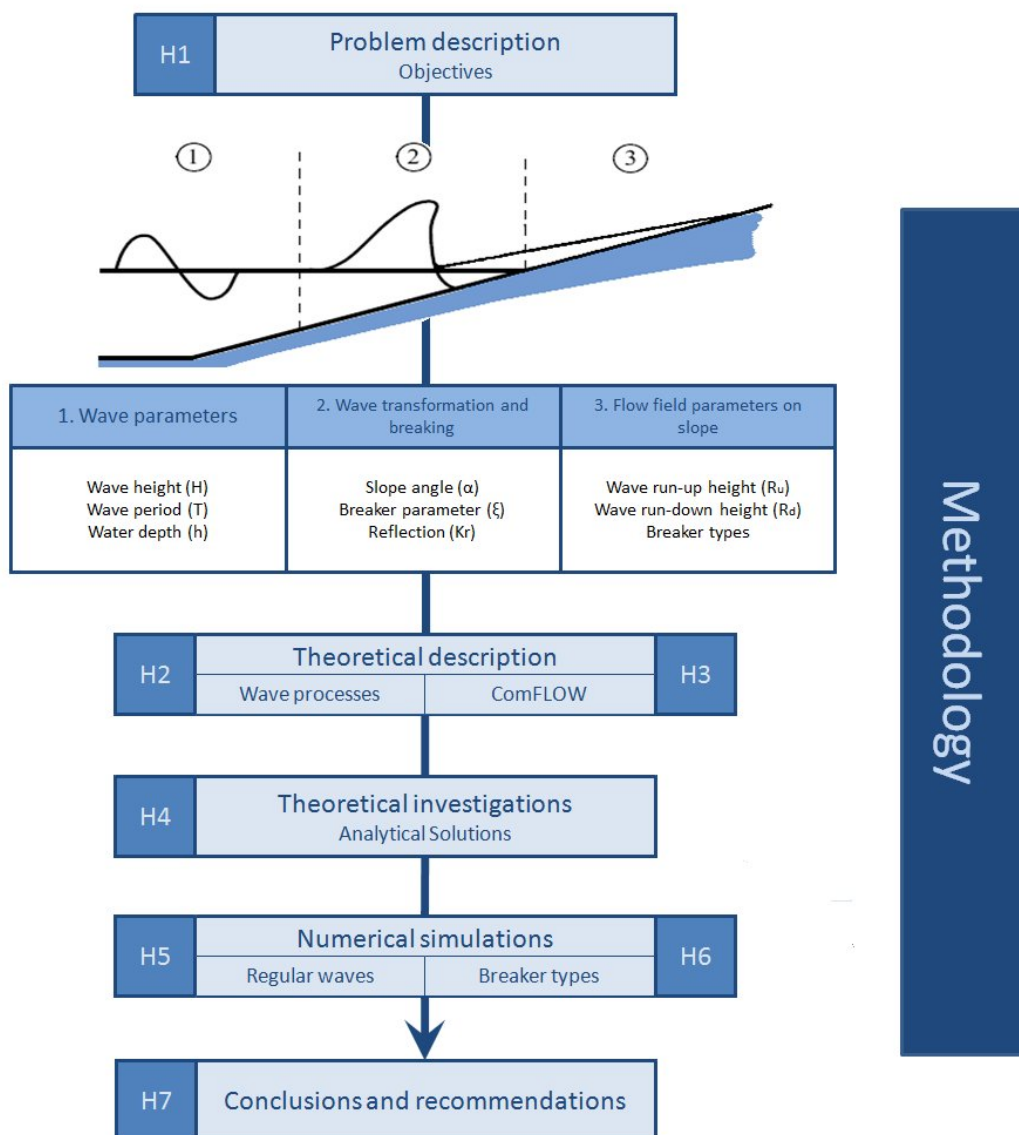


Figure 1.2: Flow-diagram methodology

2 Wave processes

This chapter will give an overview of literature and relevant theoretical background for the research of wave run-up and other relevant wave processes. Wave run-up has been subject to a lot of research, as it is an important design parameter for dikes and breakwaters. Many books and papers discuss this topic, for example lecture notes on bed, bank and shore protection (Schiereck, 2001), extensively used in this thesis. Most research has been summarized in the Overtopping Manual (Pullen et al., 2007). Since the present thesis is treating smooth, impermeable slopes with perpendicular wave attack, the presented theory focuses on these conditions.

To give a thorough analysis of the performance of the ComFLOW model for wave run-up not only run-up heights should be studied, this would give an incomplete picture. Therefore different wave processes at the seaward slope of coastal structures will be discussed, giving the characteristics of wave run-up, breaker types, reflection, and wave run-down for regular waves on impermeable structures with uniform slopes. By treating these processes the qualities (and shortcomings) of the model will be shown on multiple fronts.

2.1 Breaker parameter

The surf similarity parameter, also called breaker parameter or Iribarren number (ξ) is of importance in all kinds of shore protection problems. This parameter plays an important role in the behaviour of waves on a slope. It represents the ratio of slope steepness and deep water wave steepness, and therefore combines hydraulic and structural parameters, see equation (2.1):

$$\xi = \frac{\tan \alpha}{\sqrt{H/L_0}}$$

in which L_0 :

$$L_0 = \frac{gT^2}{2\pi}$$
(2.1)

Where:

ξ =	breaker parameter	[-]
α =	angle of the slope	[°]
H=	wave height	[m]
T =	wave period	[s]
L_0	deep water wave length	[m]
g =	gravitational acceleration	[m/s ²]

2.1.1 Wave breaker types

Near a structure, for different values of ξ , waves behave in a completely different way. Not only does this relation provide insight whether waves will break and how the wave will break, also reflection, run-up and stone stability (as non-breaking or breaking strongly determines pressures and velocities along the slope) are related to this parameter.

The different ways of breaking of waves can be classified in three main types; surging, plunging and spilling. Where the type collapsing is distinguished as a transition between surging and plunging. Figure 2.1 gives an impression of the different breaker types and the range of ξ for which they occur, obviously the transition between the types is not sharp-cut.

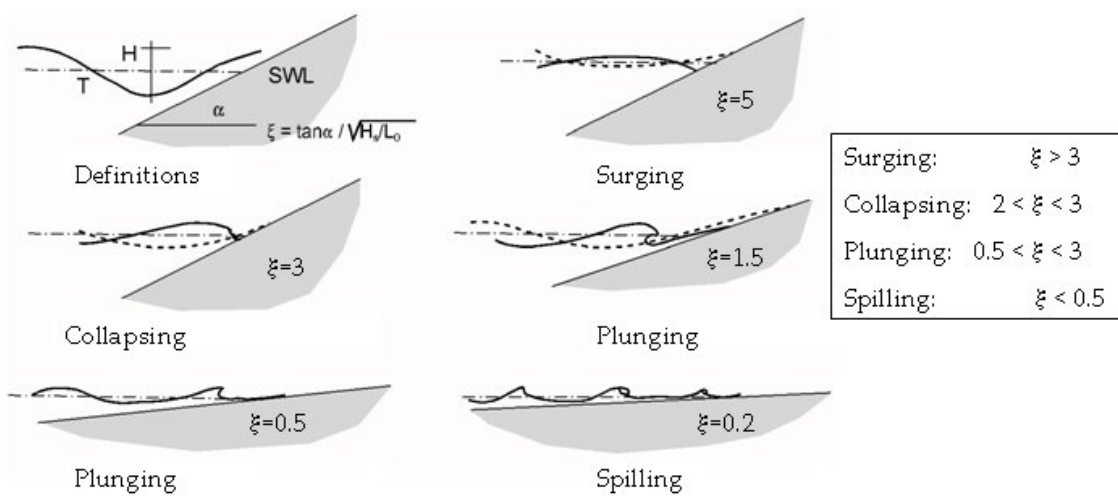


Figure 2.1: Breaker types as function of ξ

Both Iribarren (1938) and Battjes (1974) theoretically deduced the critical value for the breaker parameter, ξ_c , for which $\xi > \xi_c$ waves do not break. Iribarren came to a value of $\xi_c = 2.3$ and Battjes of $\xi_c = 2.5$. Given the coarseness of the estimation it is stated that these values are virtually the same. The range of values for breaker types presented in Figure 2.1 was deduced from physical experiments, this also shows that in this highly turbulent and complex environment it is very difficult to extract exact values for the transition between breaker types.

2.2 Wave run-up

The wave run-up height is defined in the overtopping manual (Pullen et al., 2007) as the vertical difference between the highest point of wave run-up and the still water level (SWL). For irregular waves, due to the stochastic nature of the incoming waves, each wave will possibly give a different run-up level. In case of regular waves, on the other hand, each incoming wave will give the same run-up level.



Figure 2.2: Wave run-up level R_u (Van der Meer and Janssen, 1994)

In the Netherlands as well as in Germany many dike heights have been designed using a wave run-up height $R_{u2\%}$. This is the wave run-up height which is exceeded by 2% of incoming waves at the toe of the structure. Note that the wave run-up level is related to the number of incoming waves and not to the number of run-up levels. Most of the research in the past focuses on this 2% run-up height. But for regular waves the $R_{u2\%}$ value is irrelevant, as all incoming waves should give the same run-up value.

Hunt's formula (1959)

Hunt derived this formula for regular waves, with wave height H and period T , on smooth slopes during model tests. He found that the relative wave run-up is equal to the breaker parameter (for $\xi < 2.5-3$):

$$\frac{R_u}{H} = \xi \quad (2.2)$$

Run-up appears to be maximum around $\xi=2-3$, which is just at the transition between plunging and surging (collapsing waves).

Schüttrumpf formula (2001)

For waves with values for ξ lower than 2.5, waves will break. The plunging waves hit a sheet of water that flows down from the foregoing wave (see Figure 2.1). This results in highly turbulent flows and energy dissipation, resulting in a reduction of wave run-up and reflection (see section 2.1.4). For non-breaking waves this is not the case and energy is preserved. Therefore a more or less horizontal equilibrium in relative wave run-up is reached for higher breaker parameters.

Schüttrumpf derived the following empirical function for regular waves on smooth slopes:

$$\begin{aligned} \frac{R}{H} &= c_1 \cdot \tanh(c_1^* \cdot \xi) \\ c_1 &= 2.25 \\ c_1^* &= 0.5 \end{aligned} \quad (2.3)$$

With the use of continuous, hyperbolic functions for wave run-up (and other wave processes) Schüttrumpf tried to take natural processes of the breaking of waves into account and the transition for breaking to non-breaking. In the next figure both formulas by Hunt and Schüttrumpf for regular waves are shown.

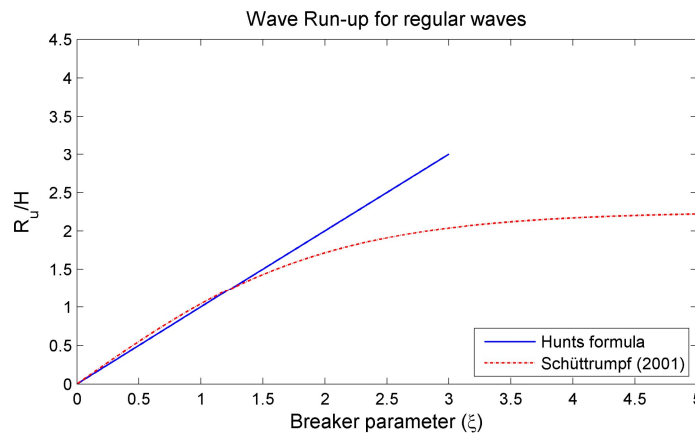


Figure 2.3: Wave run-up formulas by Hunt and Schüttrumpf for regular waves

Reduction factors

In reality the relative wave run-up depends not only on the parameters included in the breaker parameter; slope angle, wave height and wave length. There are also other factors that reduce run-up. Although these factors are not considered in this study, it is valuable to be aware of the influence of other variables. These reduction factors include: roughness, oblique wave attack and berms. The reduction factors have all been determined separately in experimental model investigations and are all between 0 and 1. Formula 2.2 now extends to:

$$\frac{R_u}{H} = \gamma_b \cdot \gamma_\beta \cdot \gamma_r \cdot \xi$$

The formula shows that a combination of reduction factors is possible that produces a very small run-up value. Since combinations of run-up reduction factors have not been investigated, a minimum total reduction factor is set to 0.5. In this section the reduction factors will shortly be discussed, to clarify the influence of these factors and which reduction factors are incorporated:

- Roughness: a rough surface will reduce the wave run-up heights. For smooth slopes this factor is 1. For grass slopes, γ_r , is between 0.95 and 1. The reduction for riprap slopes is between 0.7 and 0.55.
- Angle of attack: when waves do not approach the slope perpendicularly a reduction factor is applied. For long crested waves this reduction factor, γ_β , has a minimum of 0.7 and for short-crested waves the minimum reduction is 0.8.
- Berm: the presence of a berm also reduces wave run-up. The parameters that influence the reduction is the length of the berm, wave height and the distance between SWL and the berm level. The reduction factor is limited by $0.6 < \gamma_b < 1$.

2.3 Wave run-down

The wave run-down height, R_d , is defined as the minimum water level on a slope during a wave period relative to the SWL. It is the opposite process of the run-up level, see Figure 2.4 below.

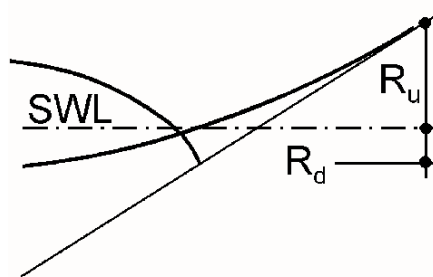


Figure 2.4: Run-down definition

Battjes (1974)

Battjes formulated a formula for wave run-down for regular waves based on experiments:

$$R_d = R_u(1 - 0.4\xi),$$

$$\frac{R_d}{H} = (1 - 0.4\xi)\xi \tag{2.4}$$

The relative run down has a positive value for $\xi < 2.5$, which means that the water level does not drop below the still water level. This is because the water in a wave that flows down on a slope, meets the water running up from the next wave. For higher Iribarren values this is not the case and the wave run-down reaches below SWL, this can be seen in Figure 2.5 where the wave run-down is illustrated.

Bruun and Günbak (1977) however analyzed the existence of this condition assuming the movement of a water mass along the smooth slope from the maximum run-up point down to SWL under the action of gravity only. This theoretical analysis showed that for smooth slopes that positive values for run-down are reached for $\xi < 1.6$. The difference between the experimental and theoretically found value is explained by the fact that effects of pressure and friction forces on the flow are neglected in the theoretical derivation. This will retard the run-down and will cause waves with higher values than 1.6 for ξ not to cross the SWL, this may occur with waves breaking on the slope. This analysis and the formula by Battjes shows that the run-down values are interrelated with the maximum run-up values.

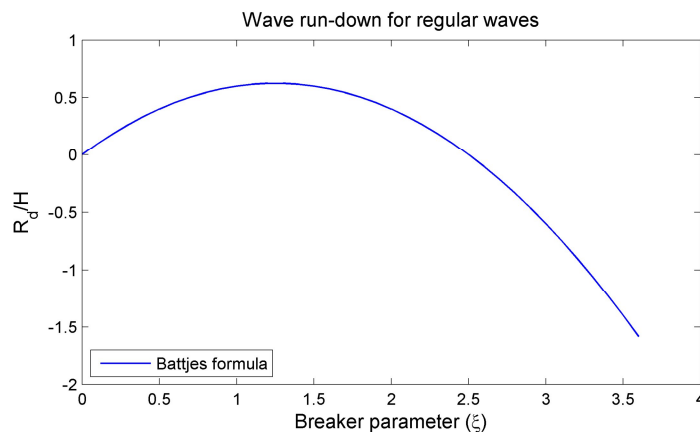


Figure 2.5: Wave run-down formula by Battjes for regular waves

The same reasoning for non-breaking waves can be used as for wave run-up, for this type of waves no energy will be lost during surging up- and down the slope and an equilibrium for relative wave run-down is reached for higher breaker parameters, which is for a matter of fact not included in the given formula.

2.4 Reflection

The extend to which waves are reflected against a structure is important for the resulting wave field near the structure. Wave breaking is the most effective, and for smooth impermeable slopes the only, mechanism of energy dissipation. There can be two extremes distinguished with respect to reflection: for non-breaking waves on steep slopes (vertical walls) reflection is almost 100%, leading to standing waves and for sufficiently gentle slopes, with breaking waves, nearly all incoming wave energy is dissipated so that reflection is negligible.

The reflection-coefficient is defined as the wave height of the reflected wave with respect to the incoming wave height:

$$\frac{H_r}{H_i} = K_r \tag{2.5}$$

The derivation of a theoretical solution for reflection of breaking waves is hardly possible. An useful approach is given by Miche. He equalized the height of the reflected waves to a limit value (H_c) of H , in case of wave breaking. This approach implies that the reflection coefficient is proportional to ξ^2 (see Battjes, 1974). For values of ξ below the breaking limit, the following formula was found experimentally:

$$K_r \approx 0.1\xi^2 \tag{2.6}$$

For $\xi > 2.5$ reflection slowly tends to 1, the value for total reflection. Figure 2.6 shows this reflection coefficient as a function of the breaker parameter, the deflection for higher breaker parameters is obviously not represented by the formula.

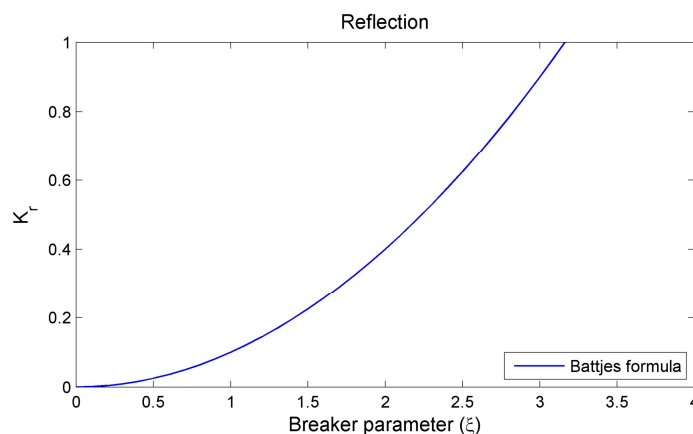


Figure 2.6: Reflection formula by Battjes, reflection coefficient as a function of ξ

2.5 Summary of wave processes

Most formulas of the described processes are curve fittings, based on the results of physical model test. Differences in the data of experiments can be explained by different scales, different measurement techniques and the fact that these highly turbulent flows are difficult to measure. Schüttrumpf and van Gent (2003) collectively wrote a paper and indicated the test set up (dike geometries and instruments) and test programmes as primary cause of discrepancies between different experimental model tests. The formulas based on curve fitting of experimental result are therefore just not exact solutions. Analysis of numerical results will be done with experimental data. In this section the used experimental data will be shown, differences and similarities are shortly discussed.

Differences in set-up of the used physical experiments are summarized here. The data of Bruun and Günbak are based on two physical experiments of regular waves on smooth slopes: one performed by Hudson (1959) and one by themselves. They used slopes of 1:3, 1:2 and 1:5, wave heights of 4 to 15 cm with periods ranging from 0.8 to 2.43 seconds and a constant water depth of 50 cm. Schüttrumpf used slopes of 1:6, 1:4 and 1:3, wave heights of 7.6 to 20 cm with periods ranging from 1.5 to 4.25 seconds and a constant water depth of 70 cm.

In Figure 2.7 the experimental data result for wave run-up of Bruun and Günbak and those of Schüttrumpf are shown. In this figure we can already discover some interesting differences. Around $2 < \xi < 3.5$ we see in the results of Bruun and Günbak a large peak, which is not present in the data of Schüttrumpf. Notable fact is that all run-up results in this peak are those of plunging waves. This peak made Bruun and Günbak say that the formula of Hunt is valid to $\xi=3$, Schüttrumpf on the other hand held this, also based on his result, to the breaking limit of $\xi=2.3$. Another remarkable difference is the fact that the results for value larger than 4 are lower and more scattered for Bruun and Günbak.

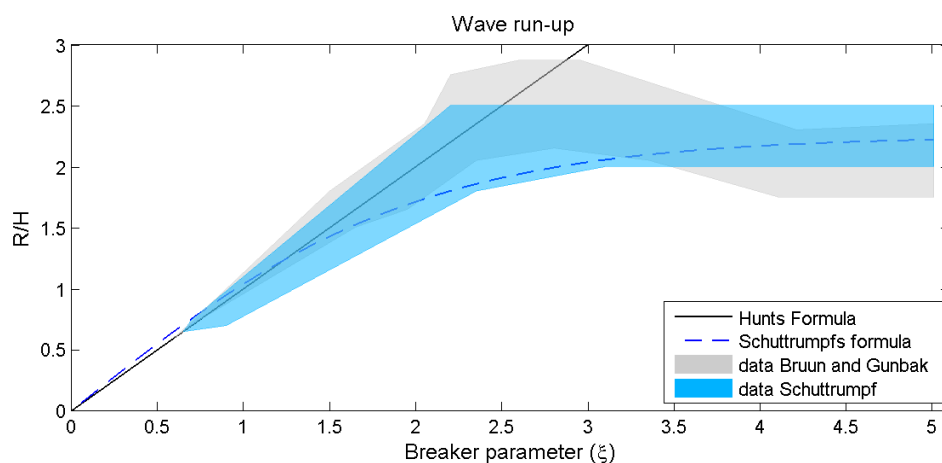


Figure 2.7: Wave run-up formulas with experimental data of Bruun and Günbak and Schüttrumpf.

The wave run-down data, in Figure 2.8, are for both experiments less scattered than the run-up data. Most notable fact is that the data is for both experiments lower than the formula of Battjes and that all results of Schüttrumpf are below those of Günbak and Bruun. The last also gave a curve fitting in their paper based on the formula of Battjes, resulting in $R_d = H(1 - 0.45 \xi) \xi$. This gives a penetration of the SWL at $\xi=2.2$. Schüttrumpf based his curve fittings on a hyperbolic function, which looks more appropriate when looking at the data. However, he did not deduct this curve fitting for regular wave run-down. From his data the penetration of the SWL can be

read, which is at $\xi=1.8-1.9$. Both penetration values of the data are higher than the theoretical value of 1.6, but are lower than the 2.5 value of Battjes. This could indicate that the formula by Battjes gives too high run-up values.

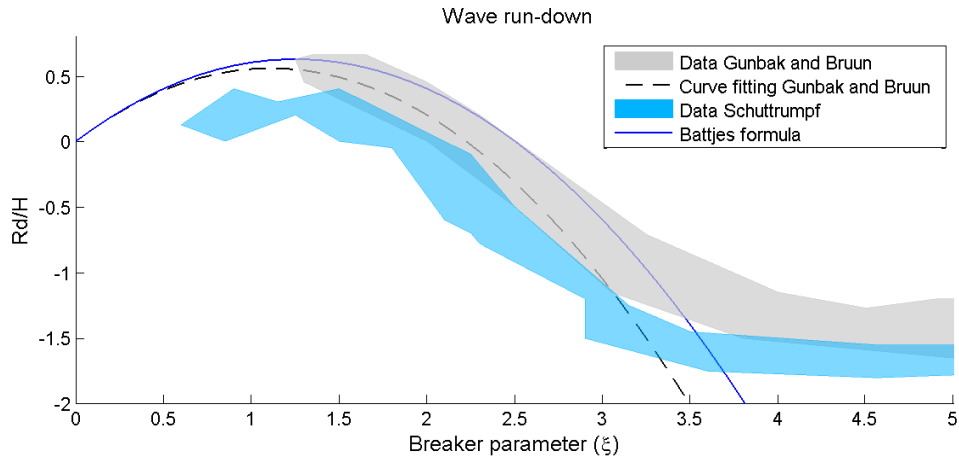


Figure 2.8: Wave run-down formulas with experimental data of Bruun and Günbak and Schüttrumpf.

The formula of the reflection coefficient is also plotted with a experimental data cloud, this cloud is extracted from the lecture notes on bed, bank and shore protection (Schiereck, 2001). Clear is the deflection from values around $\xi=2.5$, slowly tending to a value of $K_r=1$. For lower values the formula describes the data well.

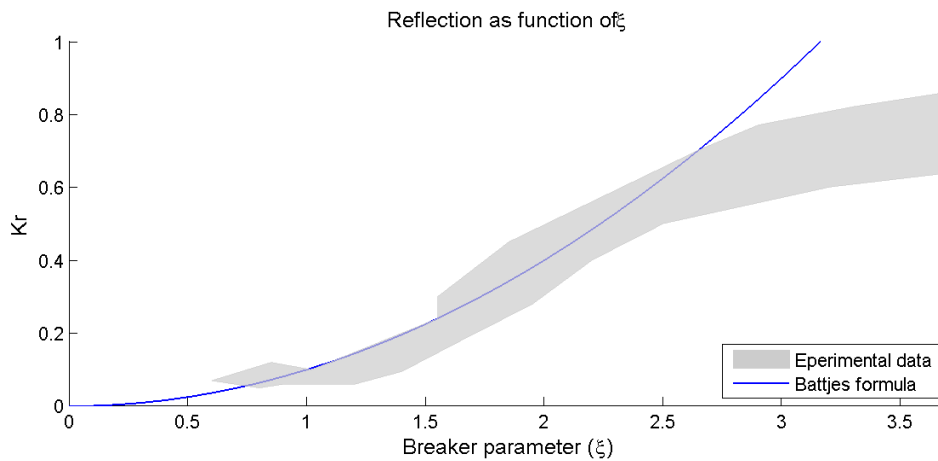


Figure 2.9: Reflection formulas with experimental data.

3

ComFLOW

ComFLOW is a model for numerical simulations of fluid flow. The code is a (3D) hydrodynamic flow model based on the incompressible Navier-Stokes equations, used in this study to simulate wave run-up and other processes. The evolution of the free water surface is described by the Volume-of-Fluid method (VOF), designed originally by Hirt and Nichols (1981). Nowadays an adapted and (highly) improved version is used in the model. For introduction a short history of ComFLOW will be given here, the mathematical and numerical model and a description of the wave generation will be discussed hereafter. In this chapter only relevant aspects of ComFLOW are highlighted, functionalities as two phase-flow or moving bodies are not included as they are not used in this study. A more extensive description of ComFLOW can be found in Kleefsman (2005), the ComFLOW manual (ComFLOW, 2008) and Wemmenhove (2008) .

History of ComFLOW

The model has initially been developed in the late seventies by the University of Groningen (RUG), by Prof. dr. Arthur Veldman, to study the sloshing of liquid fuel in satellites. This micro-gravity environment required a very accurate and robust description of the free surface.

In the late nineties, MARIN got in touch with the application at RUG and started the development and utilization of the model for offshore and maritime applications: the green water loading on the deck of ships, semi-submersibles and tension-leg platforms, motions of offshore structures, sloshing in LNG systems and air entrapment during wave impacts. This research was extended with support of a world-wide consortium of offshore-related companies in the ComFLOW-2 joint-industry project.

After the ComFLOW-2 project Deltares joint the consortium to apply and develop the simulation method in predicting impact forces on coastal protection structures. The research is part of the follow-up project, ComFLOW-3, which started in 2009. Objectives of this program are the inclusion of a sophisticated turbulence model, speed-up of the algorithms, improved functionality, less dissipative wave propagation, improvement of the generating and absorbing boundary conditions (GABC) and validation for various advanced engineering applications.

3.1 Mathematical model

3.1.1 Governing equations

Since almost a century and a half the mathematical formulation of the laws describing the motion of fluid are known. The so-called Navier-Stokes equations, formulated by the Frenchman called Claude Louis Marie Henry Navier (1785-1836) and the Irishman called George Gabriel Stokes (1819-1903). This system of partial differential equations governs the laws of conservation of mass and momentum and is in most cases unsolvable analytically due to the high non-linearity of the equations. This is the point where numerical models as ComFLOW come in. ComFLOW describes the flow of a homogeneous incompressible viscous fluid using this law of conservation of mass

and momentum. Mass and momentum conservation together give a set of differential equations, which suffice to describe the motion of water. In combination with a set of boundary conditions on the boundary of the domain of interest a problem is defined with a unique solution. The laws of conservation of mass and momentum are given by:

$$\begin{aligned} \nabla \cdot \mathbf{u} &= 0 \\ \frac{\partial \mathbf{u}}{\partial t} + \nabla (\mathbf{u} \otimes \mathbf{u}^T) &= \frac{1}{\rho} \nabla p + \frac{\mu}{\rho} \nabla^2 \mathbf{u} + \mathbf{F} \end{aligned} \quad (3.1)$$

With:

$p =$	pressure	[N/m ²]
$t =$	time	[s]
$\mathbf{u} =$	velocity vector	[m/s]
$\nabla =$	gradient operator	[-]
$\mu =$	dynamic viscosity	[kg/sm]
$\rho =$	fluid density	[kg/m ³]
$\mathbf{F} =$	dissymmetric forcing term	[m/s ²]

Note that the dynamic viscosity and fluid density are assumed constant as in the model no turbulence model is included. And $\mathbf{u}=(u,v,w)$ the velocity vector with u,v and w the velocities in the three coordinate directions x,y and z , respectively. This vector reduces to a scalar in one dimension and the system of equations reduces to a single equation. In case of wave run-up the only external force is gravity, given by:

$$\mathbf{F} = \mathbf{g} = (g_x; g_y; g_z) = (0; 0; -9,81) \quad (3.2)$$

The continuity and Navier-Stokes equations will be solved inside one fluid: water. In the simulations a second fluid will be present, air, for which no equations will be solved. Both fluids are separated from each other by a free surface. The evolution of free surface is described by the following equation:

$$\frac{Ds}{Dt} = \frac{\partial s}{\partial t} + (\mathbf{u} \cdot \nabla)s = 0 \quad (3.3)$$

Where $s(x,t)=0$ gives the actual position of the free surface. A piecewise constant reconstruction of the free surface is used, where the free surface is displaced by changing the VOF value in a cell using calculated fluxes through cell faces. The flux through a cell face is calculated as the velocity time the area of the cell face A and the time step δt .

3.1.2 Boundary conditions

To solve the foregoing flow equations, boundary conditions are required at all fluid boundaries. At solid boundaries the no-slip boundary condition for viscous fluids is applied.

$$\mathbf{u} = \mathbf{u}_b \quad (3.4)$$

With $\mathbf{u}_b=0$ for fixed objects and solid domain boundaries. This means that no fluid can go through the wall and also the velocity tangential to the solid boundary is zero.

At the domain boundaries a free-slip boundary condition is applied.

$$\begin{aligned} u_n &= \underline{u} \cdot \underline{n} = 0 \\ u_t &= \underline{u} \cdot \underline{t} \\ \frac{\partial u_t}{\partial n} &= 0 \end{aligned} \quad (3.5)$$

Where u_n and u_t denote the normal and tangential component of the velocity to the solid boundary respectively. This boundary condition implies velocity normal to the wall are zero and the gradient of velocities parallel to the wall are zero. Free slip denotes that there is no friction between fluid and wall.

At the free surface the forces are balanced. Continuity of normal stresses and tangential stresses lead to the boundary conditions for the pressure and velocity at the free surface. When the fluid is assumed incompressible and the curvature of the free surface is neglected in the viscous stress terms, this results in the following equations (split in the normal and tangential direction):

$$-p + 2\mu \frac{\partial u_n}{\partial x_n} = -p_0 + \sigma \kappa_c \quad (3.6)$$

$$\mu \left(\frac{\partial u_n}{\partial x_t} + \frac{\partial u_t}{\partial x_n} \right) = 0 \quad (3.7)$$

In the equation x_n denotes the normal of the free surface and x_t is the tangential direction, u_n and u_t denote the normal and tangential component of the velocity to the free surface respectively, p_0 is the atmospheric pressure, σ is the surface tension, and κ_c the total curvature of the free surface. This formula is based on the assumption of laminar flow.

3.2 Numerical model

3.2.1 Grid and geometry definition

To numerically solve the Navier-Stokes equations the computational domain is covered by a fixed Cartesian grid. A Cartesian grid is a simple rectangular grid. The grid can be defined in two ways: uniform, a grid in which all grid cells have the same dimension, or stretched, the size of the grid cells varies in one or more dimensions. The grid will always be of rectangular shape. The simplicity of the grid is an advantage; it gives an easy geometric framework in which the position and slope of the surface can be more accurately described than other grid types, as preferred for the application in wave run-up. Moreover, it gives relatively simple and efficient data structures.

The form of a defined geometry is mostly not rectilinear and will cut through the rectangular, Cartesian grid cells, resulting in cut cells. For the definition of the geometry on the Cartesian grid, volume and edge apertures are introduced. To indicate which part of a cell volume and cell face is open for fluid for every cell has a volume aperture (F_b) and edge apertures (A^x , A^y , A^z). Three aperture options are indicated:

- F_b or $A=0$, the cell or edge is blocked for fluid (indicates solid body);
- $0 < F_b$ or $A < 1$, the cell or edge is (partly) open for fluid;

- F_b or $A=1$, the cell or edge is completely open for fluid.

An illustration is given in Figure 3.1, on the left side all information on the apertures is given.

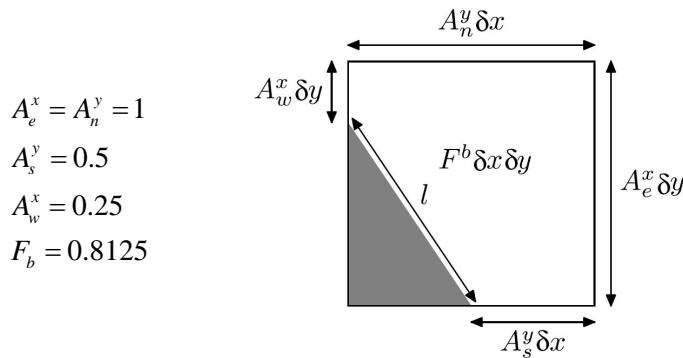


Figure 3.1: Grid cell, volume aperture and edge apertures. (Figure 2.8 Kleefsman (2005))

As showed in the illustration volume and edge apertures contain all relevant geometrical information for the discretization of the flow equations. However, this information is not exact and limited by the number of integration points (nrinp), specified by the user. ComFLOW checks for this number of points per grid cell whether this point is inside or outside the geometry. This number of integration points therefore actually defines the 'smoothness' of the geometry. A value of 1 will give a staircase geometry, while higher values give more fluent geometries. Figure 3.2 shows an example with two integration points. In this figure the bold lines on the outer part of the cells denotes the closed apertures by ComFLOW. The black, sloping line is the actual defined geometry by the user, dark grey denotes the part of the cell filled denoted as body by ComFLOW. Light grey denotes possible presence of geometry, which is not known by the model. More integration points result in a smoother geometry and make the uncertain part of the area (light grey) smaller.

$A_e^x = A_n^y = 1$	$A_e^x = 0.5$	$A_e^x = A_w^x = 0.5$
$A_w^x = 1$	$A_s^y = 0.0$	$A_s^y = 0.0$
$A_s^y = 0.0$	$A_n^y = A_w^x = 1$	$A_n^y = 1$
$F_b = 1$	$F_b = 0.5$	$F_b = 0.5$

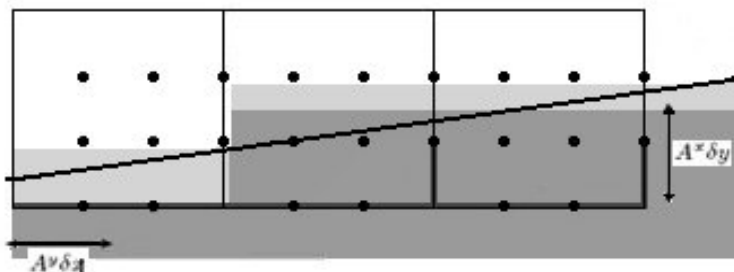


Figure 3.2: Aperture calculation using two integration points. The more integration points, the smoother the geometry. Given for the cells volume and edge apertures.

3.2.2 Free surface description

Besides the volume apertures another function has been introduced to identify the fraction of a cell that is filled with fluid: the Volume-Of-Fluid (VOF) function, denoted by F_s . The time-dependent fluid aperture F_s indicates which fraction of a cell is actually occupied by fluid, and hereby tracks the free surface. The same statements as for the aperture cells can be distinguished for F_s . Because there can be no more fluid in the cell than the open part of the cell, the VOF-function is limited by $0 \leq F_s \leq F_b \leq 1$.

A piecewise constant reconstruction of the free surface is used where the free surface is displaced by changing the F_s value in a cell using the calculated fluxes through cell faces. The evolution of the free surface is given by equation (3.3). In ComFLOW an adapted and improved version of original (Hirt and Nichols, 1981) VOF-method is used, see Kleefsman et. Al (2005). By combining the VOF-method with a local height function, strict mass conservation is ensured and almost no 'flotsam and jetsam' occurs, thereby avoiding two main drawbacks of the original VOF method.

3.2.3 Cell labeling

Cell labeling is introduced to distinguish cells of different character. After the apertures have been assigned to the grid cells, every cell is given a label to distinguish boundary, air and fluid:

- B(boundary)-cells : Cells that are completely in the solid geometry.
- E(empty) -cells : Cells that contain no fluid, air.
- S(surface)-cells : Cells that contain fluid adjacent to empty cells.
- F(fluid) -cells : Remaining cells that contain fluid.

In Figure 3.3 an example of cell-labeling is given.

E	E	E	E	E
E	E	S	B	B
S	S	F	F	B
F	F	F	F	F
F	F	F	F	F

Figure 3.3: Cell labelling: dark grey denotes solid body; light grey is liquid. (Figure 1, (Kleefsman et al., 2005))

Notes: S-cells always contain part of the free surface and F-cells do not have to be completely filled with fluid.

3.2.4 Discretization of the continuity and Navier-Stokes equations

The Navier-Stokes equations are discretised in time and space. The finite volume method is used for the spatial discretization. This means integration of the equations over a suitably chosen

control volume and application of Gauss divergence theorem. Conservation of mass and momentum is in this way ensured.

In the method the variables are staggered on the Cartesian grid, which means that the pressure is defined in cell centers and the velocities on cell faces. The advantage of a staggered grid is that mass conservation can be satisfied easily in a cell, without interpolations.

A first-order upwind spatial discretization for the convection term is used in this study, ComFLOW this scheme can be adapted. For the time discretization the first order Forward-Euler method is adopted. The time step Δt is automatically adapted during the simulation. It is halved when the CFL-number exceeds *cflmax* (specified by the user), or doubled when it is smaller than *cflmin* for ten successive time steps. The CFL-number is defined as:

$$CFL = \max_{i,j,k} \left(\frac{|u_{i,j,k}| \Delta t}{\Delta x_i} + \frac{|v_{i,j,k}| \Delta t}{\Delta y_j} + \frac{|w_{i,j,k}| \Delta t}{\Delta z_k} \right) \quad (3.8)$$

Where *u,v* and *w* are the velocity components, indices *i,j,k* refer to the cell number.

For the solution of the discretised Navier-Stokes equation, a Poisson equation must be solved for the pressure, which is solved using Successive Over-Relaxation (SOR) iteration with an automatically adapted relaxation parameter, when one-phase flow without GABC boundaries is used (see next section). When absorbing boundary conditions are used the CGSTAB pressure solver should be used.

3.2.5 Free surface boundary conditions: velocities

Velocities in the neighbourhood of the free surface can be grouped in different classes (see Figure 3.4). The first class contains the velocities between two F-cells, two S-cells and S- and F-cell. These velocities are determined by solving the momentum equation. The second class are the SE-velocities and these are solved by an engineering mix between extrapolation from interior velocity field and mass conservation. This combination results in a highly accurate and robust method. The last class consists of velocities between two E-cells that are sometimes needed to solve the momentum equation. These are determined using the tangential free-surface condition, equation (3.7). An extensive description is given in (Kleefsman, 2005: page 38-46).

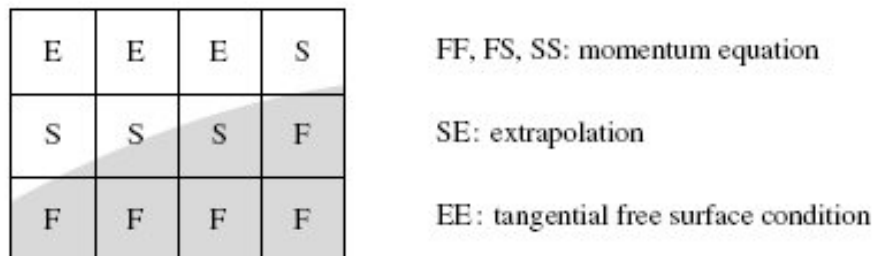


Figure 3.4: Different classes of velocities near the surface (Kleefsman et al., 2005)

3.3 Wave generation and boundary conditions

3.3.1 Description of wave generation

A wave description theory is used to generate waves at the inflow boundary of the domain. At the inflow boundary positive and negative velocities can occur, so fluid can flow in and out.

In ComFLOW the waves are prescribed at the inflow boundary using a theoretical description of the waves. In this model the wave is traveling in positive x-direction, making the left domain wall the inflow boundary, with an angle of incidence of 0 degrees. The wave that can be imposed in ComFLOW are based on Airy wave theory describing linear waves and 2nd order Stokes, 5th order Stokes or the Rienecker Fenton theory describing nonlinear waves. A superposition of linear wave components can be used to generate an irregular wave.

When using linear waves (Airy wave), the wave elevation is defined by a cosine:

$$\eta(x,t) = A \cos(\omega t - \kappa x + \phi) \quad (3.9)$$

With A the amplitude, ω the frequency, κ the wave number and Φ the phase.

When generating irregular waves, the variables A, ω , κ , Φ should be prescribed by the user and the wave is defined as:

$$\eta(x,t) = \sum_{i=1}^n a(i) \cos(\omega(i) \cdot t - \kappa(i) \cdot x + \phi(i)) \quad (3.10)$$

For steeper waves, where in general the crests become higher and the troughs flatter, linear theory does no longer hold. To prescribe nonlinear waves, a solution to potential theory is used. The Rienecker-Fenton wave theory gives more accurate wave kinematics than 5th order Stokes in shallow water and for steep waves. The Rienecker-Fenton wave is constructed by using a finite Fourier series to give a set of equations that can be solved using Newton's method (Rienecker and Fenton, 1981). The only approximation for a Rienecker-Fenton wave is the truncation of this Fourier series. The advantage of Rienecker Fenton compared to other wave theories are its applicability to all wave lengths and possibility to describe the propagation of steep non-linear waves.

3.3.2 Generation and Absorbing Boundary Condition (GABC)

At the outflow boundary conditions should be imposed, such that the wave can leave the domain undisturbed and prevent reflection. Therefore a generating and absorbing boundary condition (GABC) has been implemented in ComFLOW (Wellens et al., 2009), it ensures wave generation and wave absorption at the same time. The Sommerfield radiation boundary condition for a velocity potential is the basis for the GABC, is given by:

$$\frac{\partial \phi}{\partial t} + \frac{c \partial \phi}{\partial x} = r h s d \quad (3.11)$$

Where the left-hand side absorbs outgoing waves, and the right-hand side is used to prescribe incident waves. Recognizing that the velocity and dynamic pressure are in the potential theory given by respectively $u = \delta \phi / \delta x$ and $q = - \delta \phi / \delta t$, the expression can than be rewritten as:

$$-cu + q = rhd \quad (3.12)$$

The difficulty with evaluation of this expression is that the celerity of the outgoing waves is unknown. In the GABC the celerity is computed from a numerical solution, the Padé-approximation of the linear dispersion relation is used for this:

$$c_a = \sqrt{gh} \frac{a_0 + a_1(kh)^2}{1 + b_1(kh)^2} \quad (3.13)$$

This is an essential ingredient in the GABC procedure as a_0 , a_1 , b_1 need to be specified by the user. Combining equation (3.11), (3.13) and relations following from linear theory give an expression for the GABC boundary condition:

$$-\sqrt{gh} \left(a_0 u + a_1 h^2 \frac{\partial^2 u}{\partial z^2} \right) u + \left(q + b_1 h^2 \frac{\partial^2 q}{\partial z^2} \right) = rhd \quad (3.14)$$

A more extensive explanation and numerical evaluation can be found in (Wellens et al., 2009).

3.4 Numerical default settings

In this section the numerical setting that are used for all simulations are discussed. In this study it was decided to call these settings the numerical default settings, as they are for all simulation kept the same. This will be referred to as the default settings. For some simulations exceptions are made, but this will be explained at the corresponding section on.

Time integration, time steps and spatial discretization

The following settings are used:

- Space discretization: a first-order upwind spatial discretization for the convection term.
- Time integration: forward Euler.
- Initial time step: 0.01 seconds.

The time step is adapted during simulation, as described in section 3.2.4, for $cfl_{max}=0.9$ and $cfl_{min}=0.4$.

Geometry smoothness

The number of integration points specifies the smoothness of the geometry by the 'staircase' way the discretization is handled, as explained in section 3.2.1. Initially four integration points ($n_{rintp}=4$) are used for simulations, as the user manual describes this as the maximum usable (and stable) value. However personal communication with Peter Wellens revealed that according to theory the model should be stable for higher numbers of integration points. More integration points should only lead to an increase in computational time in case of moving objects in the simulation. Therefore, additional simulations are performed to analyze the results and usability for higher numbers of integration points with a value of 8.

Physical parameter settings

All simulations are one-phase flow, i.e. no physical parameters are included for air. The following physical model settings are used:

- Water density: $\rho=1000$ [kg/m³]
- Dynamic viscosity: $\mu=1.0 \times 10^{-3}$ [kg/(m.s)]
- Gravitational acceleration : $g=9,81$ [m/s²]
- Kinematic surface tension: $\sigma=0$ [N/m]

As can be seen the kinematic surface tension is neglected in these simulations.

Wave boundary conditions

The left domain boundary condition needs to be specified by the user when (regular) waves need to be generated and absorbed at this boundary. The incoming waves have a wave height equal to H and a wave period equal to T . The GABC boundary condition (see section 2.2.4) is used for all simulations that include waves. Wenneker (2010) proposed to use more robust settings than the default values described in the user manual. With the robust settings the effect of the second derivatives in the vertical is absent which destabilized the solution. This is realised by putting $a_1=b_1=0$. Equation (3.13) then reduces to $c_a = a_0 \sqrt{gh}$ and now a_0 needs to be specified. As most wave energy is stored in wave period T and this waves propagate at speed $c = \sqrt{g \tanh(kh)} / kh$, this leads to the following suitable value for a_0 :

$$a_0 = \sqrt{\frac{\tanh(kh)}{(kh)}} \quad (3.15)$$

4 Analytical solutions

To investigate whether different mathematical aspects for relevant processes are solved well by the numerical system, simulation results will be compared with analytical solutions known from literature. Three cases are chosen which show resemblance with the wave run-up processes that will be studied in the next chapter. These tests should give more insight in the causes of the differences and resemblances that occur during wave run-up simulations and the overall performance of the model. From these test cases the performance of the model with respect to accuracy of shoreline movement, flooding of the domain at high speed, velocities along geometries and similarity to the analytical solution will be investigated.

Three test cases are used, the classical dam break test with a horizontal bed, the dam break test with an upward sloping bed and periodic non-breaking waves on a sloping beach formulated by Carrier and Greenspan which both include different elements that will be important for the wave run-up process.

Theoretical run-up analysis mainly investigate the behaviour of a propagating bore on a slope, leaving wave breaking out of the analysis. If there is no breaking of waves the motion is smooth, incident waves are reflected and the water layer propagation along the slope can be describe well by linear theory for slopes, see Whitham (1979), or by solutions of the nonlinear shallow-water equations. The dam break test and the test of Carrier and Greenspan (1958) are solutions of these shallow water equations.

4.1 Dam break test

A dam wave break is the flow resulting from a sudden release of a mass of fluid in a channel. The work on the dam break problem was initiated by major dam break catastrophes that caused numerous losses of lives. In point of fact the dam break test is a propagating flood wave in a channel without any wave breaking. Here two cases are investigated a horizontal channel and an upward sloping channel. This test is suited to investigate the ability of the model to simulate the propagation of the leading edge of a wave with high velocities. In the case of a sloping bed the run-up under influence of gravity can be investigated. Difficulties that arise for the dam break test are: the thickness of the water layer at the front becomes infinitely small in the analytical solution, this is difficult in a numerical representation, and the initial gradient of the water front is very large, flooding the dry part of the domain at a very high speed which causes often problems in numerical models.

4.1.1 Horizontal channel, dry bed

The dam break test is a classical test widely applied to validate the performance of numerical models, examples are Fraccarollo and Toro (1995), Stelling and Duijnmeijer (2003) and Kroon (2009). Kleefsman (2005) performed the dam break test with ComFLOW and compared it with lab

experiments. In this test a closed tank was used with a cube halfway the tank with pressure sensors. Yet the test is performed again with ComFLOW for two reasons. First, Kleefsman focuses on pressures and compares only with lab experiments. In this research interest is in the ability to represent the analytical solution and occurring velocities. Secondly, the test is extended with an upward sloping channel to investigate the influence of the presence of a slope, the classical test is then needed as a basis simulation.

The dam break test is based upon the development of a simple analytical solution for instantaneous dam break of the Saint-Venant equations (1871) and method of characteristics (Stoker, 1957). The solution relies on some basic assumptions: the flow is one-dimensional, the streamline curvature is very small and the pressure distributions are hydrostatic, the flow is not affected by viscosity or bed friction, the water density is constant and the channel has fixed boundaries. In other words this solution assumes non-linear shallow water (NLSW) equations, ComFLOW on the other hand is based on the Navier-Stokes equations in which vertical acceleration is included. This will cause some deviations between the results.

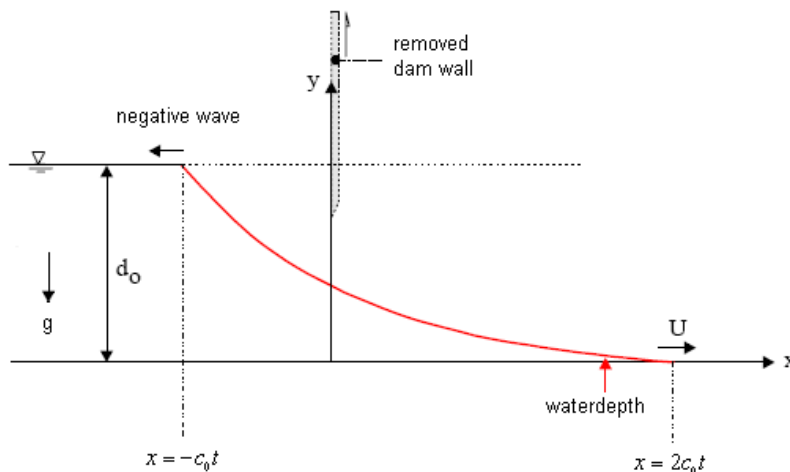


Figure 4.1: Sketch of the dam break problem in a dry, frictionless channel with zero initial velocity. Red line is solution at time t . (Chanson 2005: 24).

Analytical description

In this case a dam break on a dry, horizontal, frictionless channel is analyzed. The method to solve the wave profile was first proposed by Ritter in 1892. For an upstream water mass that is initially at rest ($h=h_0$) behind a vertical wall at $x=0$ and a downstream water level equal to zero. At $t=0$ the water mass is released and a negative wave propagates upstream and a flood wave moves downstream. The solution describes the ideal fluid flow between the position of these waves, $x=-c_0 t$ and $x=2c_0 t$ by (Stoker, 1957):

$$\begin{aligned}
 h &= \frac{1}{g} \left(\frac{2}{3} c_0 - \frac{1}{3} \frac{x}{t} \right)^2, \\
 u &= \frac{2}{3} \left(c_0 + \frac{x}{t} \right), \text{ with} \\
 c_0 &= \sqrt{gh_0}
 \end{aligned} \tag{4.1}$$

Numerical setup

The test is performed three times, with the numerical default settings (as explained in section 3.4). The domain boundaries are closed. The domain is 40 meters long en 2 meters high (see Figure 4.2). Three different grids are applied of $\Delta x = \Delta z = 0,025; 0,05; 0,1$ respectively. The initial water level is set to 1 m behind a virtual wall at $x=0$. The simulation time is set to 6 seconds. No input file for the geometry needs to be specified, therefore we deal with free-slip boundary conditions at the horizontal bed.

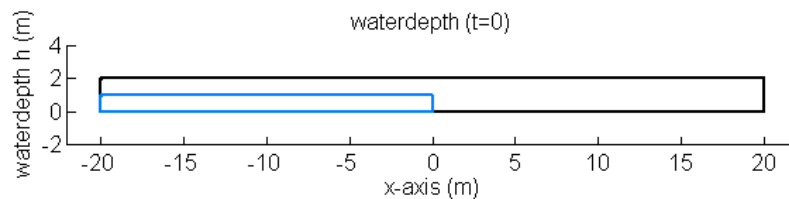


Figure 4.2: Domain setup dam break problem horizontal channel

Results and analysis

The results obtained for three different grid sizes are presented in Figure 4.3. The results for the water depth and velocity with respect to the analytical solution are shown at $t=3$ seconds. All grids give similar results and represent the analytical solution well, but the finest grid size gives the best fit. The propagating flood wave is close to the solution, observed wiggles in the velocity profile of the coarser grids are suppressed by the refinement and the velocity lag is the smallest. Therefore further analysis will focus on the results obtained on this grid.

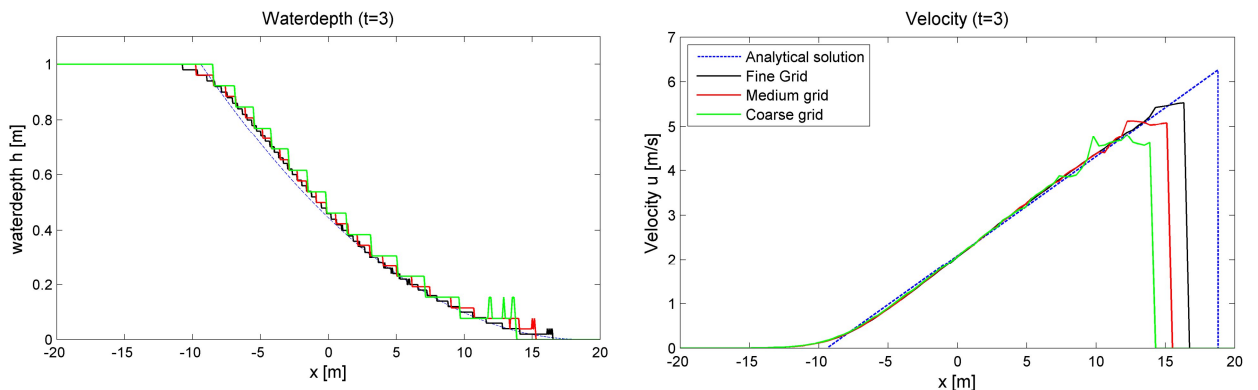


Figure 4.3: Results for the dam break problem at $t=3$ s, for three different grid sizes.

Figure 4.4 presents the results for the finest grid size, the figure shows the water depth at $t=1,2, 3,$ and 4 seconds. The four graphs show that the same agreements and disagreements with respect to the analytical solution are present during the propagation of the flood wave. The parabolic shape of the water height is well represented, and is improving during the simulation. In the analytical solution the thickness of the water layer becomes infinitely small in the leading edge of the wave, this is hard to represent in a numerical model. The leading edge indeed lags behind in the numerical results, but no artificial bore is created as in many other numerical schemes.

For the negative wave front the transition is smoother than in the analytical solution. This is created in the first half of a second and is caused by numerical dissipation. The effect of dissipation is that sharp gradients, discontinuities in the solution are smeared out. This is caused by the fact that the higher frequency components being damped more than lower frequency components.

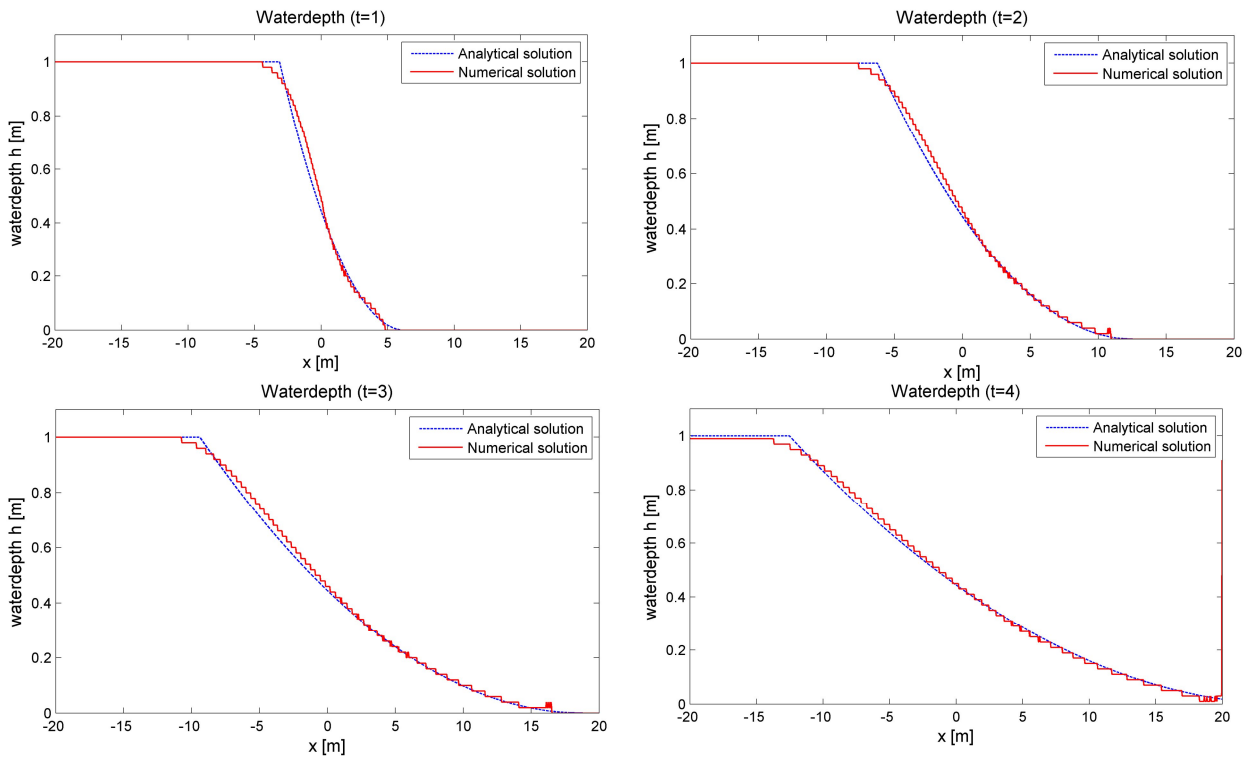
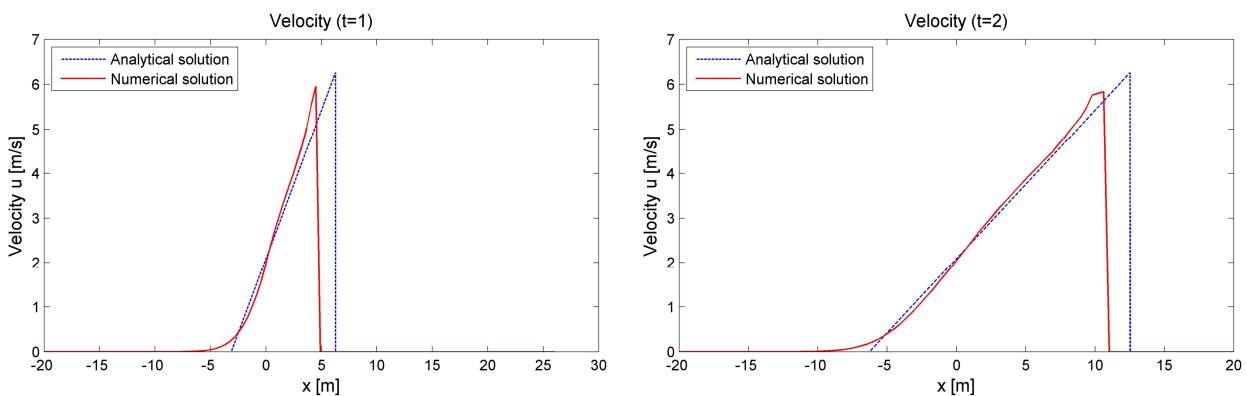


Figure 4.4: Results for the dam break problem at $t=1, 2, 3$ and $t=4$ s, showing water depths solved on a fine grid.

In Figure 4.5 the graphs represent the velocity in the x-domain. The velocities are represented quite well by the numerical model. Nevertheless a velocity lag in space and in speed is apparent, which is growing during the simulation. Part of this problem lies in the fact that the analytical solution is based on NLSW equations (pressure is assumed hydrostatic), whereas ComFLOW solves the Navier-Stokes equations including vertical accelerations. Therefore, the analytical solution is actually not valid for the initial stage of the simulation. In this phase the numerical scheme develops a lag in the propagation of the leading edge of the wave, but this lag should not increase in time.



Results for the dam break problem at $t=1$ and 2 s showing velocities solved on a fine grid. ($t=3$ and 4 s on next page)

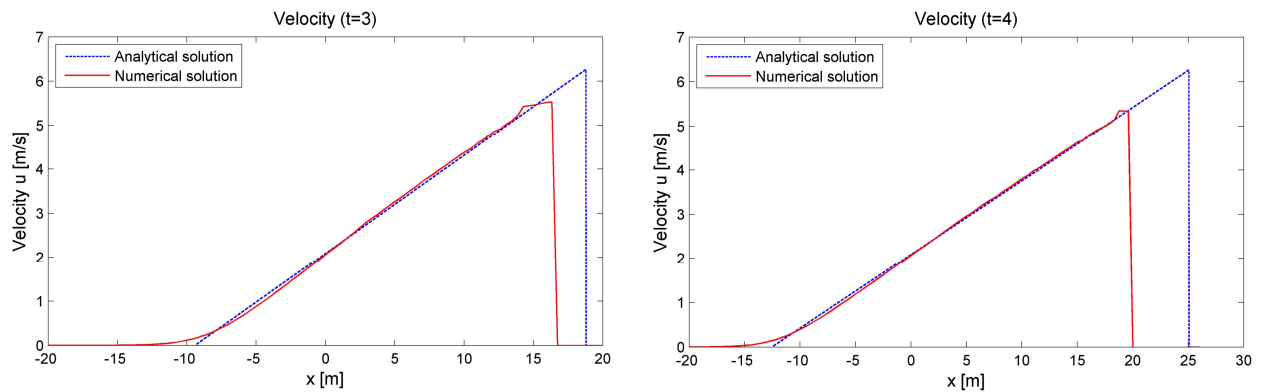


Figure 4.5: Results for the dam break problem at $t=1, 2, 3$ and 4 s, showing velocities solved on a fine grid.

However, from Figure 4.5 it is apparent that the wave front is lagging further behind. Secondly, according to the analytical solution the maximum velocity of $2 \cdot c_0$ is constant in time, but the maximum velocity in the simulation decreases. This indicates that some kind of resistance is encountered in the model. Figure 4.6 shows that this resistance is (probably) not created by free-slip boundary conditions at the domain boundary. Observed is a hydrostatic pressure distribution, a fairly straight velocity profile and no boundary layers are formed at the bottom, indicating that there is hardly friction between wall and fluid. Part of the answer may be found in the artificial viscosity, this will be discussed in section 5.5.1, this leads to an increase of the viscosity at higher speeds, in combination with the imposed boundary conditions this can lead to deceleration of the leading edge of the wave. As for a larger grid size the artificial viscosity increases, the worse performance for the coarser grids may also partly be explained by this influence.

Secondly the wetting and drying algorithm can have a contribution to this deceleration. Before empty cells (E) become fluid cells (F) or surface cells (S) the velocities should be calculated, this is done with a combination of linear extrapolation and mass conservation, see section 3.2.5. In the numerical model of ComFLOW the following restriction applies. If two adjacent cells are considered, the first cell contains some fluid and it a surface cells, the adjacent second cell contains no fluid which makes it an empty cell. The first cell has to be filled completely before it can transmit fluid to its neighbouring cell. This restriction decelerates the flooding process for high speeds. This influence is less with a smaller mesh size.

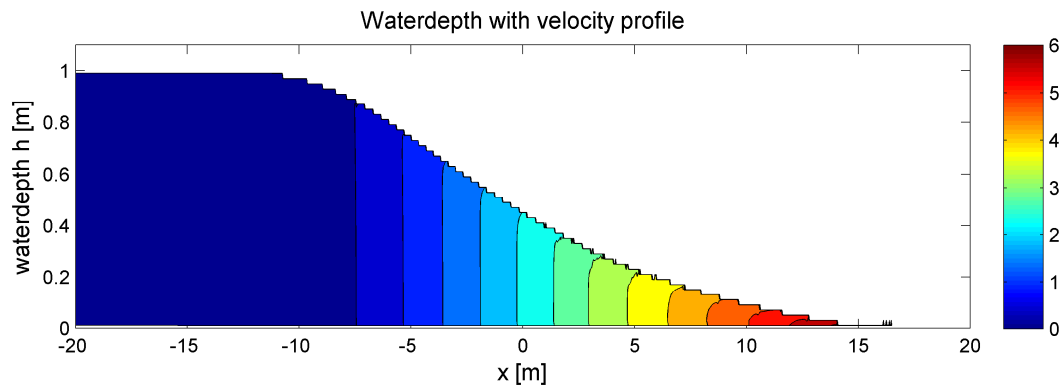


Figure 4.6: Result for dam break test at $t=3$ s showing velocity profile over the water depth.

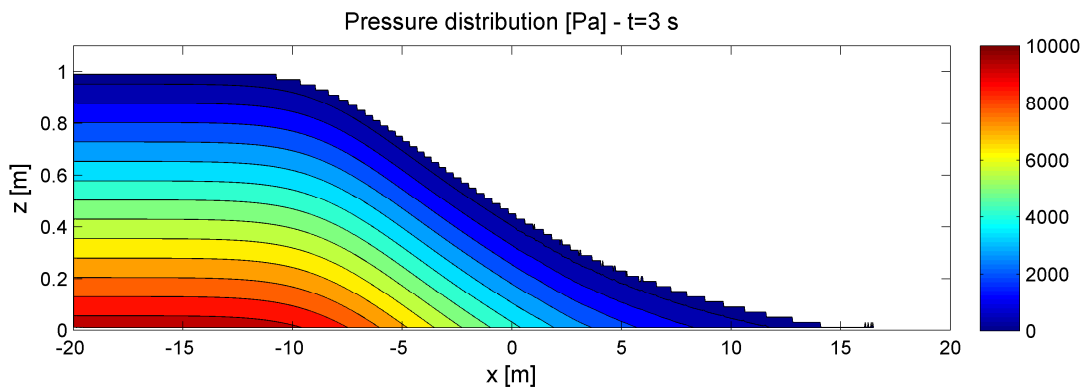


Figure 4.7: Result for dam break test at $t=3s$ showing pressures over the water depth.

Above it was stated that the analytical solution is not valid for the early stages of the dam breaking, due to vertical acceleration the NLSW equations would not be appropriate to describe the processes. For $t=3$ seconds it is shown, in Figure 4.7, that the pressure distribution is hydrostatic.

If the above stated is true the pressure should be non-hydrostatic in the beginning of the simulation. In Figure 4.8 the pressure at $t=0.5$ and $t=1$ s are shown, observed is that the pressures at $t=0.5$ second are indeed non-hydrostatic, between $x=0$ and $x=1$ m. For $t=1$ second the pressures are nearly hydrostatic. These figures show that the analytical solution is indeed not valid for the early stages of the test and that this statement is correct. If one is aware of this problem, the test is still very suitable to investigate the performance of the numerical model.

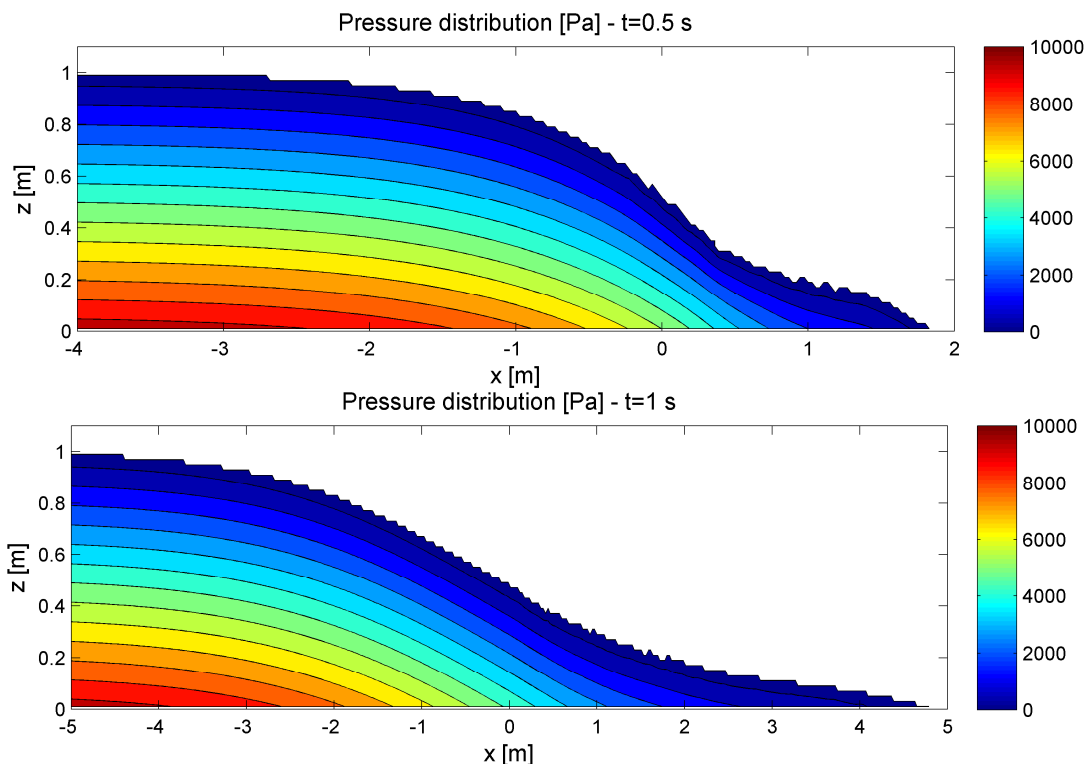


Figure 4.8: Pressure distribution for the dam break test at $t=0.5s$ in the upper figure and $t=1.0s$ in the lower figure.

4.1.2 Sloping channel, dry bed

An extended solution of the ideal flow solutions of the dam break problem is described by Chanson (2005). He presents the solution of the dam break problem for an upward sloping channel. However his solution is limited to the development of the initial stage of the dam breaking and to small bed slope angles. The initial conditions used by Chanson are based on real life basins behind a dam on a sloped channel, which severely complicated the solution mathematically.

In this research, focus is on the propagation of the wave front on a slope, occurring velocities and maximum run-up. Personal communication with R.J. Laheur led to the decision to rewrite the solution to a dam break test on a sloping bottom, which can be applied for all slopes and time periods. This solution is obtained by rotating the initial conditions of the classic test, as described in section 4.1.1, by the slope angle and solving this with the method of characteristics. The problem is sketched in Figure 4.9, which reveals that the problem is basically the same as the previous problem, but with an extra gravitational acceleration in the horizontal plane and a decreased gravitational acceleration in the vertical plane. A more extensive explanation can be found in appendix A.

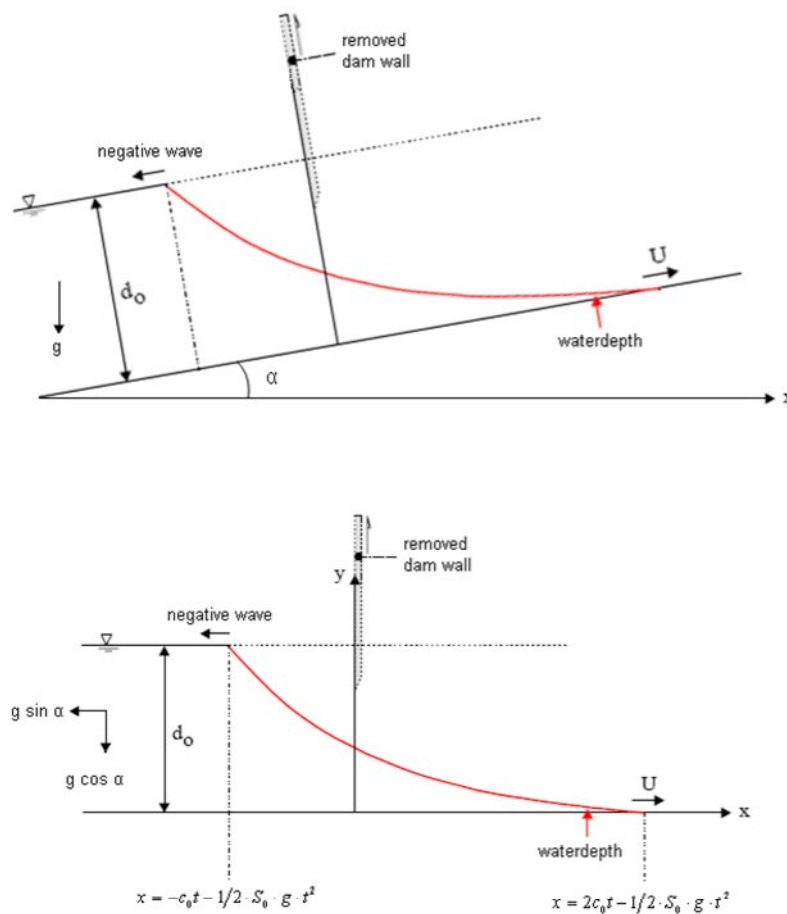


Figure 4.9: Sketch of the dam break problem in a dry, frictionless, sloping upward channel with zero initial velocity.

Analytical description

The solution represents a dam break in a dry, frictionless, upward sloping channel bed with zero initial velocity, in a prismatic wide rectangular channel. The solution for a sloping channel gives different solutions for the propagating waves as the velocity will decrease in time by gravitational force. The solution between the negative propagating wave, $x = -c_0 t - 1/2 \cdot S_0 \cdot g \cdot t^2$ and the leading edge of the wave, $x = 2c_0 t - 1/2 \cdot S_0 \cdot g \cdot t^2$, is described by:

$$\begin{aligned}
 u &= \frac{2}{3} \left(c_0 - S_0 \cdot g \cdot t + \frac{x}{t} \right), \\
 h &= \frac{1}{g'} \left(\frac{2}{3} - \frac{1}{6} S_0 \cdot g \cdot t - \frac{1}{3} \frac{x}{t} \right)^2, \text{ with} \\
 c_0 &= \sqrt{g' h_0} \\
 g' &= g \cdot \cos \alpha \\
 S_0 &= \sin \alpha
 \end{aligned}
 \tag{4.2}$$

In which, α is the angle between the bed and the horizontal plane and $\alpha > 0$ for an upward slope. For an upward slope, the maximum elevation reached by the wave front is $z_{\max} = 2 \cdot h_0$ at $x = 2/\tan \alpha$, for $t = 2 c_0/g \cdot S_0$, this result is independent of the bed slope.

Numerical setup

This test is performed with the numerical default settings and the simulation time again 6 seconds. Five different bed slopes are applied; 1,2, 5, 10 and 15 degrees. Note that a slope of 10 degrees is in the same order as a slope of 1:6 and that 15 degrees is in the order of 1:4, which will be used during the run-up simulations. The simulations are performed in two main differenced ways: one with an actual sloping channel and one with a horizontal channel with rotated g-forces (see for theoretical description section 3.1.2 and equation 3.2). The simulations are in fact graphically shown in the lower sketch of Figure 4.9 and the set-up of the domains in the numerical model are shown in Figure 4.10.

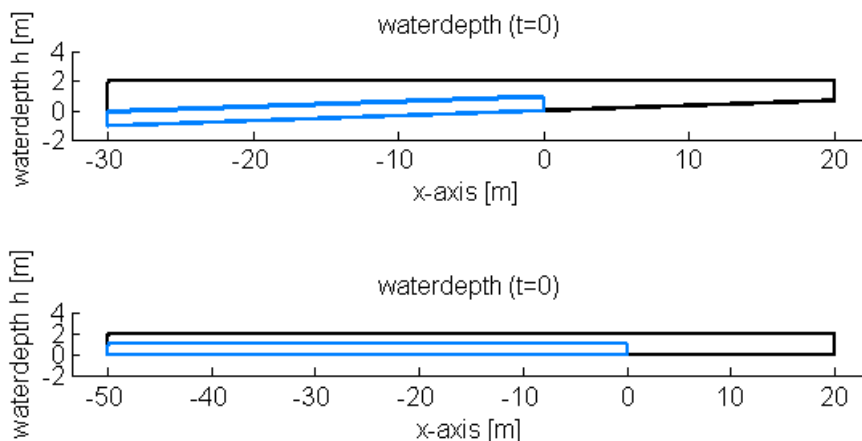


Figure 4.10: Domain setup dam break test for sloping bed channel. Top with defined geometry, down with rotated g-force.

Simulation with bed slopes of 1,2 and 5 are performed with a sloping channel and a defined geometry in ComFLOW. Two different values of integration points (nrinp 4 and 8) are used, see section 3.4.

For all slopes the simulation is performed with a horizontal channel with a rotated g-force. This results in simulations with a free-slip boundary condition at the bottom. At last two simulations were performed with the horizontal channel and rotated g-force, but with a defined cube on the bottom of the domain. This cube imposes a no-slip boundary condition at the bottom. In table 4.1 an overview is given of the 13 performed simulations.

Table 4.1: Overview of simulations dam break test with an upward sloping channel

Slope	Rotated Channel Nrinp 4	Rotated Channel Nrinp 8	Rotated g-force 'free-slip'	Rotated g-force 'no-slip'
1	√	√	√	-
2	√	√	√	-
5	√	√	√	√
10	-	-	√	√
15	-	-	√	-

√ = simulation performed, - = not performed

In all 13 simulations for the analytical solution with a sloping channel a natural effect caused by the gravitational forces could influence the results. Water will not only travel in positive x-direction, as in section 4.1.1, but under influence of gravity the water mass will also start flow in opposite direction. With the closed domain boundaries a sort of tank is created in the model. The water will flow against the left wall and leading to an accumulation of water, as showed in Figure 4.11. This process should not influence the results, therefore the domain is enlarged in the x-direction to -50 m and just as in the previous simulations only the results till -20 m are analyzed.

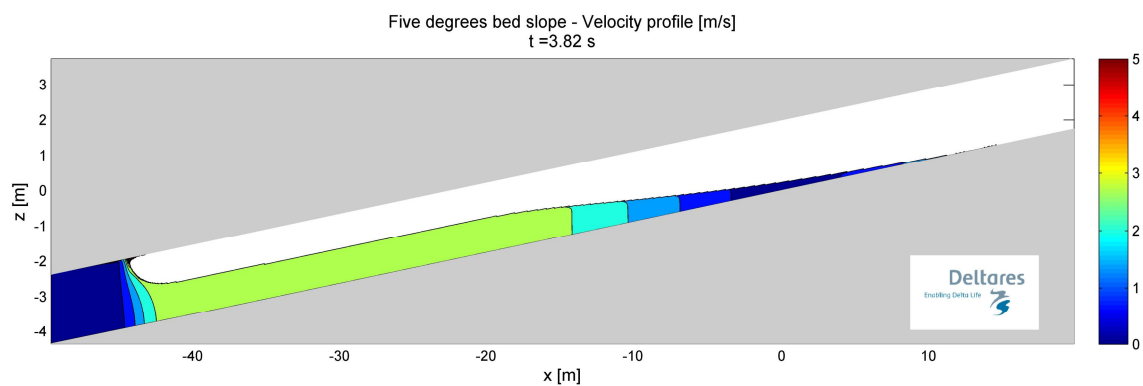


Figure 4.11: Results for the five degree bed slope at $t=3.82s$ illustrating the water accumulation at the left domain boundary.

The mesh size was set on $\Delta x = \Delta z = 0.03$. It turned out that ComFLOW has a limited number of grid cells, therefore it was not possible to have the same grid size for all simulations. The problem lies in the fact that the domain height increases with the increase of slope steepness, this leads to a situation where more grid cells are needed to obtain the same grid size. The problem caused the grid size for the 5 degrees bed slope with a geometry to be coarser, the smallest possible grid size is $\Delta x = \Delta z = 0.04$. This problem is the reason that the slopes of 10 and 15 degrees are only performed with the rotated g-force setting. With these even steeper slopes the grid would end up too coarse to make a good comparison between the results of the two methods.

Results and analysis

Figure 4.12 shows the results of the dam break test with a sloped channel giving the location of the propagating flood wave as a function of time. It illustrates that the leading edge is represented quite well. It is somewhat behind the analytical solution and is lagging behind further in time, giving the same image as in the previous section. The graphs show that increasing the number of integration points indeed improves the results of the wave propagation, the use of eight points leads to less deceleration. However this improvement is far less significant than for the rotated g-force, the simulations with the rotated g-force are less dissipative than the ones with the geometry. The computed location of leading edge of the wave is much closer to the analytical solution and the wave front is less decelerated in time.

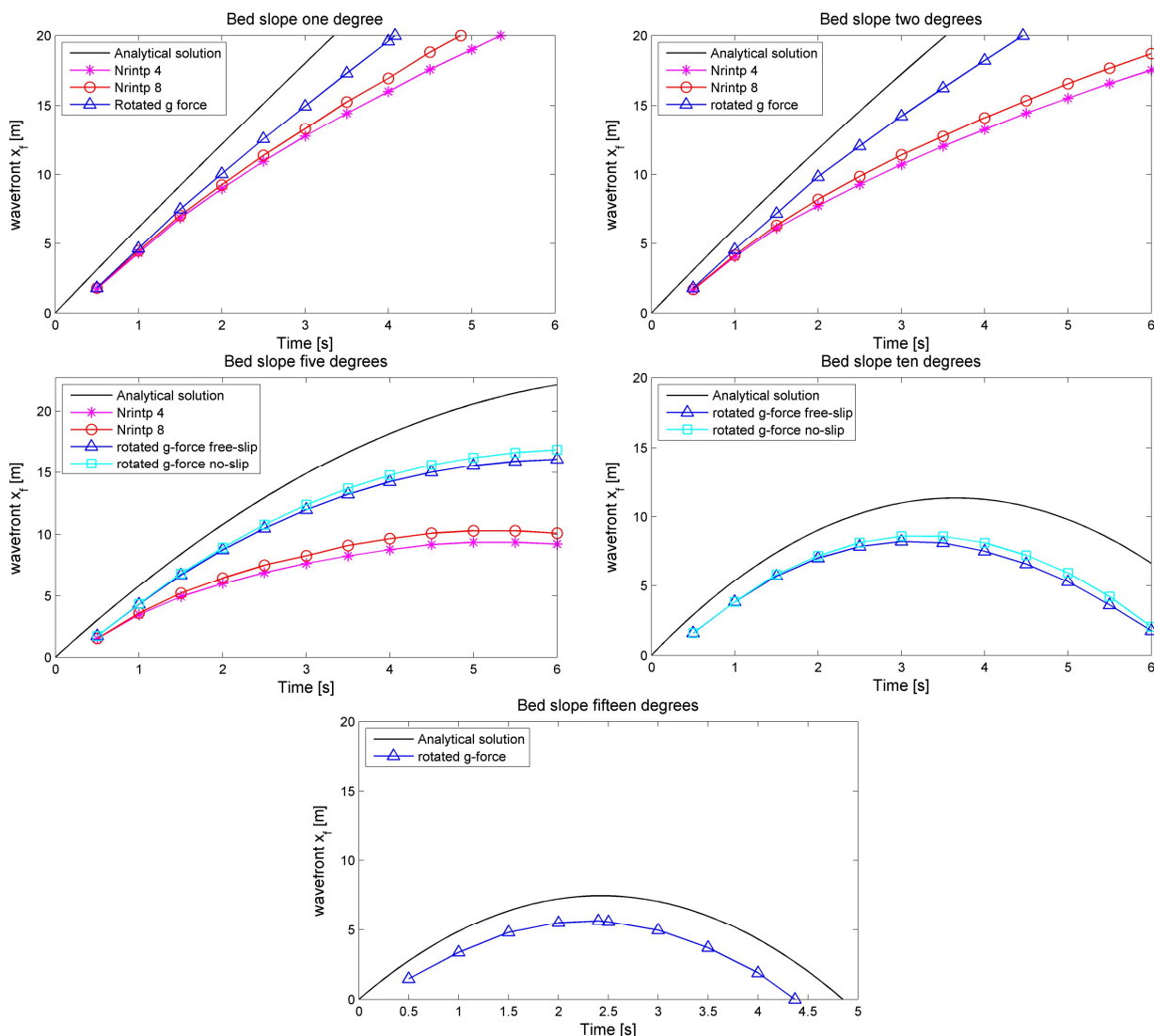


Figure 4.12: Results dam break problem showing the wave front as a function of time for all bed slopes and simulations.

For the ten and fifteen degrees bed slope, which are conform the slope angles of 1:6 and 1:4, the maximum run-up of the flood wave is only slightly underestimated for the rotated simulations. One should keep in mind that the underestimation is also partly caused due to the fact that the thickness of the water layer at the front becomes infinitely small in the analytical solution, this is not represented in the numerical model. Therefore in terms of run-up we can say that the model

performs very well for the simulation with the rotated g-force. Remarkable is that the down-rush is at the same speed as the analytical solution and that it seems that the maximum run-up is better approached for steeper slopes. The results on the sloped bottoms for the 1, 2 and 5 degree show the opposite process, gentler slopes give better results. For the five degrees bed slope it must be noted that, as already mentioned, the simulations with nrintp=4 and 8 are on a coarser grid. Therefore it is expected that a grid size of 0.03 m should have improved the results and that the difference between the results should have been smaller.

Two significant differences between the simulations with rotated g-force and the sloping bed channel can be distinguished. First the free-slip at the horizontal bed and the no-slip boundary condition at the geometry body. Apparent from the simulations with no-slip boundary condition at the bottom for the rotated g-force, for five and ten degrees, is that the results of these simulations are quite similar to the ones with the free-slip boundary conditions. Second difference is the totally smooth bottom at the horizontal bed and that the discretization of the defined geometry for the sloping bed is not completely smooth, the geometry is handled in a 'staircase way'. This discretization of the geometry is the main cause of the deceleration of the wave front and it is creating a sort of numerical roughness at the slope.

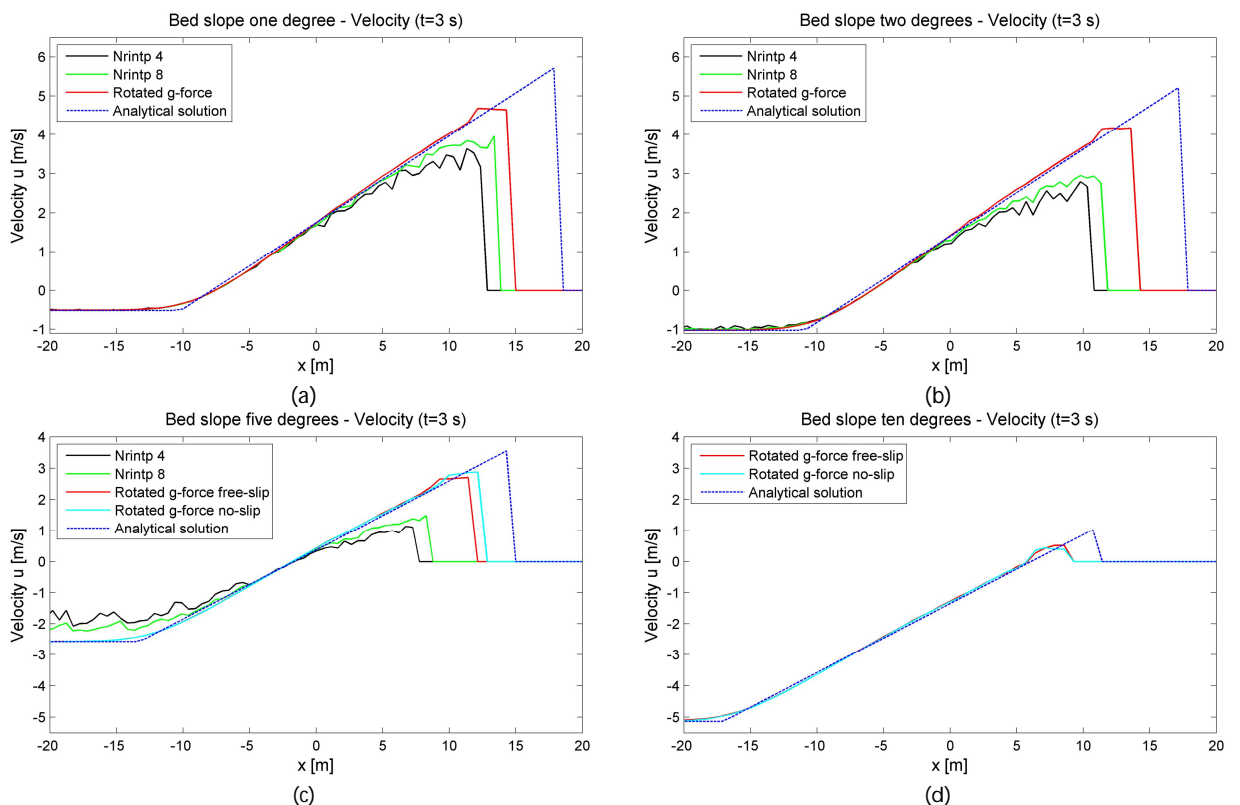


Figure 4.13: Results for dam break problem with sloped channel showing velocities as a function of x at $t=3$ s for slope 1 (a), 2 (b), 5 (c) and 10 (d) degrees and for different model settings.

The results for the velocities at $t=3$ are showed in Figure 4.13. The velocities are simulated quite well for the simulations with a rotated g-force, the results for a sloped bottom are less and more wiggly. A velocity lag is observed, this lag is smaller for the simulations with rotated g-force. The analysis of the velocities is in agreement with the analysis of the leading edge of the wave. Figure 4.14 (a) shows that the wiggles in the velocities of the simulations with sloped bottom are caused by the fact that the defined geometry is causing the development of boundary layers. In

the velocity profiles of simulations with the rotated g-force, for both free-slip and no-slip conditions this forming is not present at all. This observation is in agreement with the earlier statement that the discretization of a sloped geometry leads to friction between fluid and the solid geometry.

The velocities of the water flowing in opposite direction (Figure 4.11) are simulated well. These are the negative velocity values in Figure 4.13 for $x < 0$. For the steeper slopes (Figure 4.13c) the simulations with the sloped geometry (nrinp 4 & 8) the velocities are too low compared to the analytical solution. This is caused by the influence of the numerical roughness. In Figure 4.14a small boundary layers are formed in the water mass that is running down the slope, for example around $x = -10$ m.

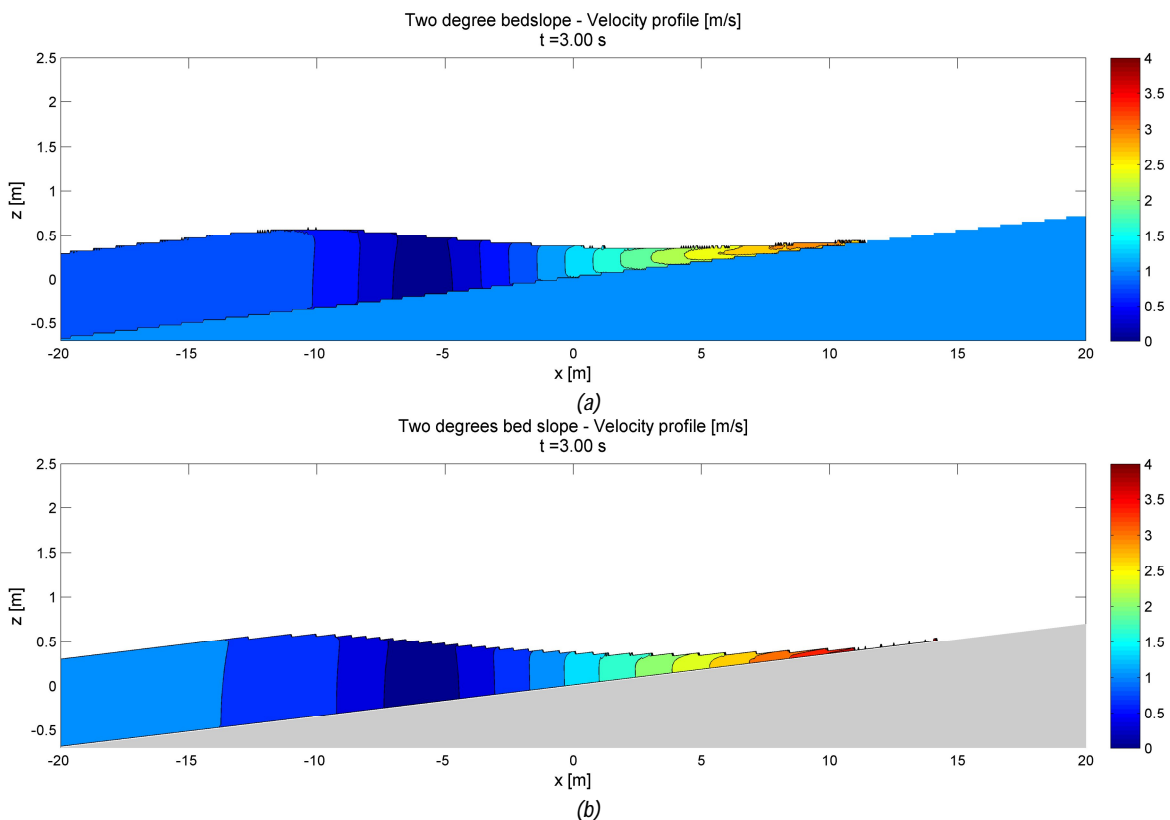


Figure 4.14: Velocity profiles on a slope of two degrees for $t = 3s$, a: results for nrinp 8 and b: results for rotated g-force.

During the analysis of the simulation it was found that ripples arise on the propagating wave, as shown in Figure 4.15. These ripples occur in all simulations. This type of problem occurs more often in numerical simulations with flooding of cells at high speed. In the dam break test performed by Kleefsman in 3d mode also ripples arose during the simulation. She concluded that these ripples are probably caused by post-processing. It was advised (Kleefsman et al., 2005) to use a piece-wise linear reconstruction of the free surface, instead of the reconstruction aligned with the coordinate axes as used in ComFLOW, this is a constant reconstruction of the free surface. These ripples do not seem to affect the results, so they are not considered as a problem.

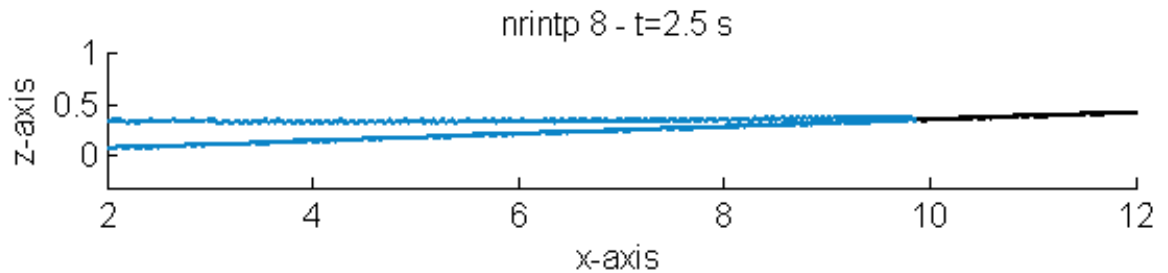


Figure 4.15: The forming of ripples on propagating flood wave, results for a bed slope of two degrees.

4.2 Waves on a sloping beach

Numerous times numerical models have been compared with the analytical solution of standing waves on a slope given by Carrier and Greenspan (1958), amongst others by Stelling and Zijlema (2008) and van Gent (1995).

Carrier and Greenspan show in their paper that waves can climb a sloping beach without breaking. In this classical test a sinusoidal wave runs up and down a frictionless, sloping beach without breaking. The test is particularly suited to verify the accuracy and quality of the calculated shoreline movement, during up-rush and down-rush. Maximum run-up and run-down and also the correct representation of the location of nodes of the standing wave can be checked.

Analytical description

Carrier and Greenspan derive their conclusions by using dimensionless quantities, and writing the solution in terms of the independent variables λ and σ .

$$\begin{aligned}\lambda &= 2(v+t) \\ \sigma &= 4c\end{aligned}\tag{4.3}$$

Where v , t and c are respectively the dimensionless velocity, time and propagation speed. The velocity, water surface elevation distance and time with respect to these variables are then written as:

$$\begin{aligned}v &= \sigma^{-1} \phi_{\sigma}(\sigma, \lambda), \\ x &= \frac{\phi_{\lambda}}{4} - \frac{\sigma^2}{16} - \frac{v^2}{2}, \\ \eta &= \frac{\phi_{\lambda}}{4} - \frac{v^2}{2}, \\ t &= \frac{\lambda}{2} - v, \text{ with} \\ \phi &= AJ_0(\sigma) \cos(\lambda).\end{aligned}\tag{4.4}$$

Where J_0 is the Bessel function of the first kind. This short analytical description is extracted from Kroon (2009). From the analytical solution a relation between the amplitude of sinusoidal incident waves (η_{in}) and the vertical amplitude at the shoreline (A_s) can be derived (van Gent, 1995):

$$A_s = \eta_{in} \cdot \pi / \sqrt{(sT / 8 \cdot \sqrt{(g / h_0)})}$$

Breaking at the slope does not occur if :

$$A_s \leq 1 / (4 \cdot \pi^2) \cdot g \cdot T^2 \cdot s^2,$$

$$\eta_{in} = 1 / (\sqrt{128} \cdot \pi^3) \cdot s^{2.5} \cdot T^{2.5} \cdot g^{1.25} \cdot h_0^{-0.25}$$

Numerical setup

The parameters used in this study are the same as those used by van Gent (1995). He took for comparison with numerical model results an incident wave with amplitude equal to the maximum amplitude without occurrence of breaking waves. For a slope 1:4, a wave period of 5.0 s and a still water level of $h_0 = 2.0$ m at the toe of the slope is used giving an incident wave height of 0.15m.

The simulation is done on two grids, with a mesh size of $\Delta x = \Delta z = 0.025$ m and a refined grid with $\Delta z = \Delta x = 0.015$ m. At the left in- and outflow boundary the generating and absorbing boundary condition (GABC) has been used, see also section 3.3.2. For the discretization of the geometry 8 integration points of integration are used. Use is made of linear wave theory and Airy waves are used to prescribe the incoming waves. Again the numerical default settings are used.

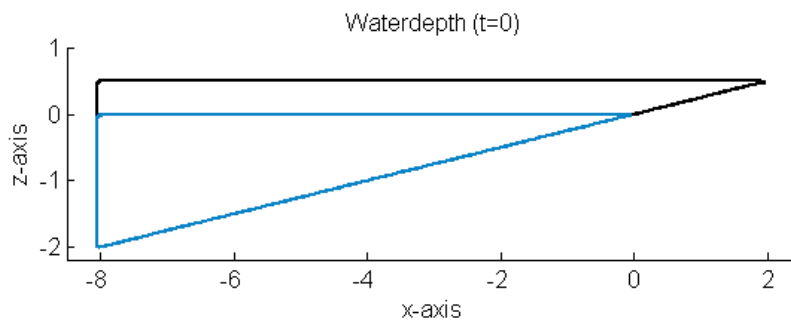


Figure 4.16: Domain setup Carrier Greenspan, slope 1:4, still water level 2,0 m.

Results and analysis

It must be emphasized that the chosen parameters are near the breaking criterion, this is one of the most difficult choices of parameters for a model to represent the Carrier Greenspan test. Keeping this in mind we can evaluate the results of the model rather good. The results of the medium and the fine grid are similar, maximum run-up and down values are equal. The finest grid is shown in the figures, only because the representation is smoother. The results during up-rush and down-rush are analyzed separately.

The numerical results obtained with the finest grid during up-rush are presented in Figure 4.17. The model is quite well able to represent the location of the node of a standing wave, although the node is more concentrated in one point compared to the analytical solution the position on x-axis is the same.

The wave shape is represented moderate, although the profiles of the extreme values are represented well. For intermediate time steps the wave shape, especially behind the node, is rather different. Friction at the slope deforms the wave profile and small bores are formed. Another possible factor of influence is the hydrostatic character of the analytical solution. ComFLOW includes non-hydrostatic components and this could cause the wave to form into a different shape. However as this is mostly dependent on the ratio of wavelength and water depth the influence should not be too large.

Analyzing the results for the vertical amplitude at shoreline it can be seen that the maximum run-up and run-down values of the analytical solution are represented well by the numerical results. Although in Figure 4.17 the lowest water level is still somewhat behind, in the intermediate period

the maximum run-down value is reached. Observed is that the amplitude at the shoreline is behind the analytical solution for the lower water levels at the shoreline, but the numerical results catches up and the amplitude at the shoreline is at the same location as the analytical solution during the remaining up-rush, despite the different wave shape.

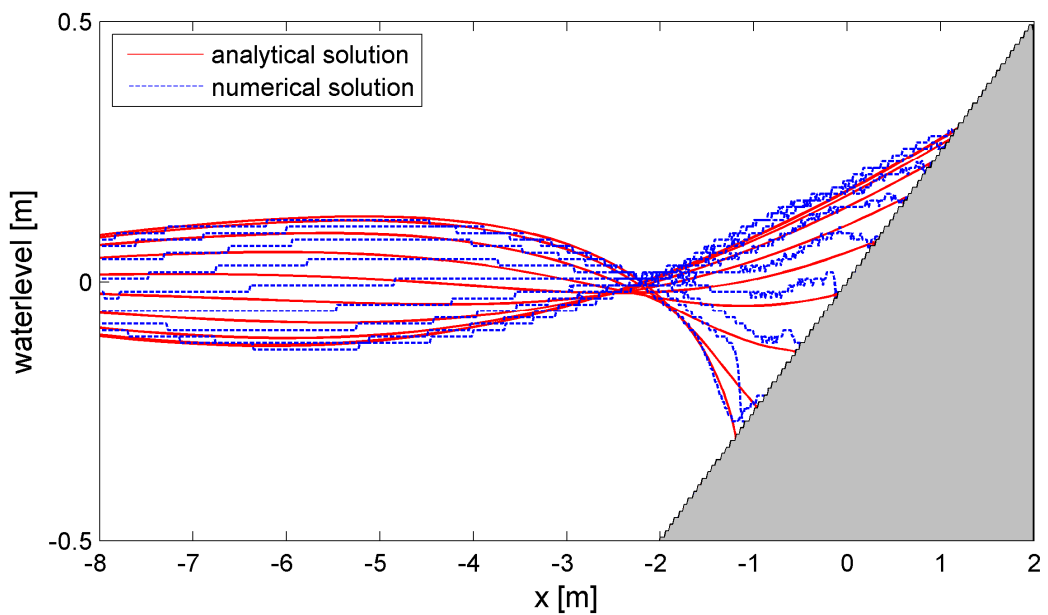


Figure 4.17: The analytical water level compared to the numerical water level for the Carrier and Greenspan test during up-rush.

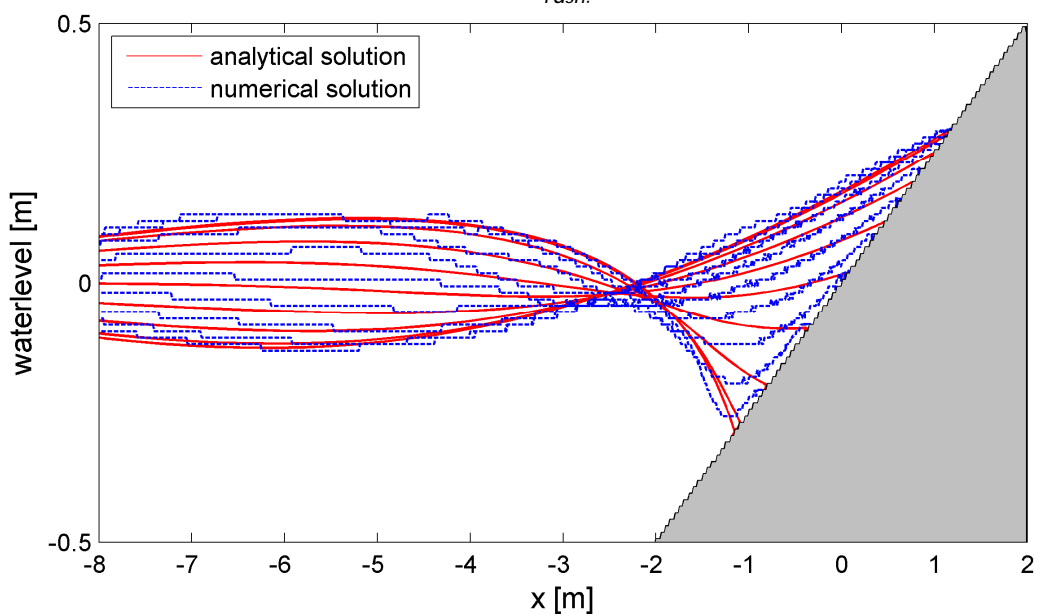


Figure 4.18: The analytical water level compared to the numerical water level for the Carrier and Greenspan test during down-rush.

In Figure 4.18 the numerical results compared to the analytical solution during down-rush are presented. The location of the node is again in the correct place. The node is less clustered and at some points the water levels are too low compared to the analytical solution.

The wave shape behind the node is again represented rather different from the analytical solution. During down-rush the water is sticking to the slope, causing the vertical amplitude to fall behind the analytical solution. As already stated for up-rush the maximum run-up and down is represented quite well by the numerical solution, as can be seen in the next Figure.

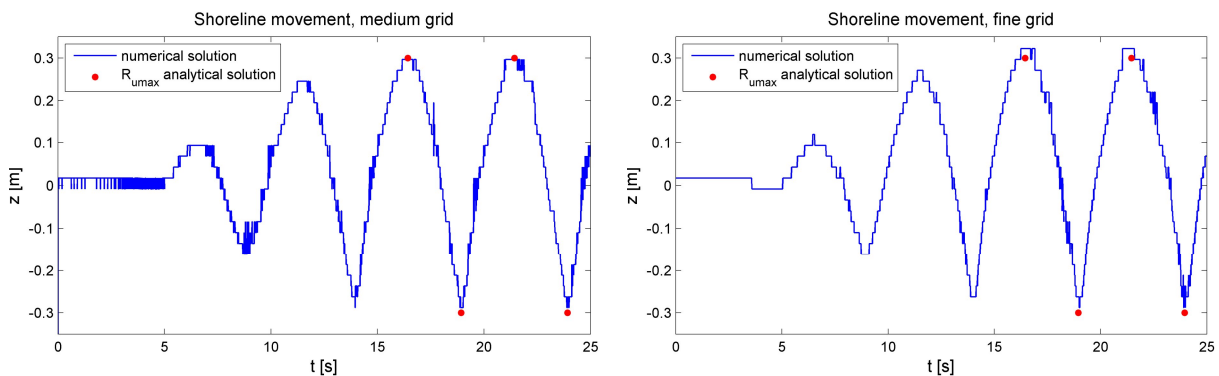


Figure 4.19: Numerical results of shoreline movement and maximum run-up value for analytical solution. Left: results medium grid, right: results fine grid.

During the simulation on the fine grid we encountered a small form of, the so called flotsam and jetsam, the accumulation of unphysical small scale fluid bodies. Forming of this droplets does not influence the results and are this is extensively discussed chapter 5, section 5.4.

4.3 Discussion and concluding remarks

The goal of this chapter was to investigate whether different mathematical aspects for relevant processes are solved well by the numerical system. To that end to simulation results are compared with analytical solutions known from literature. Three test cases are used, the classical dam break test with a horizontal bed, the dam break test with an upward sloping bed and periodic non-breaking waves on a sloping beach formulated by Carrier and Greenspan.

Most important finding in this chapter is the large influence of discretization of the geometry in both tests where a geometry is present. The 'staircase' way of the discretization is creating a numerical roughness at solid (sloped) structures in the model. This numerical roughness is possibly of negative influence for the run-up and run-down results in the next chapter, as this will cause a decrease in velocities, deceleration of up-rush and down-rush of waves. Further findings are split between the test cases.

Dam break test

Horizontal channel test

- The analysis of the dam break test on a horizontal slope, showed that in this test the leading edge of the wave was decelerated in time, in spite of the fact in this test no sloped, solid geometry was present. Two causes were identified: artificial viscosity and a restriction in the algorithm of the flooding of dry cells.

Sloping channel test

- The smoother geometry, with a number of integration point of eight, shows improvement compared to the use of four integration points, but the results for both simulations show much more dissipation than the simulations with a rotated g-force on a horizontal bed.

- During the dam break test with a sloping channel the no-slip and free-slip boundary conditions gave similar results. Implying that the no-slip boundary condition at the boundary of defined structures in ComFLOW is not causing the numerical roughness.
- For the dam break test with rotated g-force simulations, where no influence of the discretization is present, the maximum run-up heights are represented well. Some small underestimation is observed, but the analytical solution becomes infinitely small in this area and that is difficult to represent in the numerical solution.
- Results on maximum run-up are better for the steeper slopes for the simulations with the rotated g-force on a horizontal bed. The results with the sloped bottom and with the roughness present show a opposite image, for the steeper slopes more dissipation is observed, causing more deceleration of the leading edge of the wave and less maximum run-up.
- It was stated that the analytical solution becomes infinitely small in the area of the leading edge of the wave and that is difficult to represent in the numerical solution. Visually it was observed that no bores were formed in the numerical results, but more detailed investigation on the relation of mesh size and layer thickness in the wave front could be a contribution to the study of wave run-up.

Carrier and Greenspan

- In the test of Carrier and Greenspan the location of the node of the standing wave is represented well, which suggests that wave energy is correctly reflected at the structure. This should lead to good results on calculation of the reflection coefficients.
- The effect of the numerical roughness at the slope is clearly visible in the results of this test case. Clearly is the sticking to the slope during the down-rush of the wave, making the water levels at the slope fall behind the analytical solution. During up-rush this lag in water level is not present, but the wave shape is clearly deformed, resulting in the forming of small bores.
- Interesting enough the extreme values of the vertical amplitude are reached by the numerical model, so this is promising for run-up and run-down results of the simulations with regular waves.
- In their paper Carrier and Greenspan also give the solution for occurring velocities. In the analysis of the results the velocities were not included. It could be rewarding to study the velocities in more detail in future research, as this could give more insights in the differences and resemblances that occur during the run-up simulations.

5

Run-up simulations with regular waves

To test the performance of ComFLOW for wave run-up, simulations with regular waves are executed. Regular waves should, as known from physical experiments, give the same run-up height for each incoming wave. These simulations are compared with data from physical experiments.

In the first part of this chapter a description of the model setup is given and the simulation setup will be presented; the wave conditions that are used and which output is generated. Hereafter the results of the simulations are analysed and discussed. The results are analysed on general qualitative performance and for the wave processes for regular waves presented in section 2.2. This are wave run-up, wave run-down, and reflection. At last a discussion on artificial viscosity, robustness, sensitivity of the monitoring lines and CPU time is given.

5.1 Numerical setup

In this section the numerical setup of the model is discussed. The domain width and height, the defined geometries, the boundary conditions and the grid sizes used. In all simulations the numerical default settings are used, as discussed in section 3.4.

5.1.1 Domain, geometry and boundary conditions

The simulations are done in 2DV, which means a horizontal x-direction and a vertical z-direction. The y-direction does not influence the results and is not considered. This type of domain can be regarded as a numerical wave flume, dimensions are also based on physical model tests in a wave flume. Table 5.1 gives the coordinates of the domain. It is important to choose the coordinates suitably; maximum water level should not reach the (upper) boundaries of the computational domain, which would lead to unrealistic and unwanted reflections. On the other hand a too large domain will lead to unnecessary long computational time. The chosen domain height is therefore based on the maximum used wave height and the maximum calculated run-up height.

Table 5.1: Coordinates of the computational domain for regular waves

	Min value [m]	Max value [m]	Length [m]
x-direction	0	23.4	23.4
z-direction	-0.7	0.7	1.4

Three different geometries are used in the computations, dikes with a uniform slope of 1:6, 1:4 and 1:3 respectively. These slopes are typical for dikes in the Netherlands. To keep the computational conditions equal for all simulations, the same domain is used. For all geometries the toe of the dike is situated at the same point ($x=15\text{m}$) from the boundary, this distance is twice the wave length of the longest wave length used in the simulations. The offshore water depth is 0.7m. The choice for these variables (including wave conditions which will be discussed in section 3.2.1) is

based on physical experiment conditions, mainly on the experiments of Schüttrumpf (2001). In the next figure the three domain setups are shown.

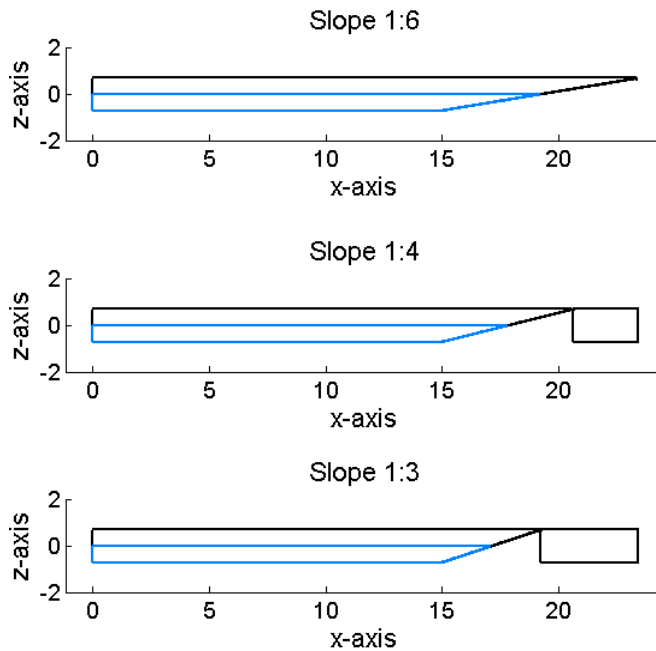


Figure 5.1: Domain setup for three different geometries: slope 1:6, 1:4 and 1:3

At the right domain boundary a defined geometry is present, here a no-slip boundary condition holds, at the bottom of the domain a free-slip condition. Use is made of the GABC boundary condition as default setting, in Table 5.3 the values for kh are presented for each wave condition.

5.1.2 Grid size

For the simulations three different grids sizes are used, coarse, medium and fine. Grid refinement is done with a factor 2 and these grids are based on the number of horizontal grid cells per wave length and vertical grid cells per wave height as based on Wenneker (2010):

- The number of horizontal grid cells per wave length is taken roughly 85 for a coarse grid, 170 for a medium and 340 for a fine grid.
- The number of vertical grid cells per wave height is taken roughly 2-3 for coarse, 4-6 for medium and 7-12 for a fine grid.

The grid sizes are presented in Table 5.2, where the number of grid cells in different directions is indicated by N .

Table 5.2: Gridsises regular wave simulations

	N_x	N_z	N_{total}	Δx [m]	Δz [m]
Coarse	330	36	11880	0.07	0.04
Medium	670	40	26800	0.035	0.035
Fine	1300	78	101400	0.018	0.018
Fine extra	1300	120	156000	0.018	0.012

The grid cell sizes in the horizontal and vertical direction (indicated by Δx and Δz) are taken equal for the medium and fine grid. This is done because hydrodynamics in horizontal and vertical length scales have about the same magnitude.

For some of the used waves heights this grid sizes did not meet the proposed number of grid cells and grid refinement in vertical direction was applied. For the coarse grid this refinement is done for all simulations, because most wave heights were otherwise around the same size as the grid cell height and performance was expected to be poor.

The same holds for the two lowest wave heights (0.04 and 0.06 m, see table 5.3) on the fine grid, and the 'fine extra' grid was introduced for all simulations with these two waves. For these waves the fine grid did not reach the 4-6 grid cells per wave height and results of (test) simulations were poor.

5.2 Simulation setup

This section gives an overview of the performed simulations. All simulations start with water at rest and waves start to develop and entering the domain at the beginning of the simulation. It takes about 5 seconds for the waves to reach the given wave height and 10 to 15 seconds to reach the toe of the dike. The simulation period is set to 35 seconds, to make sure enough waves reach the slope and to obtain a regular wave signal.

5.2.1 Wave conditions

All geometries are exposed to six wave conditions, chosen in line with the guidelines for the number of grid cells per wave length and height. The waves are non-breaking (Miche-criterion), and satisfy the ratio $h/H > 3.0$, where flow characteristics are assumed unaffected from the depth. Iribarren numbers are in the range of the validity of the run-up formulas ($0.8 < \xi < 5$) and wave heights and periods are in the same ranges as Schüttrumpf (2001) used.

Table 5.3: Overview regular waves used in ComFLOW modelling

Wave	H [cm]	T [s]	L [m]	kh	Slope*
1	11.6	1.96	5.998	0.85	All
2	9.3	2.2	7.557	0.76	All
3	20.0	2.2	7.557	0.76	All
4	11.6	1.5	3.513	1.12	All
5	6.0	2.2	7.557	0.76	All
6a	4.0	2.2	7.557	0.76	All
6b	20.0	1.5	3.513	1.12	1:3 & 1:4

(*) Last column gives an overview which slopes are used for simulations

For wave conditions 1 to 5 simulations with three grids are done (coarse, medium, fine). Wave condition 6a and 6b are added in a later stage to obtain information on lower and higher Iribarren numbers respectively, the simulations are only done with the finest grids. Wave condition 6b was not performed on slope 1:6, because it resulted in a too low breaker parameter.

As already mentioned in section 2.2.4 different ways to prescribe waves are available in ComFLOW. In this study two of these are used during the simulations, based on the Airy wave theory and based on the Rienecker-Fenton wave theory. The Rienecker-Fenton waves are chosen, because this theory gives the most accurate wave kinematics. The Airy wave theory is frequently used to prescribe irregular wave fields and it is therefore important to assess the possible

shortcomings of prescribing linear waves. All individual simulations were done for both theories, doubling the amount of simulations.

As described in section 3.1.3 the number of integration points (n_{rintp}) defines the geometry smoothness. Two values for n_{rintp} are used, 4 and 8. The four points of integration are used for all grids, but the higher value of eight is only used on the medium and fine grid.

Hence the six wave conditions, three slopes, three grid sizes, two number of integration points, and two methods to prescribe wave results in a total of 170 simulations.

5.2.2 Output ComFLOW

ComFLOW has many possibilities to generate output. The output files used in this thesis are specified below:

- During each simulation 250 2D snapshot files are generated, uniformly distributed in time. Each of these files contain the pressures and velocities in all grid cells at a given time level,. Figure 3.1 and 3.14-3.16 are generated using data of such a snapshot file.
- A number of fill boxes are generated per simulation, defined by the user. These files contain time series of the computed amount of fluid in a vertical box with dimension equal to domain height. The signals of these files are used as a kind of wave gauge. The boxes are distributed uniformly over the horizontal domain, each 0.01 meter along the slope of the structure, and for the simulations used to calculate reflection 20 are placed in front of the structure.
- Monitoring lines are generated, specified by the user, containing time series of computed velocities and pressures. Along this line 100 monitoring points are positioned at uniformly distributed distances to measure the velocities and pressures. This monitoring points are used to extract the maximum run-up on the slope. The lines are situated parallel to the structure at 0.01, 0.03 and 0.05m distance.

Both fill boxes and monitoring lines can be used to extract wave run-up along the slope. As the fill boxes could only be read every 5 centimeter, the monitoring lines turned out to be more precise. The extraction of run-up heights from the monitoring lines was also less time consuming. In appendix B it is explained how maximum run-up heights are extracted from the monitoring lines. It is important to remark here that the maximum inaccuracy in run-up and run-down heights is a correlation between the Δz of the grid size and the vertical distance between the monitoring points on the monitoring line. For all simulations this vertical distance is 0.0143 m, as the hundred points are evenly distributed along the monitoring line along the whole height of the structure 1.4 m.

5.3 Results and analysis of physical processes

In this section the results of the simulations for physical processes are presented. The results of the run-up heights, the run-down heights, reflection coefficients are analyzed. The section will start with an analysis of the qualitative performance of the model on wave-structure interaction.

5.3.1 General wave-structure interaction performance

In section 2.2.1 it was stated that for different values of ξ waves break in a completely different way. From visual observations three main classifications are made in the transformation of waves

on a slope: plunging, surging and spilling, also collapsing is defined as a transition state between plunging and surging (see Figure 2.1). However the transitions between the breaker types are not sharp-cut.

In this section it is analyzed whether ComFLOW simulates the wave transformation on the slope and the general performance of the simulations is analyzed. In order to do this three waves with different values of ξ were selected; one plunging, one surging and one collapsing. The type of wave breaking is analyzed using snapshots in time.

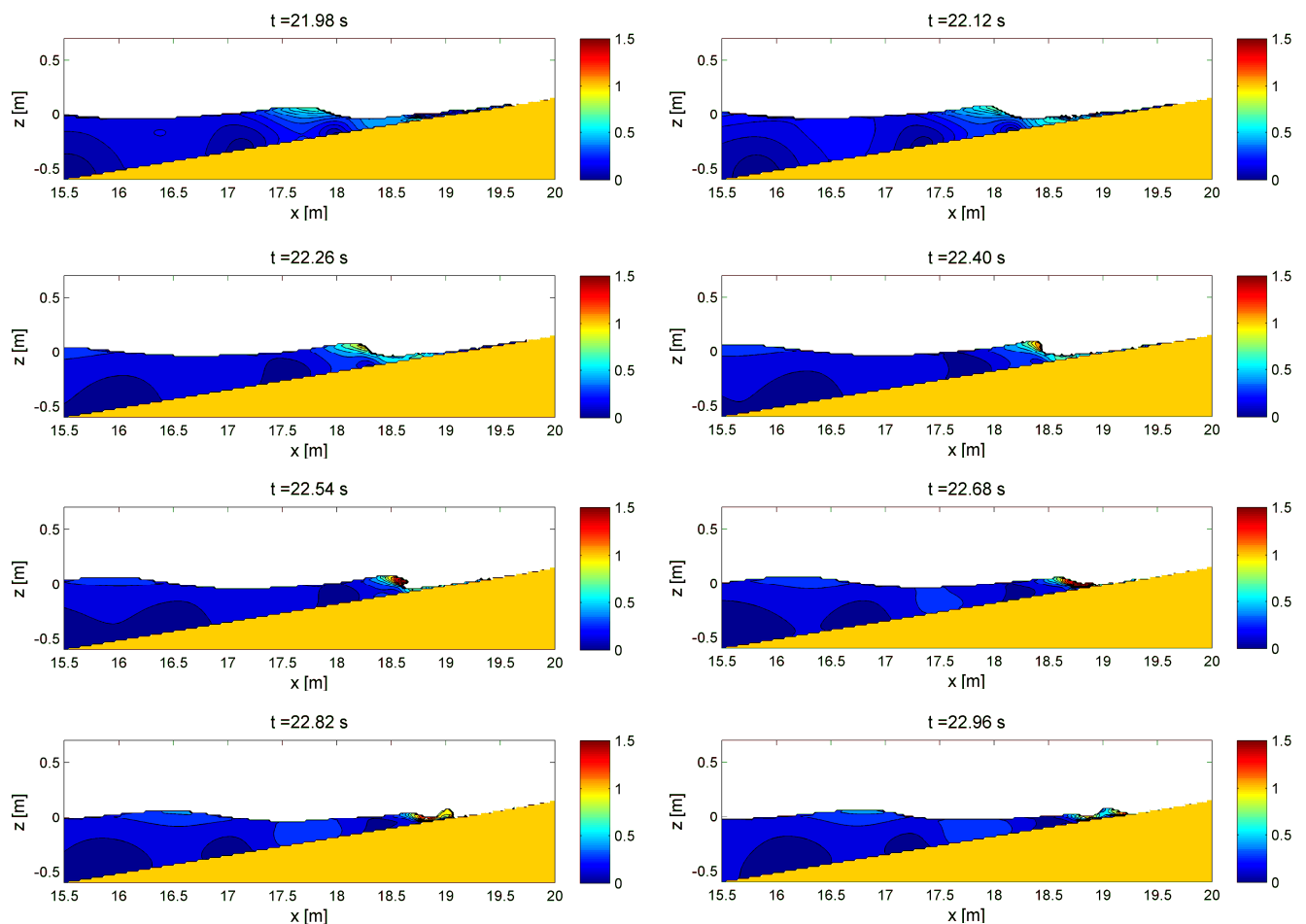


Figure 5.2: ComFLOW simulation with $\xi=0.92$, a plunging wave on slope 1:6 with velocity profile [m/s].

Figure 5.2 shows a ComFLOW simulation of a plunging wave according to the breaker parameter. When looking at the snapshots, with time steps of 0.14 seconds, it is observed that the waves in the simulation indeed have the visual appearance of a plunging wave. The incoming wave is overtaking the previous wave which is still drawing back, as mentioned in theory for wave run-down (section 2.1.3). The waves are breaking and having impact on a water sheet of the withdrawing wave front of the previous wave, this would result in a turbulent flow in reality. In the model no turbulence model is implemented, so this is not caught in the numerical results. In the model the impact results in some wobbling in the flow.

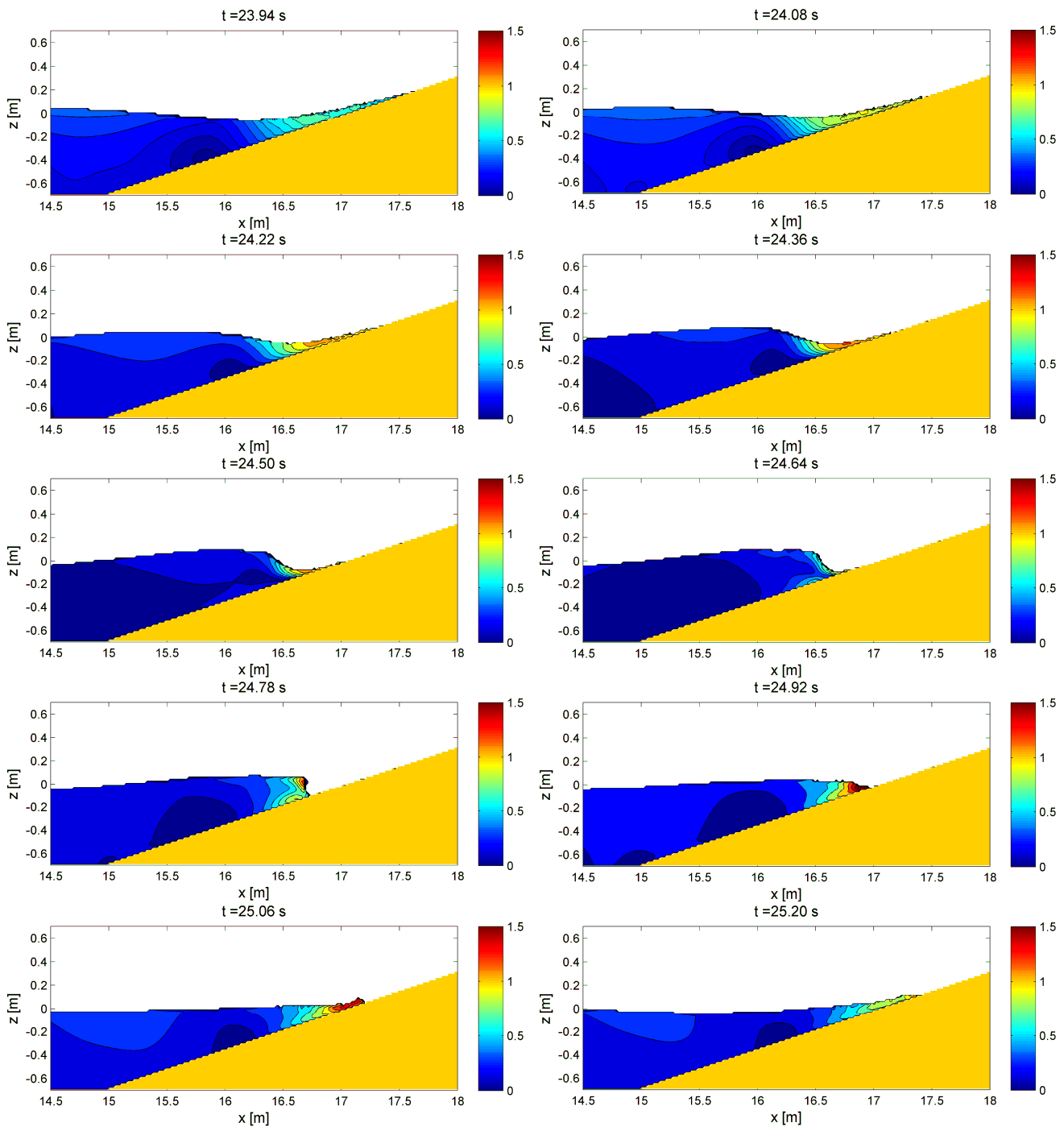


Figure 5.3: ComFLOW simulation with $\xi=2.4$, a collapsing wave on slope 1:3 with velocity profile [m/s].

Figure 5.3 shows a ComFLOW simulation of a collapsing wave according to the breaker parameter, when looking at the time frames one can say that the simulation indeed has the visual appearance of a collapsing wave. Waves are breaking, but unlike the plunging wave, the breaking occurs when the previous wave is withdrawn. Resulting in wave impact directly on the slope, which causes a large impact on the revetment. Furthermore it can be seen that the velocities along the slope are the highest for this wave type, according to data these waves also reach the highest relative run-up values.

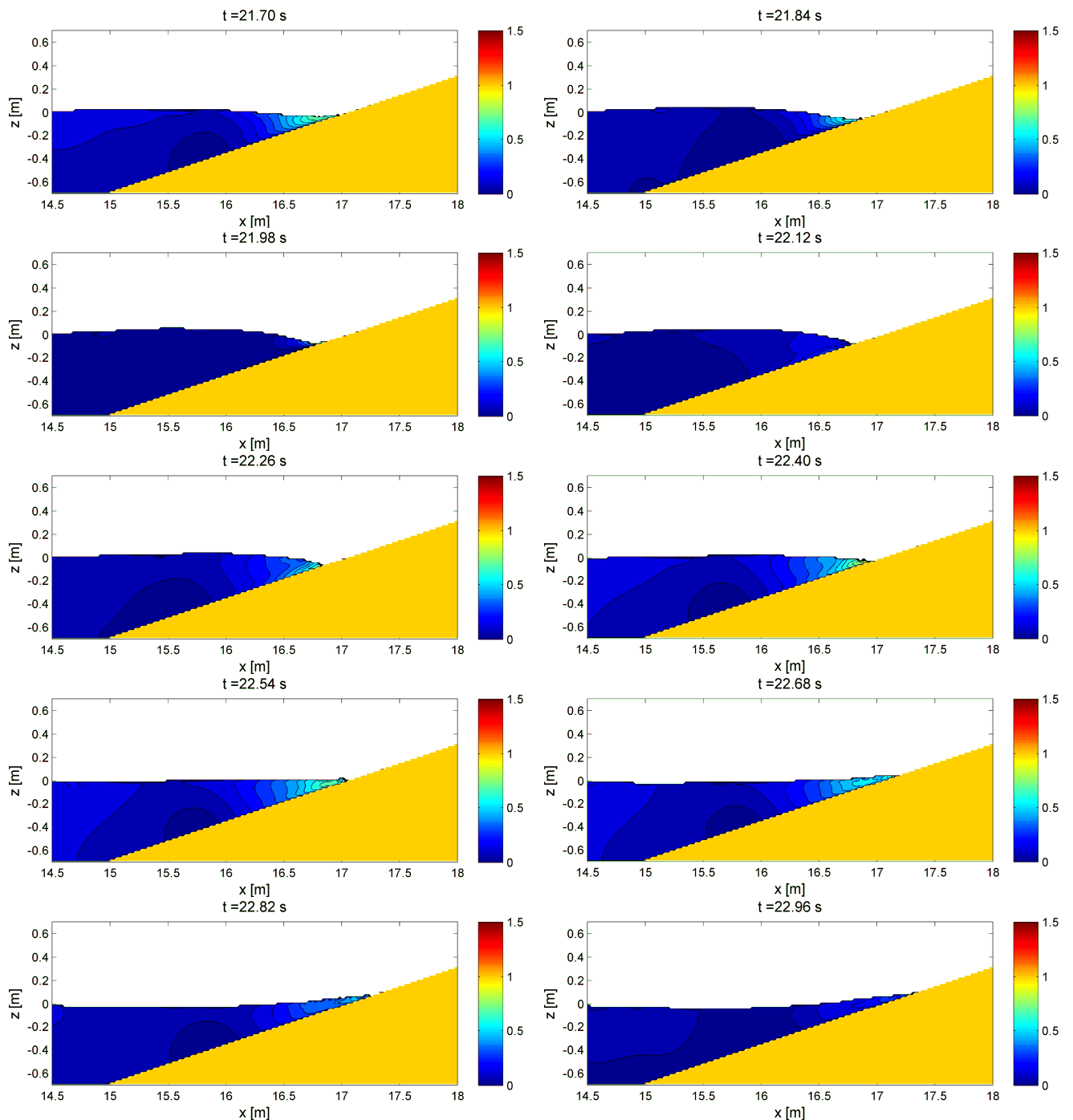


Figure 5.4: ComFLOW simulation with $\xi=3.7$, a surging wave on slope 1:3 with velocity profile [m/s].

Figure 5.4 shows a ComFLOW simulation of a surging wave according to the breaker parameter, when looking at the time frames we can say that the simulation indeed has the appearance of a surging wave. The reciprocating movement of the wave is clear, and there is not any breaking. In this section it is only possible to determine the form of the breaking waves of the numerical results and to compare it in a qualitatively way with the range of values given for the transition between breaker types. In chapter 6 the results of ComFLOW are illustrated with video recording

of real waves. Visual comparison will be used to give more insight whether the numerical results are indeed a right representation of reality.

5.3.2 Wave run-up

In Table 5.4 the results of the simulations are summarized, giving the breaker parameter, the run-up height resulting from formulas of Hunt and Schüttrumpf, the numerical results for the different grid sizes and the different points of integration. If two results are given it means that the wave theories used to prescribe the incoming waves gave a different run-up height.

The analysis of the wave run-up is divided in four parts. First the influence of the grid size is determined, giving a proposal for the relative grid fineness for this type of simulations. Hereafter the influence of the discretization of the geometry, the geometry smoothness, is analyzed, as this was indicated as an influential parameter in the previous chapter. Then the most important part of the analysis is done: the comparison with experimental data is made, giving a thorough analysis of the numerical results.

Influence of the grid size

The grid size is expected to be a parameter of large influence. The graphs of Figure 5.5 show the results for different grids with Hunt's and Schüttrumpf run-up formulas for regular waves (equation (2.2) and 2.3) for each slope. From these graphs it is clear that the overall performance is quite good and the finest grid (blue triangles) performs much better than the other two. Finer grids perform better as they are less dissipative and more accurate.

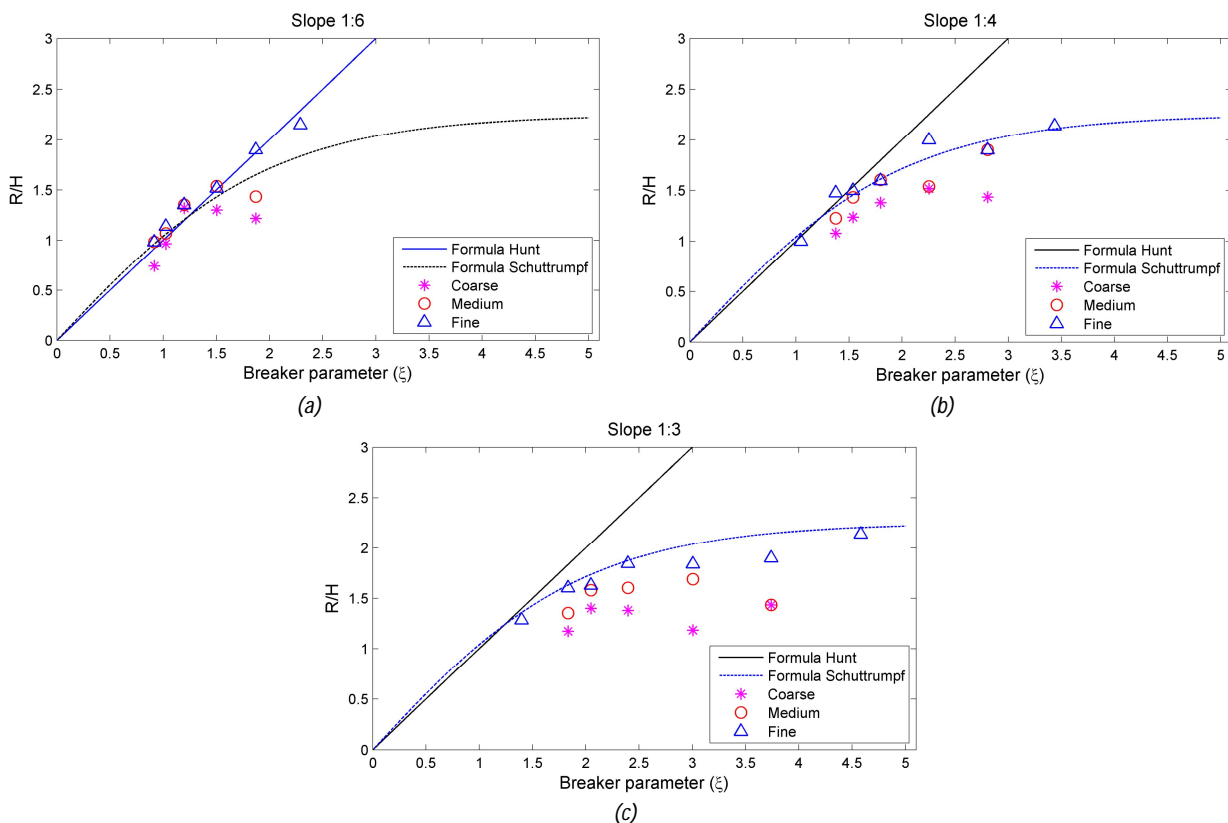


Figure 5.5: ComFLOW results for regular waves on different grids for 1:6 (a), 1:4 (b) and 1:3 (c) slopes.

Table 5.4: Results wave run-up simulations on slope 1:3, 1:4, 1:6 for different wave conditions

Wave	ξ [-]	R [cm]		Coarse		Medium		Fine				
		For. 2.2	For. 2.3			Nrintp 4	Nrintp 8	Nrintp 4	Nrintp 8			
Slope 1:6												
1	1.198	13.9	14.0	13.2	15.3	15.7	15.7	15.7	15.7	15.7		
2	1.502	14.0	13.3		12.1	14.3	14.3	15.7	12.9	15.7		
3	1.024	20.5	21.2		19.3	21.4	21.4	22.8	22.8	24.3		
4	0.917	10.6	11.2	11.4	8.6	11.4	11.4	11.4		12.9		
5	1.870	11.2	9.89		7.3	8.6	11.4	11.4		11.4		
6a	2.297	9.2	7.35		-	-	-	8.6		8.6		
Slope 1:4												
1	1.798	20.8	18.7		15.7	18.6	20	18.6	20	18.6	21.4	
2	2.254	20.9	16.9		14.3	14.3		18.6	18.6	17.2	18.6	
3	1.537	30.7	29.1		24.7	27.1	28.6	28.6	31.4	28.6	30.0	31.4
4	1.376	15.9	15.6		12.5	14.3		15.7		17.1	15.7	
5	2.806	16.8	11.9		8.6	11.4		11.4		11.4	11.4	
6a	3.436	-	8.4		-	-		-		8.6	8.6	
6b	1.048	20.9	21.6		-	-		-		20.0	21.4	
Slope 1:3												
1	2.396	27.8	21.7		16.0	20		20		21.4	21.4	
2	3.005	27.9	18.9		11.0	15.7		15.7	17.1	15.7	17.1	15.7
3	2.049	41.0	34.7	*	30	30	32.8	32.9		32.9	34.3	
4	1.834	21.3	18.9		13.6	15.7		18.6		18.6	18.6	
5	3.741	-	12.9		8.6	8.6		8.6		11.4	11.4	
6a	4.851	-	8.86		-	-		-		8.6	8.6	
6b	1.397	27.9	27.2		-	-		-		25.7	25.7	

(-) no simulation, (*) crashed simulation, if two results are given: left Airy wav theory, right Rienecker-Fenton.

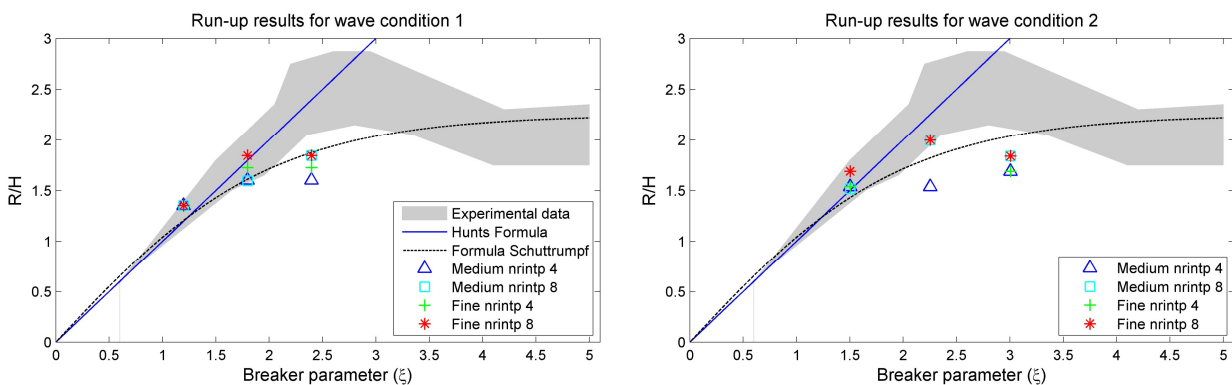
The grid size in terms fine, medium and coarse do not correspondent to some formula, therefore another expression is used to express the relative fineness of the grids. This gives a better indication of the grid size to be used for future research. The number of grid cells per wavelength and wave height expresses the relative fineness of the three grids used in dimensions of relevant physical parameters. This section focuses on question whether there is an optimum in the number of grid cells. At some point, the (exponential) increase in computational time does not counterbalance the improvement of the results.

Because different waves were used during simulation, the number of grid cells per wave length and height varies for each wave. The number of grid cells per wave length and height per grid is shown in Table 5.5 for the medium and fine grid. For wave condition 3 the grid is relative the finest.

Table 5.5: Number of grid cells (N) per wave length (L) and wave height (H) for medium and fine grid.

Wave		1	2	3	4	5
Medium	N_x/L	171.7	216.4	216.4	100.6	216.4
	N_z/H	3.3	2.7	5.7	3.3	1.7
Fine	N_x/L	333.2	419.8	419.8	195.2	419.8
	N_z/H	6.5	5.2	11.4	6.5	3.3
Fine extra	N_z/H	-	-	-	-	5.1

In Figure 5.6 for each wave the results are shown for three slopes with the medium and fine grid. It illustrates that the differences are smaller for the waves with more grids per wavelength, comparing for example wave condition 3 with 1 and 2. There is also less variation in results for lower breaker parameters independent of the number grid cells than for higher values. This indicates that the optimum run-up value is reached earlier. Wave condition 5 is a good example, for the highest breaker parameter the increase from medium to fine and to fine extra gives every refinement quite large improvement in the results. For the lower parameters this is not the case.



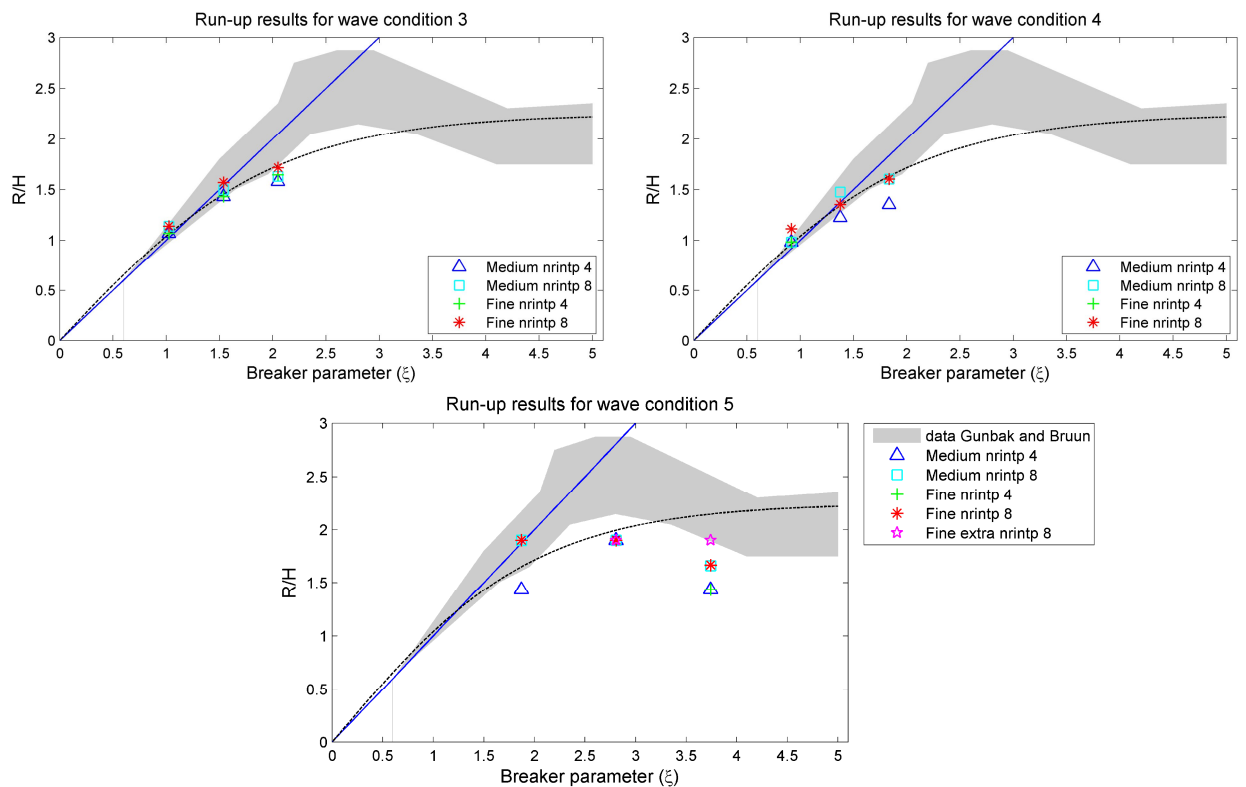


Figure 5.6: Run-up results on medium and fine grid for wave condition 1-5.

The graphs obviously show that for some point grid refinement is not leading to significantly better results and that there is an optimal grid size in terms of number of grids cells per wave height and wave length.

Considering the results in this study and the conclusion by Wenneker (2010), 200 grid cells per wave length and 4-6 grid cells per wave height would be sufficiently fine for these type of simulations. Further grid refinement will not improve results so much and does lead to an (exponential) increase in computational time (see section 3.4.3). Although one should keep in mind that extra grid refinement will decrease the uncertainty margins, as these depend on cell height, as discussed in section 3.2.2.

Influence of geometry smoothness

By defining different numbers of integration points for aperture calculation of the geometry the user can adjust the 'smoothness' of the geometry in ComFLOW. Although it is stated that smooth geometries are used in the simulation there is a difference between the number of points of integration. When using for example 1 point of integration a staircase is formed between the grid cells and a more (numerical) roughness is built in the model than when using 4 points of integration. However this roughness is not definable in terms of a roughness coefficient. In the test cases of dam break in a sloping channel already was shown that this parameter was the main cause in decelerating water layers running up. By running all simulations for medium and fine grids with both 4 and 8 number of integration points the influence of this parameters on wave run-up has been investigated.

In Figure 5.7 improvements are observed on both grids, but especially on the medium grid the results improve. These results are getting comparable with the results from the fine grid. Take again one integration point as example this larger influence is quite easily to explain; a coarser

grid will lead to bigger steps of the staircase and therefore has more roughness. For a finer grid the influence of increasing integration points decreases, the grid is smoother and will faster lead to a stable solution.

Illustrated is that for higher breaker parameters the increased number of integration points does not lead to improved results. For these values waves are of the surging type (non-breaking), in this case there are no thin water layers running up the slope and the velocities are lower, which are both phenomena largely affected by roughness.

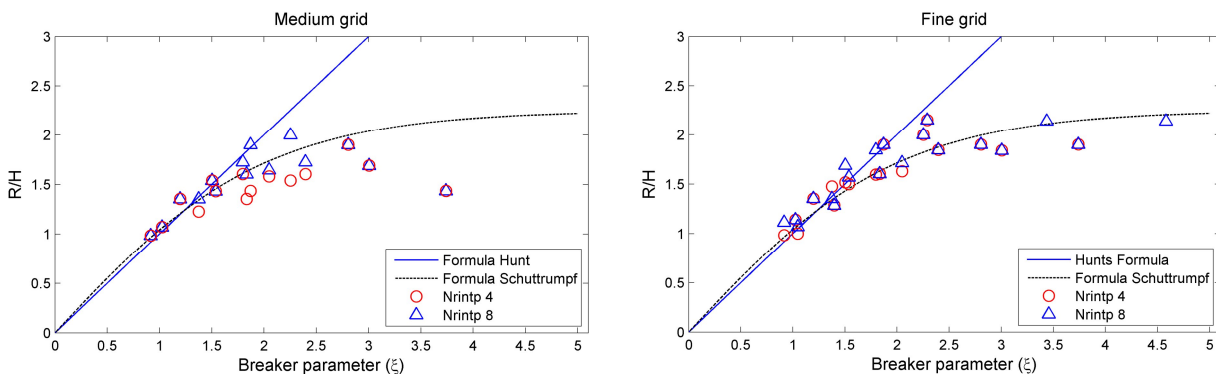


Figure 5.7: Wave Run-up results for different number of integration points. Left: medium grid. Right: fine grid.

Comparison with experimental data

In the next figure the results of all fine and medium grid simulations are gathered for the 8 number of integration points, as these gave the best results. In this figure the grey cloud displays the range of results presented by Bruun and Günbak (1977). The blue cloud displays the data Schüttrumpf collected during his experiments.

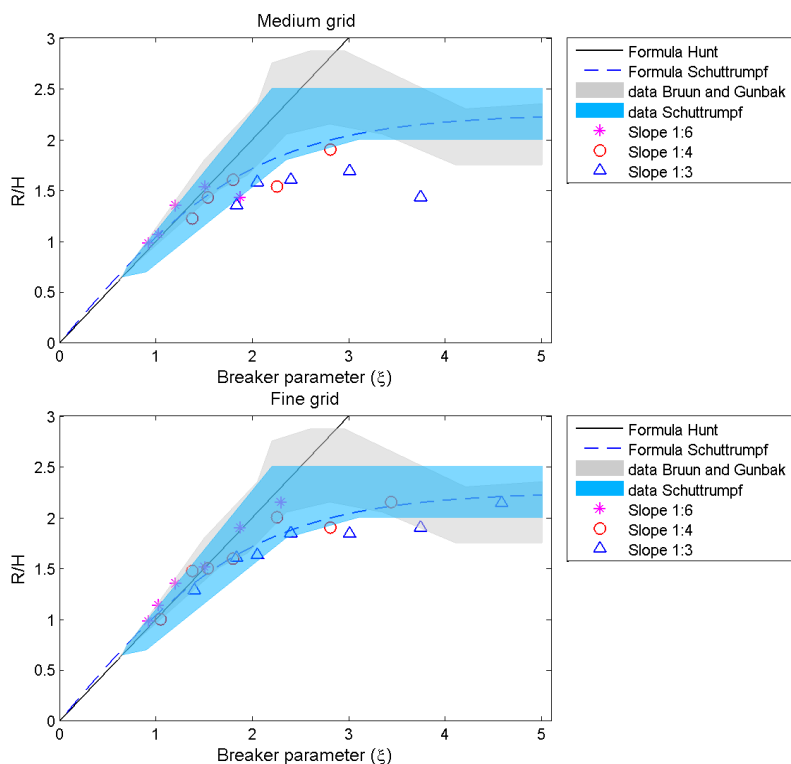


Figure 5.8: ComFLOW results for regular wave run-up. Top: medium grid, down: fine grid

The results with respect to wave run-up are convincing, having very good resemblance with data of physical experiments and show the same trend: a sharp increase in relative run-up with ξ , reaching a maximum constant around $\xi=2.5-3$. Striking is the good comparison with formula deduced by Schüttrumpf and his data cloud. The simulation set-up in this study was extracted from the conditions Schüttrumpf used in his experiment: same water depth, same magnitude of wave heights and periods and same slopes.

For lower values of the breaker parameter ($\xi < 2$), which are breaking waves, the run-up results are good and do not show a significant deviation compared to the experimental results.

The results around the intermediate breaker parameter values ($2 < \xi < 3$), are a bit too low compared to the range of data, all results are too low or in the lower regions of the experimental data. The peak Bruun and Günbak found is not observed at all in the numerical results.

In the region of non-breaking waves, where $\xi > 3$, the results tend to a more or less constant value. The values of the fine grid give rather good results and are in the experimental data cloud, although the results are in the lower regions.

For these higher breaker parameters, results of the medium grid are even less accurate and far below the experimental results. This indicates that there is too much energy loss during the interaction (numerical dissipation) of the waves with the structure. The relative influence of the numerical dissipation can partly explain this. For this steeper slopes more energy must be reflected and almost no dissipation will occur by physical processes by non-breaking waves. The relative influence of the numerical dissipation is getting larger for relative steep slopes, explaining the lower results for higher breaker parameters. The relative high numerical dissipation is hold responsible for the underestimation of relative wave run-up (Ru/H) for $\xi > 2$ of approximately 0.3 compared to the experimental data of Schüttrumpf.

It must be remarked that for the higher values the simulations were done on the 'fine extra' grid to get enough grid cells in the z-direction. For the medium grid such increase was not applied and with only 1.7 grid cells per wave height, one can imagine why the results are poor. See also the lowest graph in Figure 5.6 for the improvement of the results between of medium, fine and fine extra grid size.

Besides the good comparison of the data one last important remark should be made. Although the influence should be included in the breaker parameter, the numerical results seem to have a dependency of the slope. The results of gentler slopes give higher relative run-up heights than the steeper slope. The data points of Schüttrumpf in Figure 5.9, especially around $\xi=2$, show that these experimental results also have some dependency on the slope. However in the data of Schüttrumpf the highest values are the results for the steeper slope (1:4) and are the results for the gentler slope (1:6) fitting the formula, but in the numerical results this are the run-up heights for the gentler slope (1:6) and are the results for the steepest slope (1:3) exact on the formula. In the next section on wave run-down this slope dependency and its causes will be elaborated further.

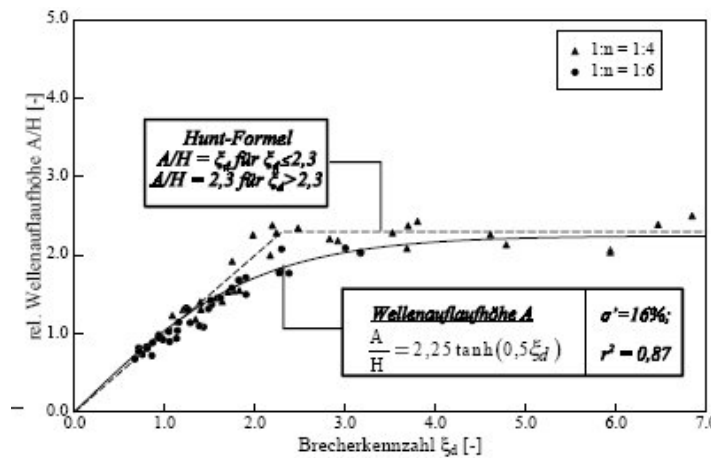


Figure 5.9: Wave run-up for regular wave, measurements Schüttrumpf (2001: abb. 4.8a)

Regularity of wave run-up

In Figure 5.10 the left graph shows wave run-up along the slope, a clear regular wave run-up pattern is visible. The right graph displays position of water as derived from the wet values along the slope, showing in the horizontal parts (scatter) water that drops behind on the slope. In the graphs the influence of the grid and the distance between the measurement points on the monitoring line are visible, giving the edgy character.

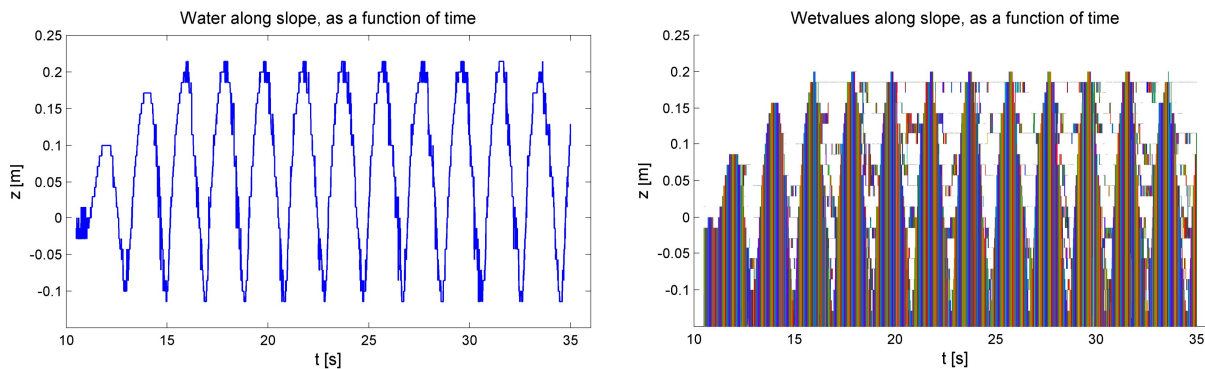


Figure 5.10: Wave signal (left) and wet values (right) along slope (For slope 1:3, wave condition 1, Airy Wave, fine grid).

Most simulations do not give this perfectly regular signal, were all waves give the same run-up or run-down value. Especially the run-down values are in most cases not that regular. Figure 5.11 shows four cases giving a less regular representation.

The influence of the discrete grid cells is clear in the irregularities of Figure 5.11. For the run-up of most waves the water is just flowing into the neighbouring grid cell, giving therefore a higher run-up height. Most of the irregularities give only one grid cell higher or lower run-up value for two or three of all incoming waves. In fact these differences are quite small and are enlarged by the discrete way the run-up is extracted. In their paper Bruun and Günbak (1977) mention an observed a deviation of 10% in run-up values during their experiments. The video recordings of physical experiments, discussed in chapter 6, also show small differences between consecutive waves. The small irregularities of wave run-up are therefore not large errors in the results and are not considered as a problem. The wave run-down results show far more irregular patterns, also for more simulations. The irregularities in the run-down in Figure 5.11 a&b look also to have a sinusoidal form.

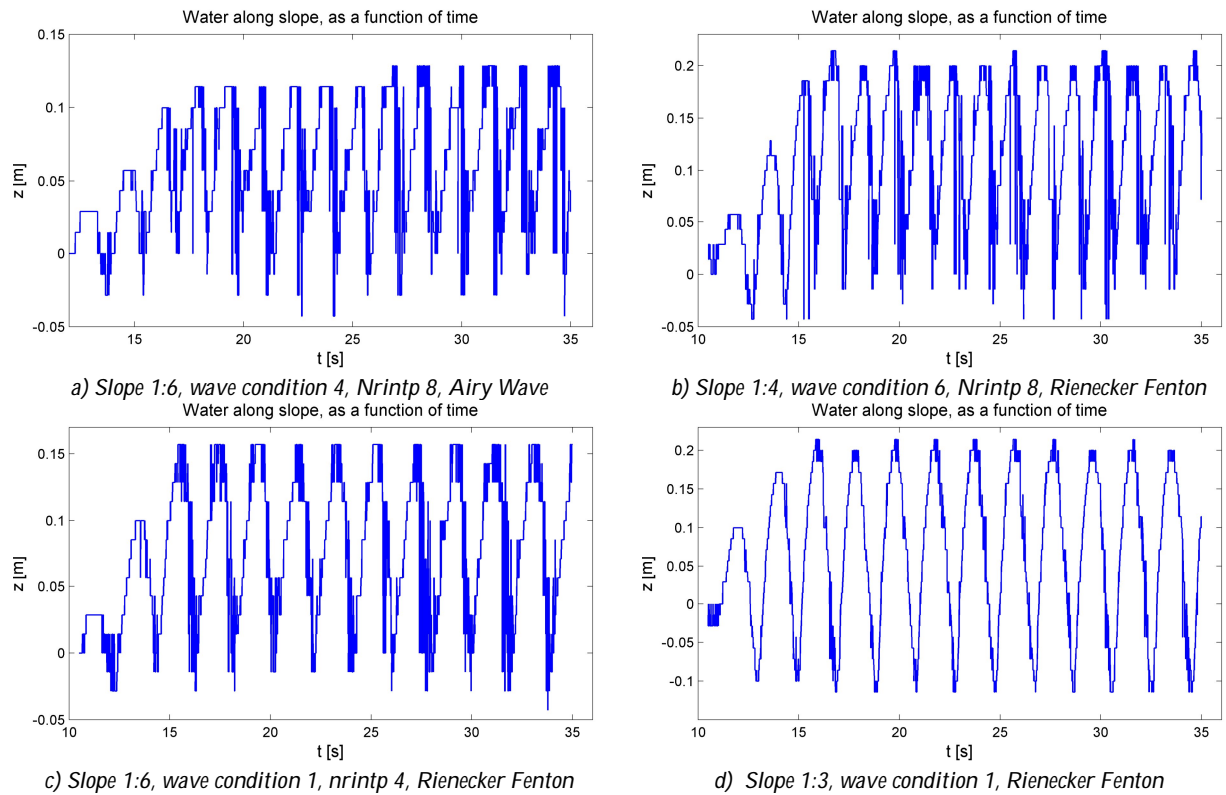


Figure 5.11: Four cases (a-d) showing wave signals along different slopes (on fine grids).

The graphs are showing different irregularities noticed in run-up patterns of the results:

- a & b: irregular run-down en run-up
- c: Irregular run-down, regular run-up
- d: Irregular run-up, regular run-down

In Figure 5.11d and Figure 5.10 are the results of the same wave conditions but for different methods (Rienecker-Fenton and Airy) to prescribe waves. Apparent are the small differences in the results, which is the case in all the simulations. Nevertheless, in most simulations the same wave run-up height is measured, but in 11 cases, see Table 5.4, the two methods give a different value.

From the four different patterns distinguishable, percentages of occurrence are given in Figure 5.12, these percentages are based on the medium and fine grid simulations for nrintp = 4 and 8, which are 2x72 simulations. From these pie charts it is apparent that the smoother geometries causing more irregular run-up patterns than the ones with 4 integration points, there is no evident explanation found for this. Furthermore it should be said that medium and fine grids have the same distribution, although this is not clear from the figure.

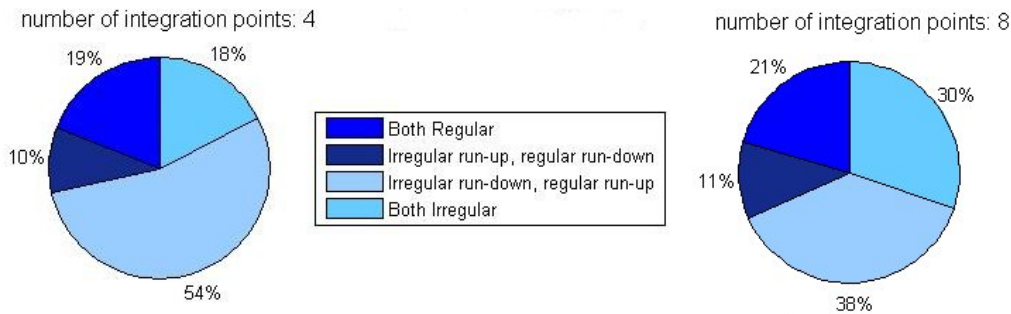


Figure 5.12: Percentage pie of 4 cases of (ir-)regularities noticed in wave run-up results of all medium and fine grid simulations with 4 and 8 number of integration points.

From the cases where irregular wave run-up occurs, 30% of the simulations gives the last 4 or 5 waves a higher value, just as can be seen in Figure 3.4a. This could indicate that not all wave energy is transported out of the domain and is reflected on the incident wave boundary, resulting in somewhat higher waves. It is important to note that these are all simulations with linear waves (Airy waves).

5.3.3 Wave run-down

The analysis of the run-down results is less straightforward than that of the run-up results. Part of this lies in the more irregular run-down patterns, as it was more problematic to retrieve one (good) run-down value from the signal. Comparison of the ComFLOW results with experimental data show less resemblance than for wave run-up as can be seen in the next figure. The relative run-down is overestimated in comparison with the experimental data and the run-down values never reach above the SWL. But for the higher values of ξ (>3) the numerical results enter the experimental data range. Just as for the run-up height the numerical results seems to be slope dependent giving lower run-down values for the steeper slope.

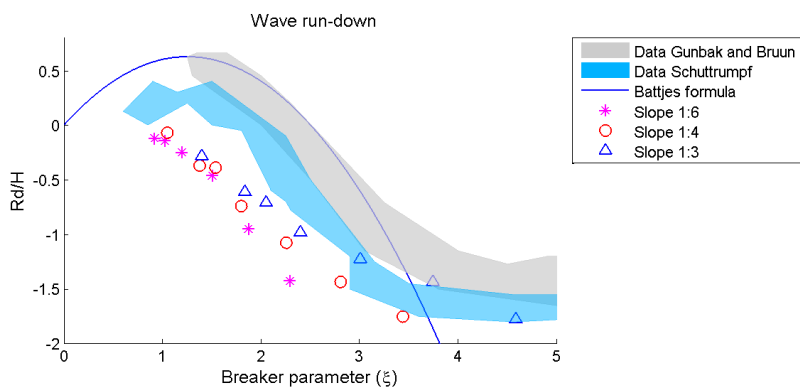


Figure 5.13: Run-down regular waves; ComFLOW results and experimental results of Bruun and Günbak and Schüttrumpf on smooth slope

Note that run-up is a more important design parameter and therefore the process has been extensively studied and described in the past. In contrast, the run-down is studied in fewer experiments. As mentioned in section 2.5, the results of both experiments show large differences. Nevertheless for wave run-down the numerical results for the run-down heights are too low for breaker parameters below a value of 3, for breaking waves. An overestimation for relative run

down (R_d/H) of approximately 0.6 compared to the data of Schüttrumpf and 1 to Bruun and Günbak is observed.

Based on the findings of the earlier analysis these lower numerical results were not expected. The numerical roughness created by the discretization of the geometry and the analysis of the test cases gave the impression that run-down would be similar to the experimental data or even somewhat higher. As run-down is related to the maximum run-up that is reached and the run-up results for the lower values of ξ are good the run-down was expected to be good. In the test case of Carrier and Greenspan (section 4.1.2), during down-rush the fluid was sticking to the slope due to numerical friction and falling behind the analytical solution, but the maximum run-down was reached in the numerical solution. In the analysis of the dam break test the down-rush was with the same speed as the analytical solution. Only in these simulations no define geometry was present, it was expected that with a structure the run-down was decelerated by the numerical roughness. Summarizing no clear explanation could be found for the mismatch of the run-down heights in earlier analysis in this study. But in other numerical studies this mismatch is observed as well. The cause may lay in the different physical properties of the processes, the run-up is a more abrupt and faster process and the run down is more smooth. Also the differences in the handling of the numerical model of flooding and drying cells may cause the mismatch.

Analyzing the observed dependency on the slope of the numerical results in both wave run-up and run-down one thing stands out. For the steeper slope the vertical amplitude at the shoreline is the smallest. In section 2.3 it was elaborated that wave run-down is dependent on the maximum run-up reached by a wave, therefore in the run-down formula the run-up height can be found. With this theory in mind the expectation is that with the lower values reached for run-up, the steeper slope would reach lower values in the wave run-down, but the opposite is happening. In the dam break test the simulations with a sloping bed showed the same trend, for steeper slopes the dissipation was larger.

Two hypothesis are formulated to find an explanation for this slope dependency in the numerical model. First hypothesis is that slope dependency can be caused by the discretization of the geometry. With different defined slope steepness this discretization creates different types of 'staircases', which could lead to a different numerical roughness. It could cause more roughness at the steeper slope than for the gentler slopes. Second hypothesis is that the number of grids cells where the wave runs through at the slope has influence on the dissipation, for steeper slopes the wave movement will run trough less grid cells.

5.3.4 Reflection

The reflection coefficient of several simulations is calculated, in order to see whether the same amount of energy is absorbed and reflected at the structure as theory prescribes. This is done by separating the incoming and reflected waves from measured wave signals. The separation was performed by a 3-gauge wave reflection method (Mansard and Funke, 1980), which uses a least square method. In this method waves can only propagate in positive x-direction (incoming waves) and negative x-direction (reflected waves) and the water depth is assumed to be uniform.

In ComFLOW fill boxes can be used as a kind of wave probe and users can define the position of this fill boxes. The boxes were placed at several positions in front of the structure. To calculate the reflection coefficient use was made of fill boxes. The location of the three fill boxes must be ordered such that $x_1 < x_2 < x_3$.

The distance between these fill boxes is determined with the range of probe spacing recommended in Mansard and Funke (1980):

$$x_{12} = L/10$$

$$L/6 < x_{13} < L/3$$

$$x_{13} \neq L/5 \text{ and } x_{13} \neq 3L/10$$

This resulted the following distances between the fill boxes, based on the different wave lengths used in the simulations:

- $x_1=6.51$ m,
- $x_2=7.56$ m, and
- $x_3=7.91$ m

Time series of the incident and reflected wave in x_1 are output of the procedure. To calculate the reflection coefficient simulations on a medium grid with a number of integration points of 8 were used with Rienecker-Fenton waves.

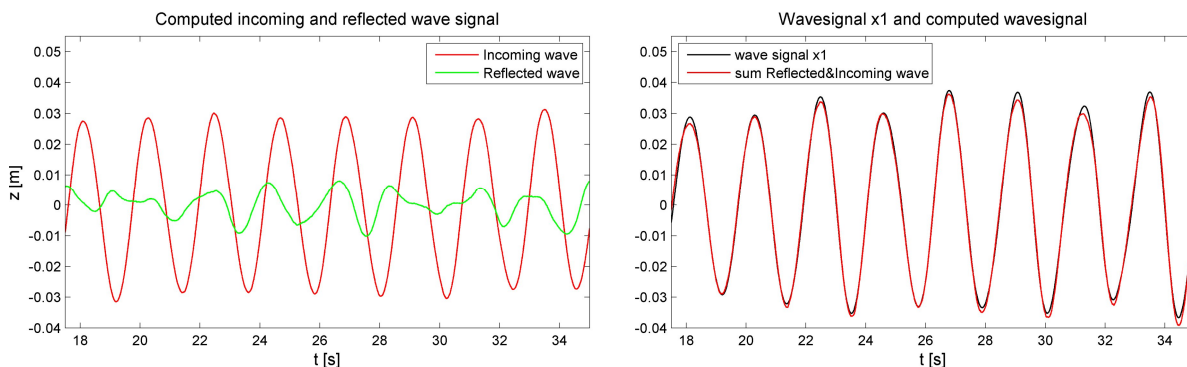


Figure 5.14: Separation of the incoming and reflected wave signal on slope 1:3, wave condition. Left: computed incoming and reflected wave signal. Right: wave signal at x_1 in ComFLOW and computed sum of incoming and reflected wave.

The sum of the reflected and incident waves, in the right graph of Figure 5.14, does not exactly fit the measured wave signal. Although the differences are small, these are a result of the fact that Mansard and Funke assume linear wave theory in their solution, while in the ComFLOW simulations non-linear waves are used. In the graph crests are higher and troughs are flatter for non-linear waves, which is according to theory. To obtain the incoming and reflected wave height from the computed incoming and reflected wave signal the following procedure is adopted for each signal:

- The number of waves and times at which zero-crossings occur are determined.
- Parameters pertaining to individual waves are determined: wave height and period, crest and trough amplitudes and time at which those occur.
- The mean and significant wave heights and periods can be determined.

With the obtained information the reflection coefficients are calculated, using the significant wave height as parameter, for this value the incoming values agreed the defined incoming wave height and period. The calculations were done for different simulations, shown in Figure 5.15.

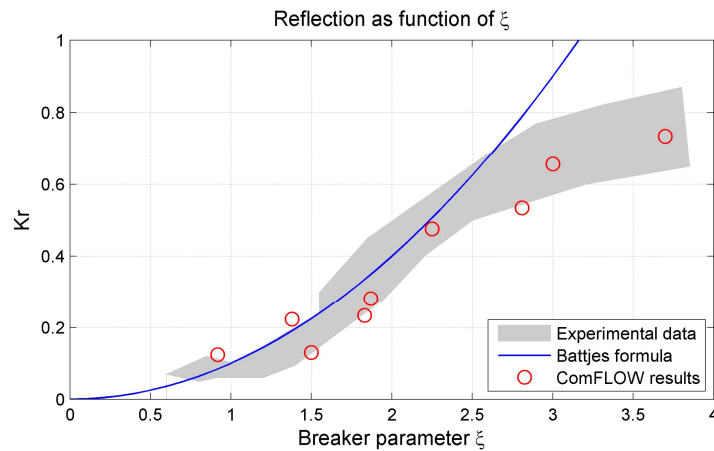


Figure 5.15: Reflection coefficients of regular waves; ComFLOW results and experimental results (Bruun and Günbak) on smooth slope.

Comparing the results, the wave reflection in ComFLOW is about the same as measured in physical model tests. All calculated reflection coefficients are practically in the grey area of the experiments of Bruun and Günbak. Although it is observed that waves for which run-up results are low (in the non-breaking range) also give less reflection. As energy is (numerical) dissipated at the slope.

To check the sensitivity of the calculations also for some other situations the reflection was calculated. This situations were the same simulations but with use of Airy Waves and the use of fill boxes with same distance in between but at different distance from the structure. It was conducted that the reflection coefficient, K_r , calculated was in the same order, a mean deviation of 0.01 with a maximum deviation of 0.04. Concluding, the used simulations are representative for the reflection and the distance of the gauges to the toe of the structure is quite indifferent.

5.4 Sensitivity analysis of the use of monitoring lines

This section is introduced to gain more insight on the use of monitoring lines in this study to obtain wave run-up and run-down values. The accuracy results of physical experiments depend often on the used measurement techniques. Different measurement techniques is one of the indicated causes for differences between results of experimental tests. Also in this study the measurement techniques, the use monitoring lines, can cause inaccuracy. Therefore this model setting is studied in more detail. First the placement of the monitoring lines at different distances from the slope is discussed and thereafter the influence on the results of uncertainty margins in the extraction of run-up and run-down values is shown.

5.4.1 Placement of monitoring lines

The placement of monitoring lines is a possible variable in the model setting that could influence the results. Lines at a larger distance possibly cannot monitor thin water layers running up the slope. The sensitivity of the results for wave run-up and wave run-down is investigated by increasing and decreasing the distance of the monitoring lines to the structure, a sketch is showed of the monitoring line in Figure 5.16. The default setting is a distance of 1 mm to the geometry. In this section the influence of the position of the line at smaller and larger distances is investigated.

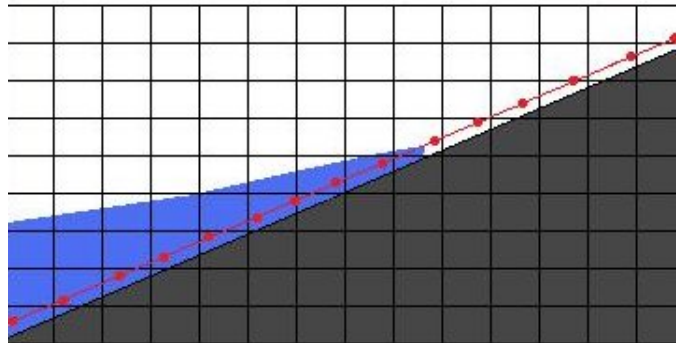


Figure 5.16: Illustrative sketch of monitoring line. Dark grey is the geometry, blue denotes fluid and red is the monitoring line with monitoring point uniformly distributed.

Decrease distance of monitoring line to structure

For some simulations in some points on the monitoring lines no output could be generated with the default value. This problem occurred on the coarse and medium grids for slope 1:4 and 1:6 with four points of integration and gives the following (lack of) output as in Figure 5.17. It is mere coincidence that this problem did not occur on the 1:3 slope. In the left figure it is showed that the wave signal can not be plotted. This signal is generated by finding the first 'no fluid present' value in the output, which is now at the blank line in the right figure.

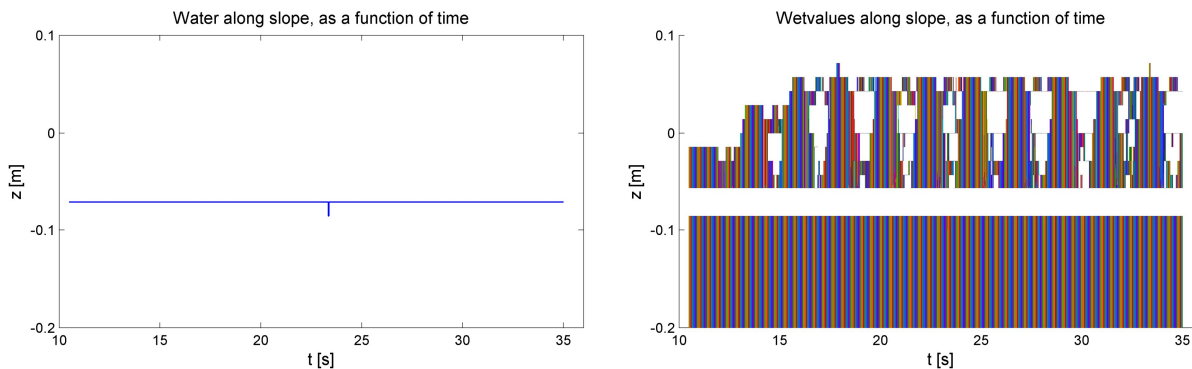


Figure 5.17: Problems with output of monitoring lines for slope 1:6, wave 5, Airy wave, medium grid. Left, waves signal along the slope. Right, wet values along the slope.

The cause for the problem lies in the discretization of the geometry (see section 2.2.3). Given a point on the monitoring line that lies at 0.01m from the structure, the grid cell in which this point lies is almost completely solid and only a small part is open for fluid. This type of cells (with small edge apertures) can give stability problems with the computation motion of the fluid, therefore ComFLOW put this edge aperture in the computation to zero. As a result this grid cell becomes a body-cell where no fluid motion is solved and no output data is generated. In the next figure the situation is sketched, the green dot denotes a part of the monitoring line where no fluid motion is solved.

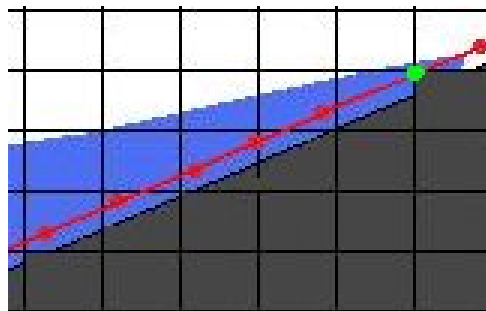


Figure 5.18: Illustrative sketch of monitoring line and the cause of problems with output generation. Green dot denotes a part of the monitoring line where no fluid motion is solved.

To solve this inconvenience there are two obvious possibilities:

- Increase the distance of the monitoring line to the structure.
- Increase the number of integration points.

As for the eight points of integration this problem did not occur, this increase was sufficient to solve the problems for these simulations. For the simulations where the problem came up, the distance of the line to the structure was increased to 0.03m to solve the problem.

As this problem already occurred at the default value the decrease of the distance of the monitoring line was not further investigated, as this would lead to more simulation where this problem would come up.

Increase distance of monitoring line to structure

The influence of the increase in distance on the accuracy of the results is investigated by looking at the output of lines at different distances (Figure 5.19).

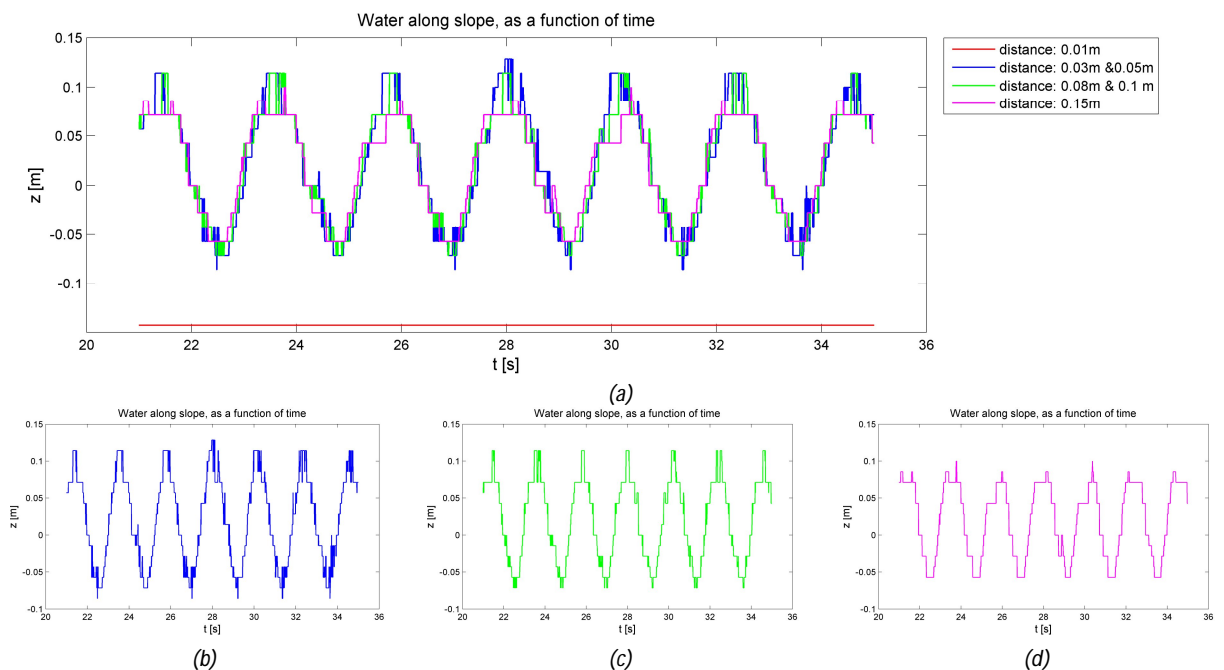


Figure 5.19: Wave signal along the slope for different distances to the structure (a) all distances, (b) 0.03 m, (c) 0.08m, (d) 0.15. For slope 1:4, condition 5, Airy Wave, medium grid.

The figure corresponds to what one would expect, monitoring lines at larger distances give lower run-up values and run-down values. It also shows that the run-up values until the distance is 0.1m do not differ that much, the blue and green line, only the monitored water layers running up until the maximum value are getting thinner.

The graphs of the wet values, Figure 5.20, are also used to check whether the larger distance of 0.03 m lead to the same accuracy. As can be seen this is indeed the case for this example.

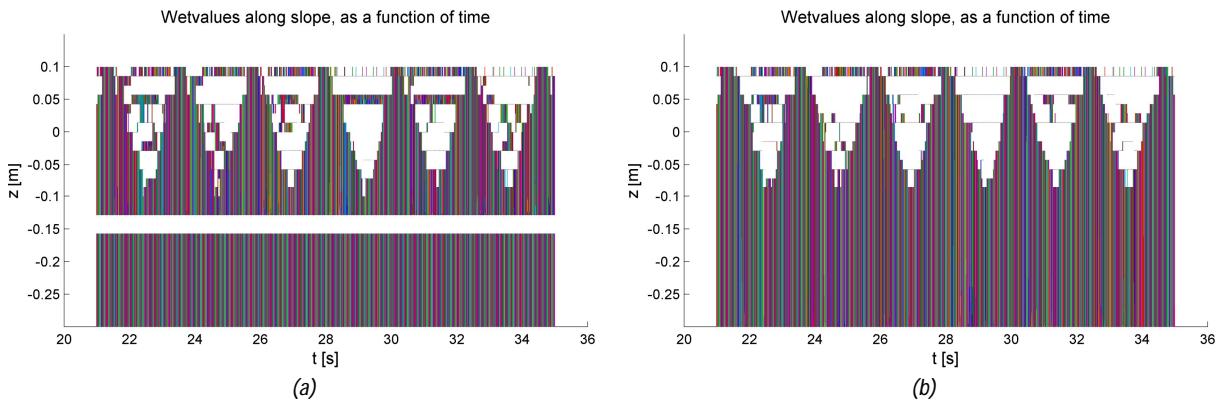


Figure 5.20: Plot of wet values on medium grid to compare accuracy of distance (a) 0.01 and (b) 0.03m. Slope 1:4, condition 5, Rienecker Fenton, medium grid.

In some simulations, it occurred that the line at 0.03m even gave higher values than the line at 0.01m, which was not as expected. Some analysis showed that this is due to the detachment of the final tip of the wave tongue.

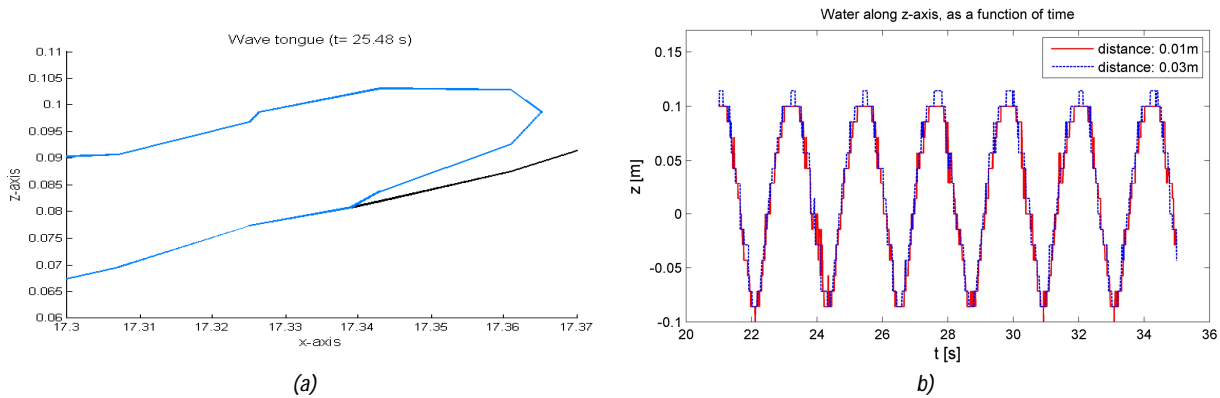


Figure 5.21: Wave run-up higher at larger distance to structure, due to detachment of tip of the wave tongue. (a) wave tongue, (b) Results for distance of 0.01 and 0.03m.

5.4.2 Uncertainty margins in wave run-up and run-down results

This section is introduced to give insight in the magnitude of the accuracy of the results on the fine grid for relative run-up and run-down, as this varies for the different wave heights used in the simulations. In Appendix B the generation of the output from ComFLOW is described. In the beginning of this chapter it was stated that the extracted run-up values were subject to a certain accuracy which was interrelated with the grid cell height and the distance between the monitoring points on the monitoring line. The data of the monitoring line contains time series of computed velocities and pressures at 100 points along the defined line. The points are uniformly distributed

along the line and the distance between the points in vertical direction is 0.0143 m. This distance is the same magnitude as the grid cell height of the finest grid. By the use of this output file the run-up results are discrete. The output is always one of the monitoring points on the monitoring line, so with steps of 0.0143 meter. With these uncertainty margins, the sensitivity on the relative run-up and run-down largely varies for different wave heights. How smaller the wave height, the larger the influence, as shown in Table 5.6.

Table 5.6: Influence of accuracy of maximum run-up and run-down values on relative run-up and down results.

Wave height H [cm]	$\Delta R/H$
11.6	0.123
9.3	0.154
20.0	0.072
6.0	0.238
4.0	0.357

With the calculation of relative run-up and run-down, it becomes clear that with the used wave heights the inaccuracy for the higher breaker parameters in this study is quite large, as can be seen in Figure 5.22.

To increase the accuracy three options are possible: decrease the height that the monitoring line should span, refine the grid cell size or adjust the simulation program and use higher waves. For the first two options one should keep in mind that the both components are interrelated and that the largest factor will be decisive.

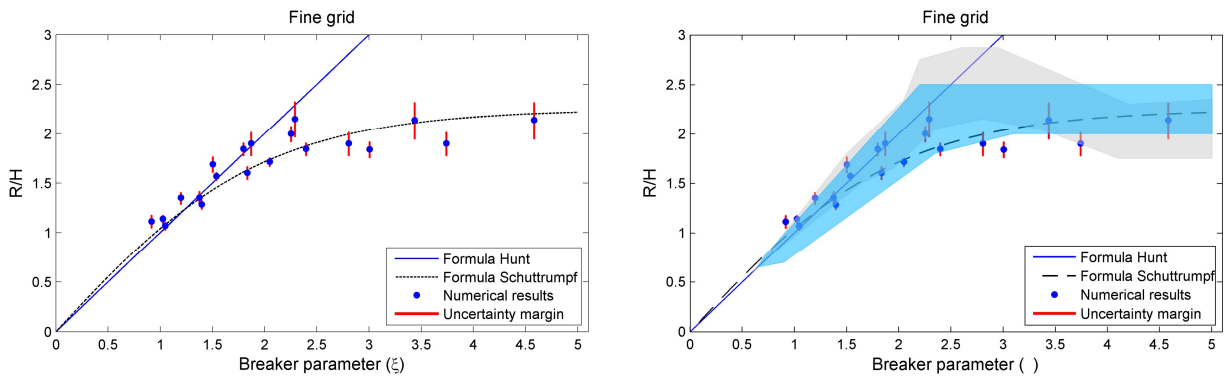


Figure 5.22: Run-up results with relative influence of the uncertainty margins with (right) and without (left) experimental data plotted.

5.5 Analysis of numerical performance

In this chapter the numerical performance is discussed and different model settings are analyzed in this matter. The chapter will start with a section on artificial viscosity or numerical diffusion, after this the robustness of the model is discussed for the performed simulations. At last the computational time (CPU time) needed for different simulations is discussed.

5.5.1 Artificial viscosity

For the discretization of the convective terms in the Navier-Stokes equations a first order upwind scheme has been used in our simulations. Although central discretization is less dissipative, it leads to wiggles in the solution and is less stable (leading to the necessity of very small grid size

and time step and thus higher computational time and costs). Compared to a central scheme, the upwind discretization can be interpreted as a central scheme plus an extra diffusive term. This term adds extra viscosity to the physical viscosity of μ/ρ and induces dissipation of energy and unphysical wave damping. An other effect is already seen by the dam break problem, the smearing out of sharp gradients.

The amount of extra viscosity is equal to $u\Delta/2$ where u is the velocity and Δ is the mesh size. So this term is dependent on the position in space. An estimate of the maximum artificial viscosity that is added can be found by calculating $u\Delta/2$. For the velocity u the mean occurring velocities on the slope during run-up are taken:

$$u \approx 1,0 \text{ m/s}$$

This results in an approximation of the maximum artificial viscosity:

$$k_{art} = u\Delta / 2 \approx 1 \cdot 0.018 / 2 = 9.0 \cdot 10^{-3} \text{ m}^2 / \text{s}$$

The approximation of the artificial viscosity above is for a fine grid, whereas the medium grid has an artificial viscosity twice as high. In comparison, the physical kinematic viscosity ν is equal to $10^{-6} \text{ m}^2/\text{s}$. This artificial viscosity can in combination with the boundary conditions for the velocities (no-slip) lead to a decrease in run-up heights.

Kleefsman (2005) investigated the influence of the numerical diffusion on wave propagation in the domain. She used a mesh size of $140/1500 = 0.0933$ and waves in the same order as the waves used in our simulations, giving k_{art} three times smaller than calculated above for our simulations. A difference is that Kleefsman used deep water for the simulations. Kleefsman showed that for wave simulation in a long domain, where many periods are simulated a clear damping is visible. After a time of 100 periods and 14 wave lengths from the inflow boundary a decrease of 22% in wave height was observed in the simulations, showed in Figure 5.23. She also proved that this loss was mainly due to the artificial viscosity, but not entirely. The dampening of waves namely also occurs with a central scheme, this part of energy dissipation is coming from the treatment of the boundaries and free surface.

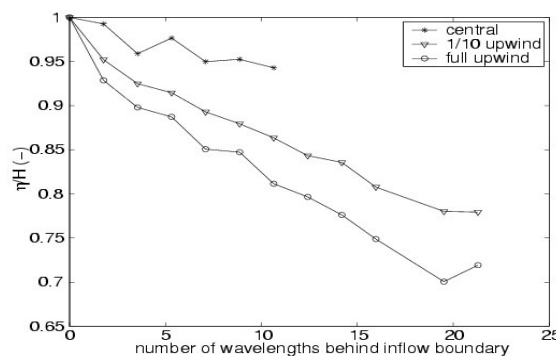


Figure 5.23: Decrease of wave height after a simulation time of 100 periods at different distances from the inflow boundary. (Kleefsman, 2005: figure 3.18)

In this study a domain of only 2-4 wavelengths and a total simulation time of maximum of 20 wave periods is used. In addition, the maximum artificial viscosity is in most simulations lower than that of Kleefsman (the coarse grid has the same magnitude). The damping of waves in our simulations is present, but will not be higher than only a few percent. This wave damping can

cause a decrease in wave run-up heights, but the effect is assumed not be very large in the used domain.

5.5.2 Robustness

The model proved to be robust during the simulations, from the 162 simulations only one could not be completed. This and some other irregularities were noticed:

- For the coarse grid, on slope 1:3, wave condition 3 with the Airy wave description the simulation could not be completed. The time step goes to zero after 30-31 seconds and the simulation crashes. Analysis of the results shows that the crash occurs suddenly and is not an accumulation of errors. This type of crash also occurred during some of the simulations of Wenneker (2010). It is possible that origin of the crash may lie in the GABC, but it is not certain.
- Despite the warning in the user manual, not to use higher values than four for the number of integration points, it appeared that the higher number of integration points of eight is stable and all simulations finished without problems. However, when trying higher values than 9 in order to obtain even smoother geometries the program gave a warning not to use higher values than 3 or 4 and the simulation was stopped.
- Unphysical small-scale fluid bodies suddenly arise in (only) four simulations. This flotsam and jetsam has the appearance of flying droplets that at one point detach from the slope of the structure and start to fly opposite direction to the inflow boundary (see Figure 5.24) in a time span of about 3 seconds. These fluid bodies do not seem to influence the result and are therefore not considered a problem.

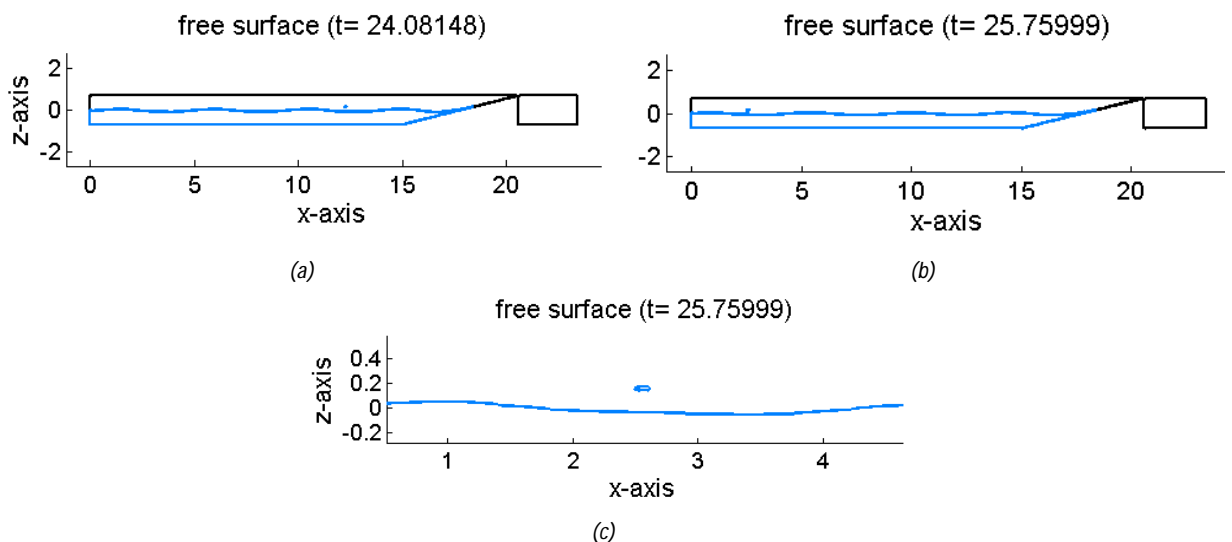


Figure 5.24 Accumulation of unphysical small-scale fluid bodies travelling to left domain boundary at (a) $t=24.1$ and (b) $t=25.7$ s (c) Enlargement of fluid body at $t=25.7$ s (For slope 1:4, wave 1, Airy wave, medium grid).

5.5.3 CPU time

This section is introduced to give insight in the increased computational time for medium and fine grids and the different methods of wave description.

Table 5.7: CPU time in minutes and time step in seconds, for medium and fine grids

	Airy Wave		Rienecker- Fenton	
	CPU time	Time step	CPU time	Time step
Medium grid	65-75	$0.3143 \cdot 10^{-2}$	120-130	$0.3143 \cdot 10^{-2}$
Fine grid	550-580	$0.1615 \cdot 10^{-2}$	940-1200	$0.1615 \cdot 10^{-2}$

From the analysis of CPU time presented in Table 5.7 some important remarks can be made:

- Airy Wave and Rienecker-Fenton waves have the same accuracy in simulating wave run-up, but twice the computational time is needed for Rienecker-Fenton waves. Evaluating time steps shows that these are the same for both methods and not causing the increase in CPU time. The doubling in time is probably caused by an inefficiency of the model, the wave kinematics are evaluated in all grid cells while it should only be necessary on in- and outflow boundaries. As Rienecker Fenton theory is more complex it takes more time to evaluate.
- Fine grids lead to more accuracy, especially for Iribarren numbers higher than 1,5 (see Figure 5.75, 5.6 and 5.8), but also lead to an increase of eight to nine times of computational time. This time increase is logical as number of grid cells double in both x- and z-direction and the time step is (almost) halved, leading to an increase of $2 \times 2 \times 2 = 8$ in CPU time.
- The increase of number of integration points does not lead to an increase of computational time.

5.6 Concluding remarks

In this last section a short summary of the main conclusions drawn in this chapter are given. These conclusions are divided in two topics, conclusions with respect to physical processes and with respect to the model settings and ComFLOW.

Physical processes

- The general performance of the numerical model is good, qualitatively the wave-structure interaction is simulated well.
- The results of run-up height are convincing, having good resemblance with data of physical experiments. Nevertheless, for waves with higher breaker parameters values ($\xi > 2$), around the transition from breaking to non-breaking and for non-breaking waves, the results are in the lower regions of the experimental data. Energy losses during structure-wave interaction and wave propagation are caused by numerical dissipation. Three possible causes for numerical dissipation are indicated:
 - Numerical roughness due to discretization of the geometry
 - Artificial viscosity
 - Restriction in flooding algorithm
- The numerical dissipation due to the created numerical roughness on the structure is seen as the main cause for energy dissipation in these simulations.

- Artificial viscosity has a damping effect on propagating waves and can decelerate the leading edge of the wave front. The damping effect on waves is in this study assumed to be very small and less influential on the results than the discretization of the geometry.
- Propagation of the leading edge of the wave front is influenced by the way flooding is treated by the numerical model. This causes the deceleration of up-rush of waves, as shown in the dam break test. In the run-up simulations in this chapter the maximum velocities are lower than the high speeds reached in the dam break test and are only reached for a short time span. The influence of this dissipation factor is therefore assumed to be small in these simulations.
- The results concerning run-down heights give a less regular pattern and are less convincing than the run-up. The results are too low compared to experimental data. No clear explanation was found for this.
- The results of the run-up and run-down values are showing slope dependency. The steepest slope gives smaller amplitudes at the shoreline than the gentler slopes. This could be caused by the fact that different slopes angles can cause different magnitude of numerical roughness in the discretization of the geometry.
- The calculated reflection coefficients gave good resemblance with experimental results, showing that the reflected wave energy is correct.
- The number of grid cells per wave length and wave height give guidance for choice of the grid size, 170-200 grid cells per wave length in the horizontal and 4-6 per wave height in the vertical are considered sufficient for this type of simulation.

ComFLOW model

- The program showed to be robust for these simulations. Only in three simulations flotsam and jetsam arose which did not influenced the results, while the accumulation of flotsam and jetsam is a known problem for VOF-models. Second only one simulation crashed out of 170 simulations in total.
- Output problems occur with the use of monitoring lines, while the program gives no warning.
- The increase of number of integration points leads to a stable solution, an improvement in run-up heights, due to the increase of smoothness of the geometry, while no extra CPU time is needed. The results improve more for coarser grids. However it must be remarked that the model does not run with values higher than 9, so at this moment the increase of 'smoothness' is not endless.
- The GABC boundary conditions works good: it proved to be robust and all wave energy of reflected waves is transported out of the domain. Only for some simulations with linear waves it seems that not all energy is transported out of the domain, for all other simulations no unwanted wave reflections at the boundaries are observed in the results.

6 Wave breaker types

To test the performance of the model in a qualitative way for wave-structure interaction, the model results are compared with video recordings. These recordings are made during experimental model tests in a wave flume with regular waves. It must be emphasized that this chapter is intended to be illustrative and no thorough analysis is made of the actual physical processes. It will give a general idea how well the breaking or non-breaking of waves with different breaker parameters on the slope is represented.

6.1 Numerical and physical model setup

The videos of the waves are recorded within the test program of Patrick van Broekhoven at the flume of the Delft University of Technology. The results of his study are still being processed and will be presented in his master thesis.

In this program different regular wave conditions are tested on smooth slopes of 1:2 and 1:1.5, respectively. The total test program of the experiment also includes irregular waves, rough slopes and permeable slopes. This part of the test program is not considered for this study, as in this study only regular waves on smooth slopes were simulated. In Figure 6.1 an overview of the flume is shown, with the set-up for a 1:2 slope. For this slope experiments are selected for analysis. The length from the wave paddle to the toe of the structure is 24.88 m, the width of the flume is 0.8 m, the slope is 1:2 and the still water depth in front of the slope is 0.5 m.

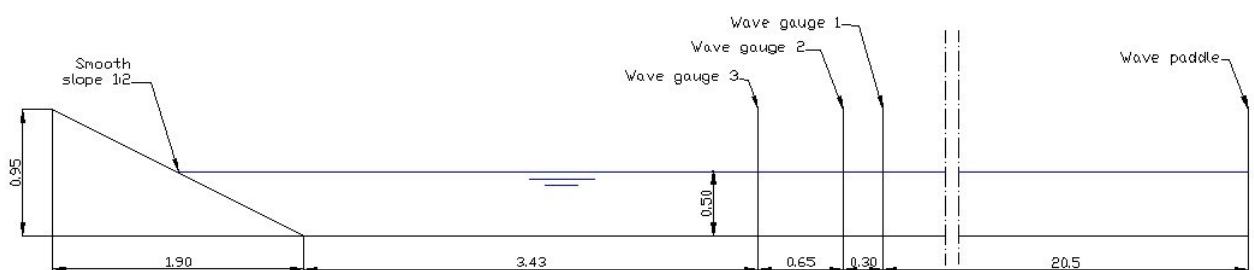


Figure 6.1: Experimental domain setup of test in TU Delft flume conducted by Patrick van Broekhoven.

The length of the computational domain was chosen much shorter than in flume, this choice reduces computational time and should have no influence on the results. In Figure 6.2 the computational domain is shown, with a length of 9.9 m from the incoming wave domain boundary to the toe of the structure. The flume is more or less two wave lengths long. Six cell per wave height are used and 350 cells per wave length, leading to $\Delta z=0.015$ and $\Delta x=0.010$. The simulation period is set to 35 seconds.

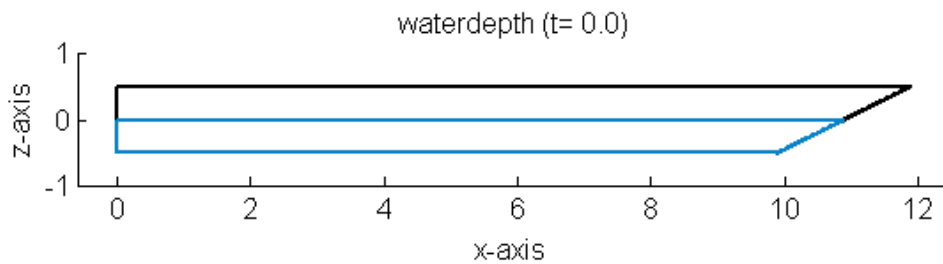


Figure 6.2: Numerical domain setup for simulations with experimental data of Patrick van Broekhoven.

Two waves are selected from the wave conditions that were tested in the flume, denoted as EGM006 and EM014. These waves are selected on their corresponding breaker parameter, a surging and a plunging wave are chosen. In Table 6.1 these two wave conditions are given, with the breaker parameter and the corresponding breaker type.

Table 6.1: Wave parameters of the incoming waves used for the simulations

Experiment	H [cm]	T [s]	ξ	Breaker type
EGM006	9.36	1.7	3.47	Surging
EM014p	8.84	0.97	2.03	Plunging/collapsing

6.2 Results

In this chapter the focus is on the comparison of the wave motion of video recording of a physical experiment and numerical representation of this wave. This will indeed be done hereafter, but first the exact computed values of wave run-up and down are given and compared with experimental results and the results of the previous chapter. The results are given in the table below.

Table 6.2: Run-up results of experiment and numerical simulations

	Experiment		ComFLOW			
	R_u	R_u/H	R_u	R_u/H	R_d	R_d/H
EGM006	20.7	2.21	15.3	1.73	-11.7	-1.25
EM014	18	2.04	13.3	1.50	-5.1	-0.58

For wave run-up the results are too low compared to the experimental results. Run-down is not analyzed in the study of Patrick van Broekhoven, so exact values cannot be compared with the physical experiment. In the next section differences and resemblances in wave motion during down-rush will be enlightened when analyzing video recordings and numerical results.

The graphs with the run-up and run-down results of the previous chapter are shown again with the results of the simulation on the 1:2 slope of this chapter, see Figure 6.3. Observed is that the ComFLOW results are for the non-breaking wave far below the experimental data range. The results are in line with the observed slope dependency in the previous chapter. The slope steepness (1:2) is steeper (maximum 1:3) than for the simulations in the previous chapter and the same trend observed. The results for run-up and run-down are again lower, giving a smaller vertical amplitude at the slope. The run-down results are therefore more in line with the experimental data of Schüttrumpf and Bruun and Gunbak.

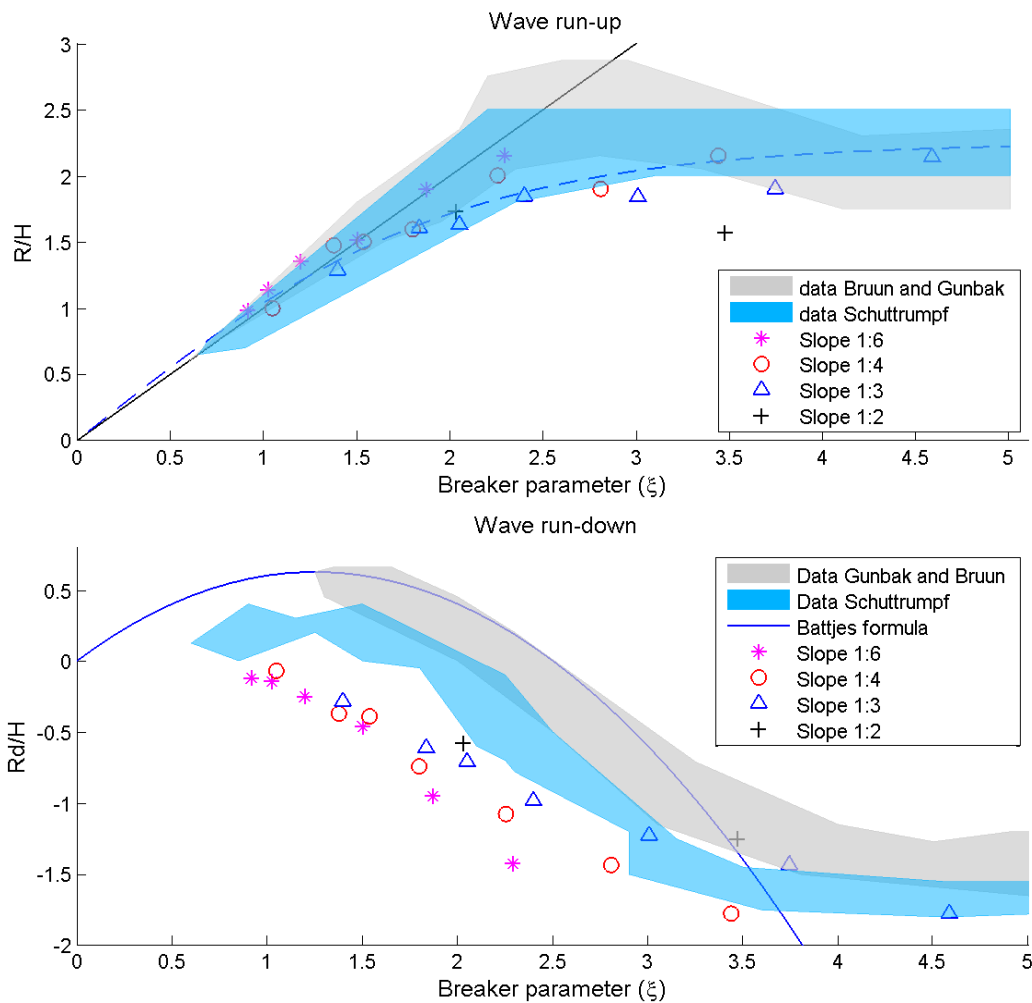
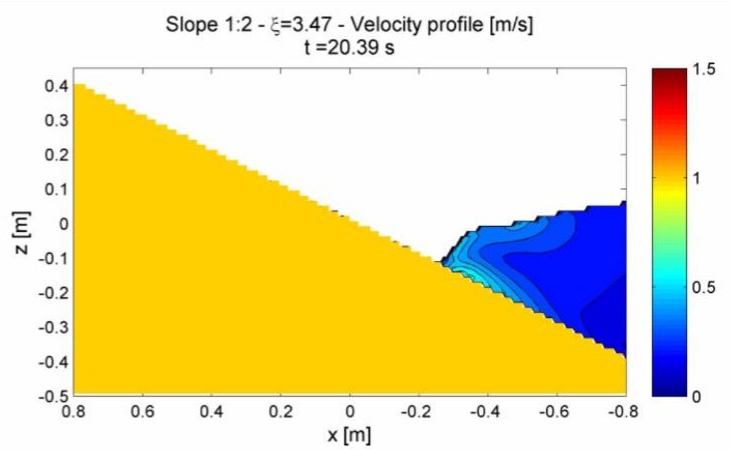
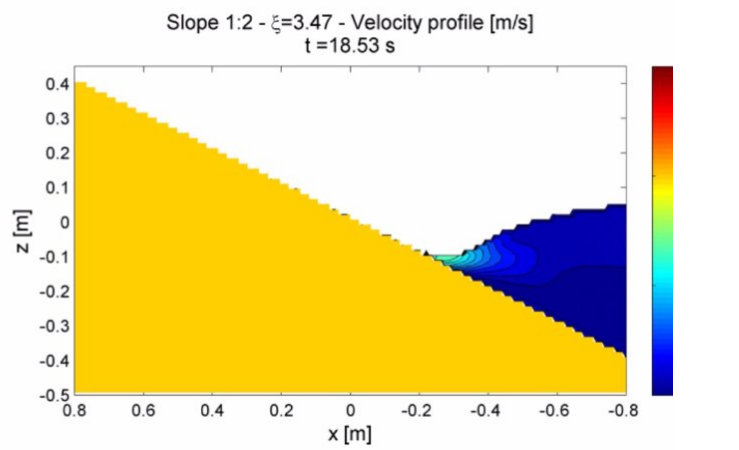
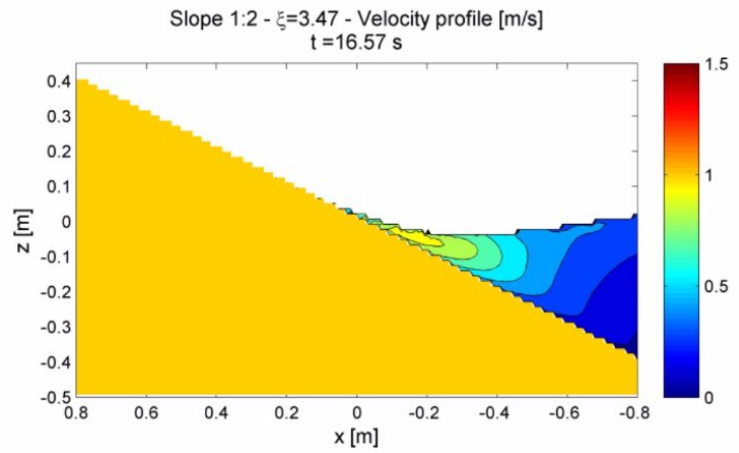


Figure 6.3: Results of regular wave run-up and run-down (figure 5.8 and 5.13), including the results of the simulations with slope 1:2.

6.2.1 Surging wave

In this section snapshots are shown of the numerical simulation and video recordings of the experiment EGM006, with a surging wave. In these snapshots good resemblance between physical model test video recordings and numerical results is observed, see Figure 6.4. General wave motion is reproduced well for all stages of the wave movement, although some small differences are observed. For example a $t=20.58$ s the wave shape is less bended in the numerical representation. The turbulent movement around maximum run-down is not represented in the numerical results, as a turbulence model is not included. This induces small differences at the slope of the structure, but the overall wave shape is quite similar. This observation is in line with the results for run-down in the previous chapter, for non-breaking waves the run-down results are comparable with experimental data (slightly overestimated).



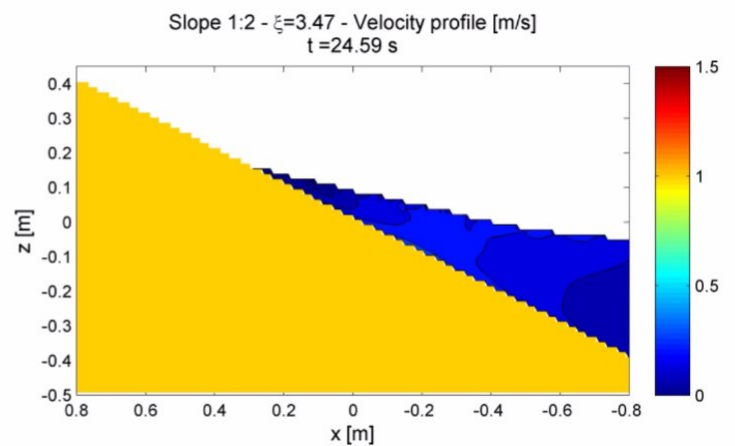
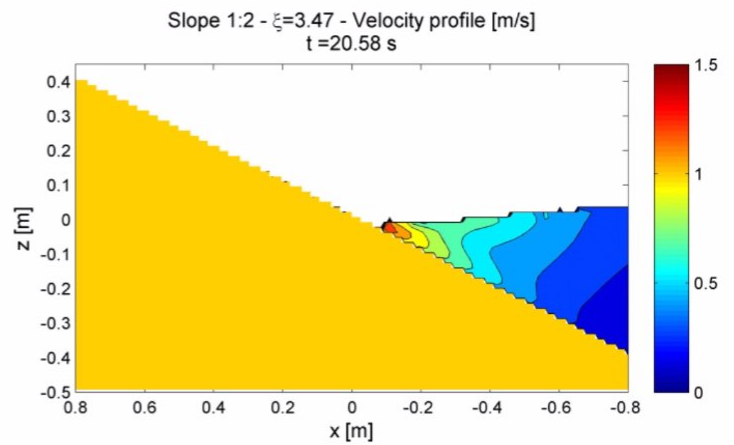
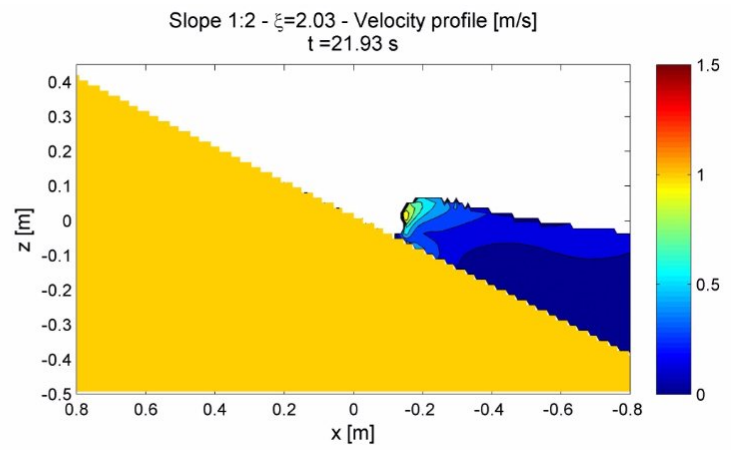
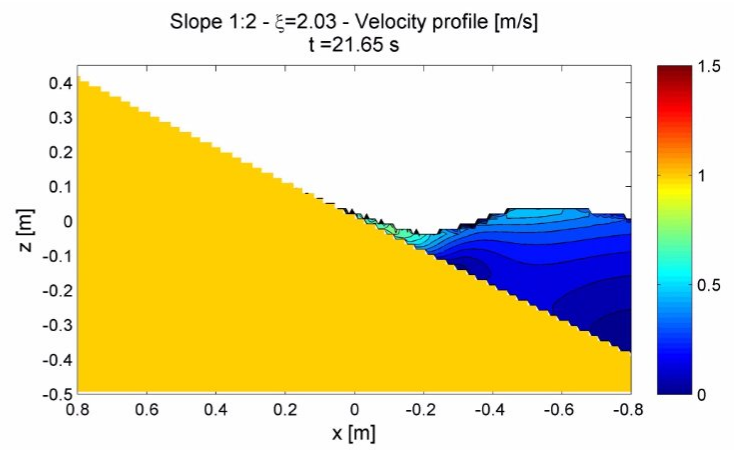
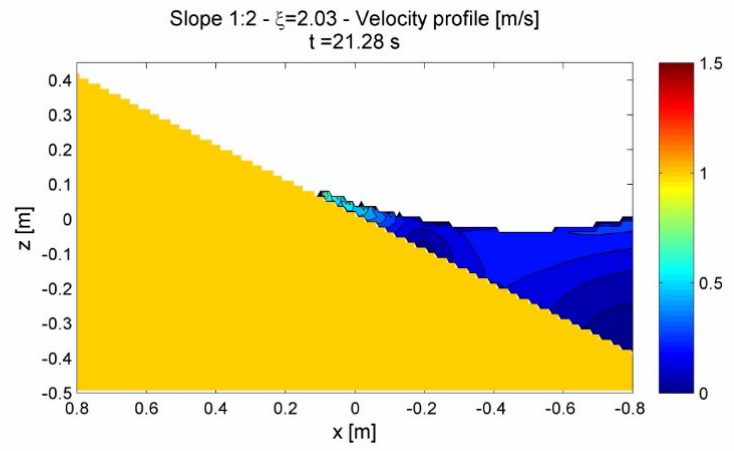


Figure 6.4: Snapshots of video recordings and ComFLOW results, displaying up- and down-rush of a surging wave.

6.2.2 Plunging wave

In this section snapshots are shown of the numerical simulations and video recording of the experiment EGM014, with a plunging wave. Comparing the video recordings and the numerical results, the same statement can be made as for surging waves: the general wave motion is reproduced well for all stages of the wave movement, see snapshots in Figure 6.5. However, the observed differences are of larger influence in for this type wave breaking, shown in the snapshots in Figure 6.6. Again it is observed that turbulence can induce some difference in wave motion, for example in the snapshot at t=21.28 s, but present in most snapshots. Furthermore duration of actual the breaking of the wave is somewhat faster in the numerical representation, compare the snapshots at t=21.93, 21.98 and 22.03 s. But the general shape of the wave is represented well.



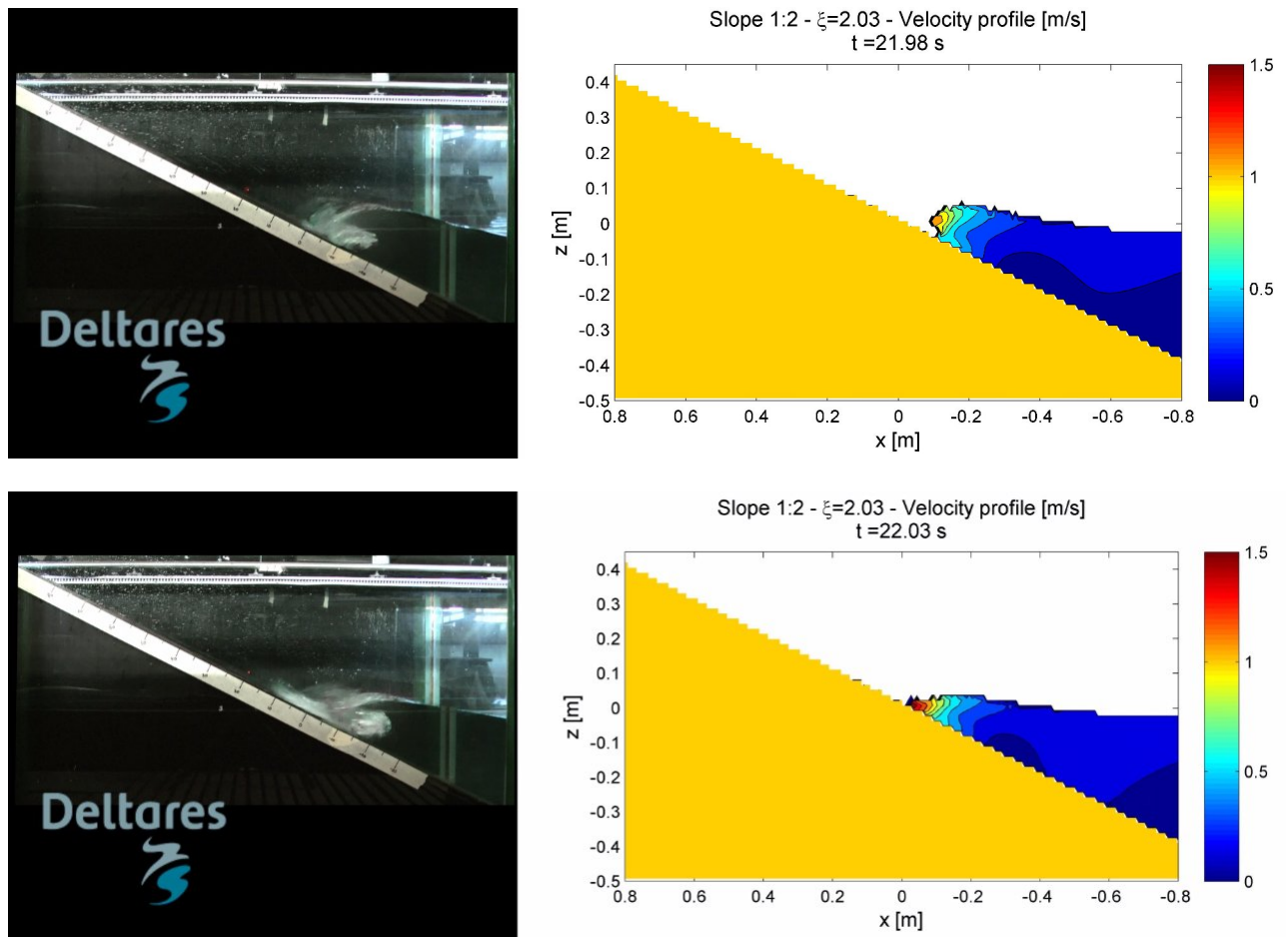


Figure 6.5: Snapshots of video recordings and ComFLOW results, displaying a plunging wave.

Figure 6.6 shows in more detailed the differences between the video recordings of the physical model test and the numerical representation, which are of influence on the run-down results. The snapshots Figure 6.6 show that during down-rush the water is retreated too fast in the numerical representation. In the numerical representation the appearance of the wave breaking is more a collapsing wave rather than a plunging one, while the video recording show a more plunging wave pattern.

This too fast retreating of the small water layer is of influence in the overestimation of the run-down results for breaking waves, as this will result in lower minimum water levels reached and thus lower wave run-down.

An important remark for this analysis must be made, that it gives an answer to which physical process is not represented well. However it does not answer the question why this is happening.

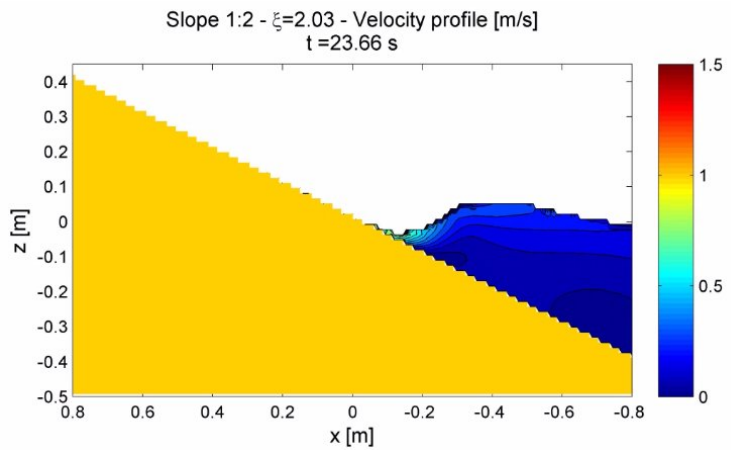
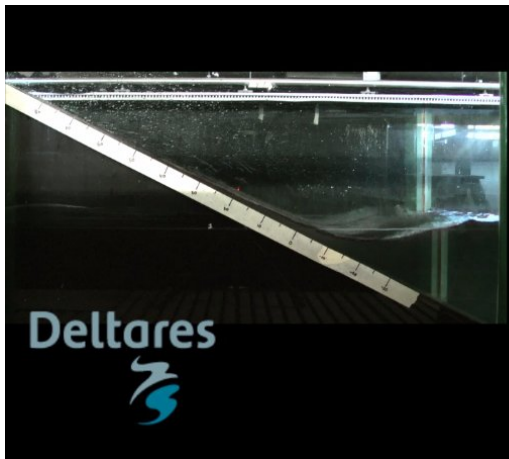
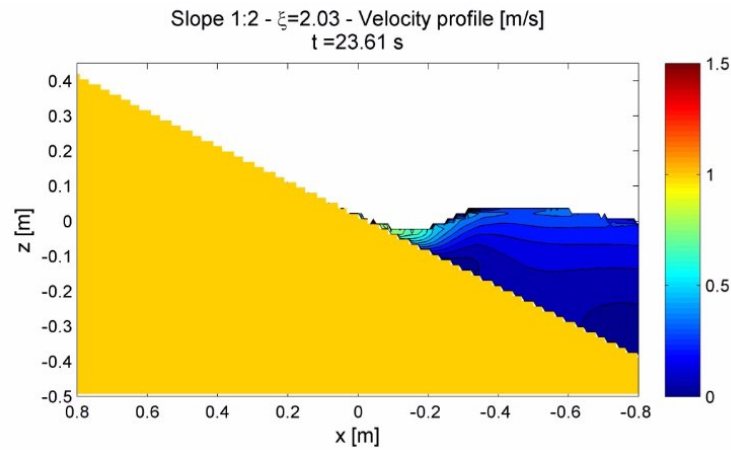
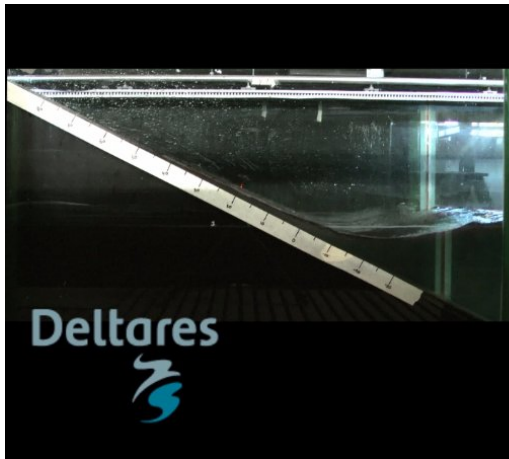
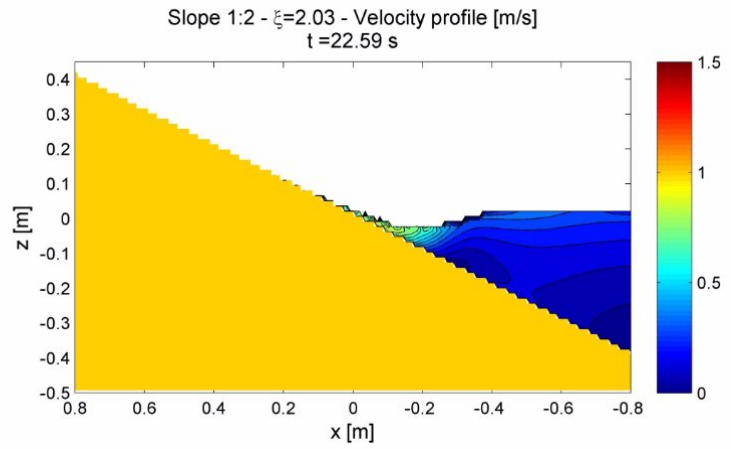
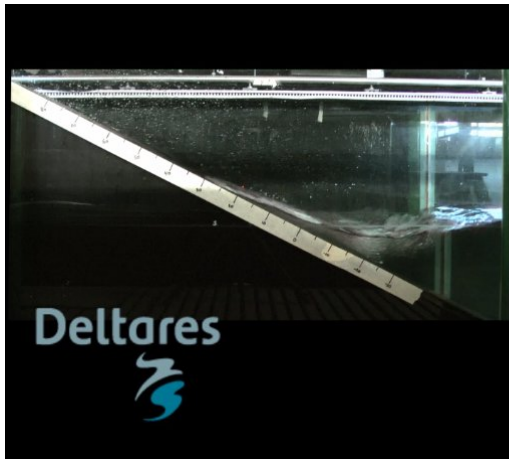


Figure 6.6: Snapshots at $t=22.59, 23.61, 23.66$ s of video recordings and ComFLOW results, displaying down-rush of a plunging wave.

7

Conclusions and recommendations

The objective of this research was to thoroughly analyze numerical simulation of wave run-up and other relevant wave-structure interaction processes on smooth and impermeable coastal structures with perpendicular wave attack. To investigate whether the Volume of Fluid (VOF) model ComFLOW is able to accurately represent these processes with 2DV simulations, if the model is robust and which model settings are to be preferred. In this chapter conclusions concerning these investigations are presented as well as recommendations with respect to further research and further development of the program.

7.1 Conclusions

To investigate whether the numerical model different mathematical aspects properly solves for relevant processes, simulation results are compared with analytical solutions. For the analysis of the different wave-structure interaction processes, simulations are performed with regular waves on impermeable structures with smooth, uniform slopes.

Overall it can be stated that the model performs well and is able to accurately simulate different wave-structure interaction processes including wave run-up. For proper numerical reproduction of wave-structure interaction, wave run-down, reflection and the type of wave breaking are considered as important processes. Also the model proved to be robust. Below this conclusion is elaborated in more detail, divided in two main topics: the physical processes and the model performance.

Physical processes

- The results with respect to wave run-up are convincing, having good resemblance with data of physical experiments, especially for lower values of the breaker parameter. For waves with higher breaker parameters values ($\xi > 2$), the (relative) numerical dissipation is too high during structure-wave interaction and is causing a decrease of approximately 0.3 in relative wave run-up (R_w/H).
- The discretization of the geometry creates numerical roughness at the slope and is indicated as the main cause of decrease in wave run-up.
- Artificial viscosity and a restriction in the algorithm of the flooding of dry cells are other processes that are indicated as other causes for numerical (energy) dissipation, but are assumed less influential in wave run-up simulations.
- The results concerning wave run-down give a less regular pattern and are less convincing than the run-up results. The relative wave run-down is overestimated (hence the lowest water level in the simulations is lower than in the experiments) compared to experimental data, especially for breaking waves ($\xi < 3$). An overestimation of approximately 0.6-1.0 in relative run-down is observed. It is observed that the numerical model simulates the retreating of the wave too fast, but no clear explanation is found for this. The answer may

lay in the different physical characteristics of wave run-up and run-down or the difference in handling of flooding and drying of cells by the numerical model.

- Both run-up and run-down results showed dependency on the slope, which already should have been accounted for in the breaker parameter. Resulting in a smaller vertical amplitude at the shoreline for steeper slopes. An explanation is found in the difference in created roughness by the discretization of the geometry for different slope steepnesses. However, some physical experiments also show dependency on the slope as well.
- The calculated reflection coefficients gave good resemblance with data from physical experiments, showing that the right amount of wave energy is reflected at the structure. Although it is observed that waves for which run-up results are low (in the non-breaking range) also give low reflection coefficients. The energy is (numerically) dissipated at the slope.
- Visual inspection of numerical results with video recordings of a physical model test showed that, the numerical model is capable of a good representation of different breaker types.

ComFLOW and model settings

- The model showed to be very robust for these simulations. Only one simulation crashed out. Only in three simulations unphysical small-scale fluid bodies (so called flotsam and jetsam) were formed, which did not influence the results.
- The number of grid cells per wave length and wave height give guidance for the choice of the grid size and determine the relative grid fineness in terms of relevant physical parameters. 170-200 grid cells per wave length and 4-6 per wave height are considered sufficient for these type of simulations.
- During the study it was found out that the maximum number of integration points could be as high as nine. This value gives stable results, reduces the created numerical roughness and does not lead to an increase of CPU-time. It is advisable to use the highest number of integration points possible when simulating smooth bodies or geometries.
- In this study it was proved that the use of the free-slip or no-slip boundary conditions did not lead to large differences in the propagation of the leading edge of the wave front along the slope.
- Artificial viscosity has a damping effect on propagating waves and causes the deceleration of the leading edge wave fronts traveling along the slope, both leading to lower run-up heights.
- The results concerning wave run-up showed that the differences in results were very small for Rienecker-Fenton waves and Airy waves. Rienecker Fenton waves however double the CPU-time, therefore it should be sufficient/advisable to use Airy waves in these type of simulations.
- The use of GABC boundary conditions with the 'robust' model setting, proposed by Wenneker (2010), works very well. All wave energy of the reflected waves is transported out of the domain, none unwanted reflections on the boundaries influencing the results and this setting proved to be stable.

7.2 Recommendations

In this section recommendations are given, concerning further research and development and usage of the ComFLOW model.

Physical processes

- It is recommended to perform more simulations with higher breaker parameters ξ . Now most simulations are done with lower ξ values, but it was recognized that higher breaker parameters gave relatively low values. More extensive research could reveal if this error is systematically and if a constant value is reached for the relative run-up.
- Other relevant wave-structure interaction parameters should be investigated in future research. Examples are velocities, and layer thickness on the slope and volumes. These processes could possibly be important for future research on overtopping, Schüttrumpf (2001) derived formulas for the velocity and layer thickness. Volume exchange formulas are described by H.D. Jumelet (2010).
- It is recommended to extend the research on wave run-up to irregular waves and compare this simulations with experimental data. Examples of possible usable experiments are van Gent (1999), Smith (1998), De Waal and Van der Meer (1992) or the experiments with irregular waves of van Broekhoven used in this study.
- Future research should include investigation on reduction factors on wave run-up. This would comprise the inclusion of angular wave attack, berms and permeable structures in the simulations. The newest version of ComFLOW includes permeable structures. Work on the calculation of reduction factors is one of the fields were interest in numerical modeling is large and future application is anticipated.
- More research should be done on the actual cause of the overestimation of the run-down values for breaking waves and the dependency on the slope. For example the dam break test with an downward sloping channel could be studied.
- It is recommended to do more research on the slope dependency that was observed and the two hypothesis that are formulated as possible explanations.
- The research should be extended to investigations on overtopping; this process is indicated as one of the most important causes for dike failure. The good performance on simulating wave run-up shows that the model has the potential for good performance on overtopping as well.

ComFLOW model

- The discretization of the geometry was indicated as the main cause of numerical energy dissipation. It is recommended to create better insight in the magnitude of the numerical roughness. If considered necessary it is recommended to asses solutions to this problem.
- Further research on the free slip and no-slip conditions and the impact on coastal engineering applications. A partial slip boundary condition at the geometry boundaries is in development (Veldman and Huijsman 2010).
- The use of Rienecker-Fenton waves needed twice CPU-time as Airy waves. Inefficient programming in ComFLOW probably causes this increase of CPU-time. As computational time is valuable it would be an improvement to eliminate this inefficiency.
- It was found that for some parts of the monitoring lines no useful data could be generated. Problems of this kind were also detected by Wenneker (2010). ComFLOW could be improved by giving a warning message with sufficient information. The user can decide to abort the computation and change the position of the monitoring line, or to neglect this warning and continue the simulation.

Bibliography

- BATTJES, J. A. (1974) Computation of Set-up, longshore Currents, Run-up and Overtopping due to wind-generated Waves. *Dissertation Delft University of Technology*.
- BRUUN, P. & GÜNBAK, A. R. (1977) Stability of sloping structures in relation to ξ risk criteria design. *Coastal Engineering*, 1, 287-322.
- CARRIER, G. F. & GREENSPAN, H. P. (1958) Water waves of finite amplitude on a sloping beach. *J. of Fluid Mech.*, 4:97-109.
- CHANSON, H. (2005) Applications of the Saint-Venant equations and method of characteristics to the dam break wave problem. *Report No. CH55/05*. Brisbane, Australia, Dept. of Civil Engineering, The University of Queensland.
- COMFLOW (2008) Manual ComFLOW V2.3. RuG 2008-002.
- DE WAAL, J. P. & VAN DER MEER, J. W. (1992) Wave run-up and overtopping on coastal structures. *Proc. ICCE'92, ASCE*. Venice.
- FRACCAROLLO, F. & TORO, E. F. (1995) Experimental and numerical assessment of the shallow water model for two-dimensional dam-break type problems. *Journal of hydraulic research*, 33 (6), 843-863.
- HIRT, C. R. & NICHOLS, B. D. (1981) Volume of fluid (VOF) method for the dynamics of free boundaries. *J. Computational Phys.*, 39, pp. 201-225.
- HUDSON, R. Y. (1959) Laboratory investigation of rubble mound breakwaters. *Proc. Am. Soc. Civ. Eng. , J. Waterw. Harbors Div.*, Vol: 85, WW3.
- HUNT, I. A. (1959) Design of seawalls and breakwaters. *Proc. ASCE*, Vol. 85, pp. 123-152.
- IRIBARREN (1938) Una Formula para el Calculo de los Diques de Escollera. *M. Bermejillo-Pasajes*. Madrid, Spain.
- JUMELET, H. D. (2010) The influence of core permeability on armour layer stability. *Hydraulic Engineering*. Delft, Delft University of Technology
- KLEEFSMAN, K. M. T. (2005) Water Impact Loading on Offshore Structures - a numerical study. PhD thesis, University of Groningen.
- KLEEFSMAN, K. M. T., BUNNIK, T. H. J. & IWANOWSKI, B. (2002) Predictions of green water and wave loading using a Navier-Stokes based simulation tool. *21ste International Conference on Offshore Mechanics and Artic Engineering*. Oslo.
- KLEEFSMAN, K. M. T., FEKKEN, G., VELDMAN, A. E. P., IWANOWSKI, B. & BUCHNER, B. (2005) A Volume-of-Fluid based simulation method for wave impact problems. *Journal of Computational Physics*, 206, 363-393.
- KROON, A. (2009) Implementation of a wetting and drying algorithm in a finite element model. *Environmental Fluid Mechanics*. Delft, Delft University of Technology.
- MANSARD, E. P. D. & FUNKE, E. R. (1980) The measurement of incident and reflected spectra using a least square method. *Proc. 17th Conference on Coastal Engineering Sydney*.
- PULLEN, T., ALLSOP, N. W. H., KORTENHAUS, A., SCHUTTRUMPF, H. & J.W., V. D. M. (2007) Wave Overtopping of Sea Defences and Related Structures: Assessment Manual. IN EUROTOP (Ed.) www.overtopping-manual.com.
- RIENECKER, M. M. & FENTON, J. D. (1981) A Fourier approximation method for steady water waves. *Journal of Fluid Mechanics*, 104, 119-137.
- RWS (2007) Sterkte en Belastingen Waterkeringen (SBW). IN RIJKSWATERSTAAT-WATERDIENST (Ed.), 7 september 2007.

- SCHIERECK, G. J. (2001) *Introduction to Bed, Bank and Shore protection*, Delft, Delft University of Technology.
- SCHÜTTRUMPF, H. F. R. (2001) Wellenüberlaufströmung bei Seedeichen- Experimentelle und theoretische Untersuchungen. *Leichtweiss-institut für Wasserbau Mitteilungen*. Technischen Universität Braunschweig.
- STELLING, G. S. & DUIJNMEIJER, S. P. A. (2003) A staggered conservative scheme for every froude number in rapidly varied shallow water flows. *Int. J. Numer. Meth. Fluids.*, 43, 1392-1345.
- STELLING, G. S. & ZIJLEMA, M. (2008) Efficient computation of surf zone waves using the nonlinear shallow water equations with non-hydrostatic pressure. *Coastal Engineering*, 55:780-790.
- STOKER, J. J. (1957) *Water waves*. Interscience. New York.
- VAN DER MEER, J. W. & JANSSEN, J. P. F. M. (1994) Wave run-up and wave overtopping at dikes and revetments. Delft, Delft Hydraulics.
- VAN GENT, M. R. A. (1995) Wave Interaction with Permeable Coastal Structures. *PhD-thesis*. Delft, Technical University of Delft.
- VAN GENT, M. R. A. (2002) Wave overtopping events at dikes. *Proc. 28th Int. Conf. on Coastal Engineering*. Cardiff.
- VELDMAN, A. E. P. & HUIJSMANS, R. H. M. (2008) *Extreme wave impact on offshore platforms and coastal structures - STW proposal*. University of Groningen, Technical University Delft.
- WELLENS, P. R., LUPPES, P., VELDMAN, A. E. P. & BORSBOOM, M. J. A. (2009) CFD simulations of a semi-submersible with absorbing boundary conditions. *Proceedings of 28th OMAE conference*. Hawai.
- WEMMENHOVE, R. (2008) Numerical simulation of two-phase flow in offshore environments. PhD thesis, University of Groningen.
- WENNEKER, I. (2010) ComFLOW simulations of Wave Impacts on a Dike. Delft, Deltares
- WHITHAM, G. B. (1979) *Lectures on Wave Propagation*, Springer-Verlag for Tata Inst. Fund. Res.

List of Tables

Table 4.1: Overview of simulations dam break test with an upward sloping channel	31
Table 5.1: Coordinates of the computational domain for regular waves	41
Table 5.2: Gridsizes regular wave simulations.....	42
Table 5.3: Overview regular waves used in ComFLOW modelling.....	43
Table 5.4: Results wave run-up simulations on slope 1:3, 1:4, 1:6 for different wave conditions....	49
Table 5.5: Number of grid cells (N) per wave length (L) and wave height (H) for medium and fine grid.....	50
Table 5.6: Influence of accuracy of maximum run-up and run-down values on relative run-up and down results.....	63
Table 5.7: CPU time in minutes and time step in seconds, for medium and fine grids.....	66
Table 6.1: Wave parameters of the incoming waves used for the simulations	70
Table 6.2: Run-up results of experiment and numerical simulations	70

List of Figures

Figure 1.1: Flow domain of wave overtopping on a dike, subdivided in five sub-flow domains. This study focuses on sub-domain 1,2 and 3. (Schüttrumpf, 2001: figure 2.8).....	2
Figure 1.2: Flow-diagram methodology	4
Figure 2.1: Breaker types as function of ξ	6
Figure 2.2: Wave run-up level R_u (Van der Meer and Janssen, 1994).....	7
Figure 2.3: Wave run-up formulas by Hunt and Schüttrumpf for regular waves.....	8
Figure 2.4: Run-down definition	9
Figure 2.5: Wave run-down formula by Battjes for regular waves.....	9
Figure 2.6: Reflection formula by Battjes, reflection coefficient as a function of ξ	10
Figure 2.7: Wave run-up formulas with experimental data of Bruun and Günbak & Schüttrumpf.....	11
Figure 2.8: Wave run-down formulas with experimental data of Bruun and Günbak and Schüttrumpf.	12
Figure 2.9: Reflection formulas with experimental data.....	12
Figure 3.1: Grid cell, volume aperture and edge apertures. (Figure 2.8 Kleefsman (2005)).....	16
Figure 3.2: Aperture calculation using two integration points. The more integration points, the smoother the geometry. Given for the cells volume and edge apertures.....	16
Figure 3.3: Cell labelling: dark grey denotes solid body; light grey is liquid. (Figure 1, (Kleefsman et al., 2005)).....	17
Figure 3.4: Different classes of velocities near the surface (Kleefsman et al., 2005).....	18
Figure 4.1: Sketch of the dam break problem in a dry, frictionless channel with zero initial velocity. Red line is solution at time t . (Chanson 2005: 24).	24
Figure 4.2: Domain setup dam break problem horizontal channel	25
Figure 4.3: Results for the dam break problem at $t=3$ s, for three different grid sizes.	25
Figure 4.4: Results for the dam break problem at $t=1, 2, 3$ and $t=4$ s, showing water depths solved on a fine grid.	26
Figure 4.5: Results for the dam break problem at $t=1, 2, 3$ and 4 s, showing velocities solved on a fine grid.	27
Figure 4.6: Result for dam break test at $t=3$ s showing velocity profile over the water depth.	27
Figure 4.7: Result for dam break test at $t=3$ s showing pressures over the water depth.	28
Figure 4.8: Pressure distribution for the dam break test at $t=0.5$ s in the upper figure and $t=1.0$ s in the lower figure.....	28
Figure 4.9: Sketch of the dam break problem in a dry, frictionless, sloping upward channel with zero initial velocity.....	29

Figure 4.10: Domain setup dam break test for sloping bed channel. Top with defined geometry, down with rotated g-force..... 30

Figure 4.11: Results for the five degree bed slope at t=3.82s illustrating the water accumulation at the left domain boundary..... 31

Figure 4.12: Results dam break problem showing the wave front as a function of time for all bed slopes and simulations. 32

Figure 4.13: Results for dam break problem with sloped channel showing velocities as a function of x at t=3 s for slope 1 (a), 2 (b), 5 (c) and 10 (d) degrees and for different model settings..... 33

Figure 4.14: Velocity profiles on a slope of two degrees for t=3s, a: results for nrintp 8 and b: results for rotated g-force. 34

Figure 4.15: The forming of ripples on propagating flood wave, results for a bed slope of two degrees..... 35

Figure 4.16: Domain setup Carrier Greenspan, slope 1:4, still water level 2,0 m..... 36

Figure 4.17: The analytical water level compared to the numerical water level for the Carrier and Greenspan test during up-rush..... 37

Figure 4.18: The analytical water level compared to the numerical water level for the Carrier and Greenspan test during down-rush..... 37

Figure 4.19: Numerical results of shoreline movement and maximum run-up value for analytical solution. Left: results medium grid, right: results fine grid..... 38

Figure 5.1: Domain setup for three different geometries: slope 1:6, 1:4 and 1:3 42

Figure 5.2: ComFLOW simulation with $\xi=0.92$, a plunging wave on slope 1:6 with velocity profile [m/s]..... 45

Figure 5.3: ComFLOW simulation with $\xi=2.4$, a collapsing wave on slope 1:3 with velocity profile [m/s]..... 46

Figure 5.4: ComFLOW simulation with $\xi=3.7$, a surging wave on slope 1:3 with velocity profile [m/s]..... 47

Figure 5.5: ComFLOW results for regular waves on different grids for 1:6 (a), 1:4 (b) and 1:3 (c) slopes. 48

Figure 5.6: Run-up results on medium and fine grid for wave condition 1-5..... 51

Figure 5.7: Wave Run-up results for different number of integration points. Left: medium grid. Right :fine grid. 52

Figure 5.8: ComFLOW results for regular wave run-up. Top: medium grid, down: fine grid..... 52

Figure 5.9: Wave run-up for regular wave, measurements Schüttrumpf (2001: abb. 4.8a) 54

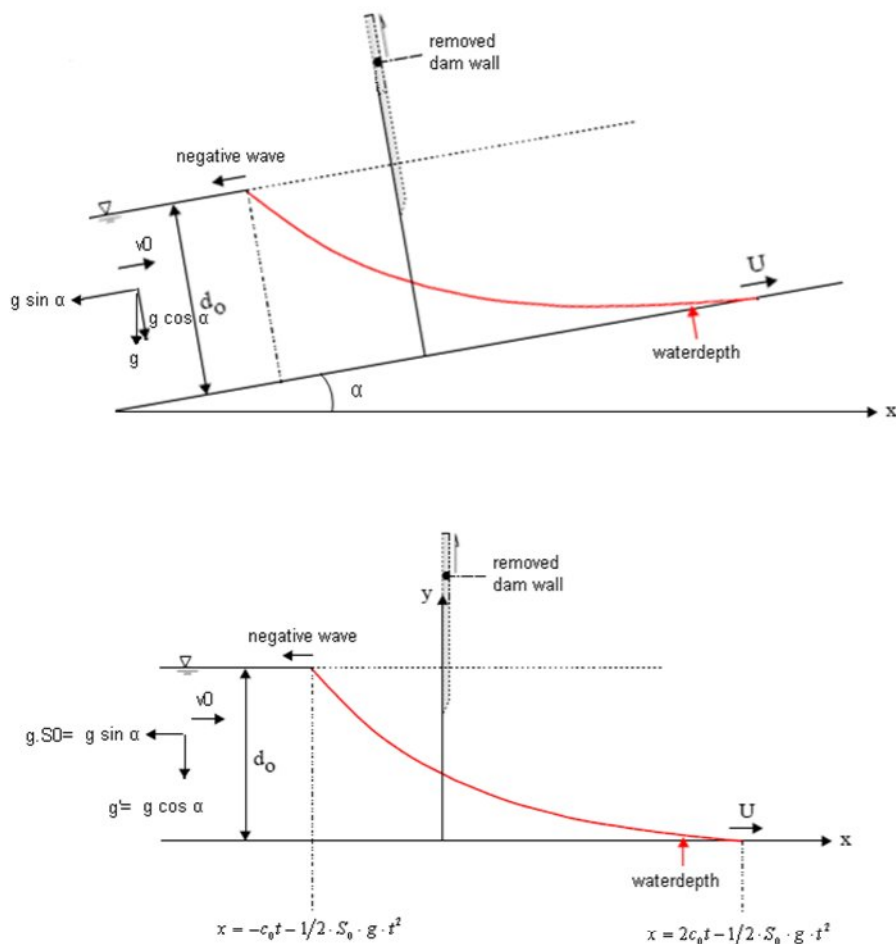
Figure 5.10: Wave signal (left) and wet values (right) along slope (For slope 1:3, wave condition 1, Airy Wave, fine grid)..... 54

Figure 5.11: Four cases (a-d) showing wave signals along different slopes (on fine grids). 55

Figure 5.12: Percentage pie of 4 cases of (ir-)regularities noticed in wave run-up results of all medium and fine grid simulations with 4 and 8 number of integration points.	56
Figure 5.13: Run-down regular waves; ComFLOW results and experimental results of Bruun and Günbak and Schüttrumpf on smooth slope	56
Figure 5.14: Separation of the incoming and reflected wave signal on slope 1:3, wave condition. Left: computed incoming and reflected wave signal. Right: wave signal at x1 in ComFLOW and computed sum of incoming and reflected wave.	58
Figure 5.15: Reflection coefficients of regular waves; ComFLOW results and experimental results (Bruun and Günbak) on smooth slope.	59
Figure 5.16: Illustrative sketch of monitoring line. Dark grey is the geometry, blue denotes fluid and red is the monitoring line with monitoring point uniformly distributed.	60
Figure 5.17: Problems with output of monitoring lines for slope 1:6, wave 5, Airy wave, medium grid. Left, waves signal along the slope. Right, wet values along the slope.	60
Figure 5.18: Illustrative sketch of monitoring line and the cause of problems with output generation. Green dot denotes a part of the monitoring line where no fluid motion is solved.	61
Figure 5.19: Wave signal along the slope for different distances to the structure (a) all distances, (b) 0.03 m, (c) 0.08m, (d) 0.15. For slope 1:4, condition 5, Airy Wave, medium grid.	61
Figure 5.20: Plot of wet values on medium grid to compare accuracy of distance (a) 0.01 and (b) 0.03m. Slope 1:4, condition 5, Rienecker Fenton, medium grid.	62
Figure 5.21: Wave run-up higher at larger distance to structure, due to detachment of tip of the wave tongue. (a) wave tongue, (b) Results for distance of 0.01 and 0.03m.	62
Figure 5.22: Run-up results with relative influence of the uncertainty margins with (right) and without (left) experimental data plotted.	63
Figure 5.23: Decrease of wave height after a simulation time of 100 periods at different distances from the inflow boundary. (Kleefsman, 2005: figure 3.18)	64
Figure 5.24 Accumulation of unphysical small-scale fluid bodies travelling to left domain boundary (For slope 1:4, wave 1, Airy wave, medium grid).	65
Figure 6.1: Experimental domain setup of test in TU Delft flume conducted by Patrick van Broekhoven.	69
Figure 6.2: Numerical domain setup for simulations with experimental data of Patrick van Broekhoven.	70
Figure 6.3: Results of regular wave run-up and run-down (figure 5.8 and 5.13), including the results of the simulations with slope 1:2.	71
Figure 6.4: Snapshots of video recordings and ComFLOW results, displaying up- and down-rush of a surging wave.	73
Figure 6.5: Snapshots of video recordings and ComFLOW results, displaying a plunging wave. .	75
Figure 6.6: Snapshots at t=22.59, 23.61, 23.66 s of video recordings and ComFLOW results, displaying down-rush of a plunging wave.	76

A Derivation of dam break test, sloped channel dry bed

The solution represents a dam break in a dry, frictionless, upward sloping channel bed with zero initial velocity, in a prismatic wide rectangular channel. The problem as formulated can be solved by advancing the solution along the characteristics. The problem is sketched in the figure below, it is shown that the rotation in fact only contributes to a constant acceleration in negative x-direction (denoted with gS_0) and a decrease in gravitational acceleration in z-direction (denoted with g'). Which causes a deceleration of the velocities in positive x-direction in time and a acceleration in negative x-direction. Although it is not used in this study we can also add an initial velocity v_0 to the problem, in this derivation this initial velocity will be included.



Assume the water occupies the region $x < 0; 0 < z < h_0$ initially held back by a dam at $x=0$. At $t=0$, the dam is removed (breaks). What is the height of the water $h(x,t)$ for $t > 0$, the initial condition is

$$h(x,0) = \begin{cases} h_0, & x < 0 \\ 0, & x > 0 \end{cases}$$

$$u(x,0) = v_0$$

On the characteristic that originates at $t=0$ for $x < 0$,

$$R_{\pm} = u \pm 2\sqrt{gh} = u \pm \sqrt{g'h_0} = C$$

Where $c_0 = \sqrt{g'h_0}$ is the initial (linear) wave speed. Along:

$$\frac{\partial}{\partial t}(u' + v' \pm 2c_0) + (u + v' \pm c_0) \cdot \frac{\partial}{\partial x}(v' + u \pm 2c_0) = -g \cdot S_0$$

Leading to constant for the forward and backward characteristic:

$$C_1 = v_0 - 2c_0 - g \cdot S_0 \cdot t$$

$$C_2 = v_0 - 2c_0 - g \cdot S_0 \cdot t$$

For the leading edge of the wave front this leads to the following equations:

$$x_+ = x_{f,0} + v_0 t + c_0 t - 1/2 \cdot S_0 \cdot g \cdot t^2$$

$$u_+ = v_0 + c_0 - S_0 \cdot g \cdot t$$

Where the velocity is the derivative of the position of the wave front in time.

For the leading edge of the negative wave this leads to the following equations:

$$x_- = 2c_0 t + v_0 t - 1/2 \cdot S_0 \cdot g \cdot t^2$$

$$u_- = 2c_0 + v_0 - S_0 \cdot g \cdot t$$

Filling these characteristics in equation 4.1, the solution between the negative propagating wave and the leading edge of the wave, is described by:

$$u = \frac{2}{3} \left(c_0 + v_0 - S_0 \cdot g \cdot t + \frac{x}{t} \right),$$

$$h = \frac{1}{g'} \left(\frac{2}{3} + \frac{1}{3} v_0 - \frac{1}{6} S_0 \cdot g \cdot t - \frac{1}{3} \frac{x}{t} \right)^2, \text{ with}$$

$$c_0 = \sqrt{g'h_0}$$

$$g' = g \cdot \cos \alpha$$

$$S_0 = \sin \alpha$$

In which, α is the angle between the bed and the horizontal plane and $\alpha > 0$ for an upward slope.

For an upward slope, the maximum elevation reached by the wave front is $Z_{\max} = 2 \cdot h_0$ at $x = 2/\tan \alpha$, for $t = 2 c_0/g \cdot S_0$. This result is independent of the bed slope.

B Generating output from ComFLOW files

Monitoring lines

To extract the run-up heights from the monitoring lines the following procedure was adopted. The data of the monitoring line contains time series of computed velocities and pressures at 100 points along the defined line. The points are uniformly distributed along the line and the distance between the points in vertical direction is 0.0143 m. In figure B-1 the monitoring line is showed, the figure shows the placement and the way the run-up vaules are extracted.

For all the 100 points on monitoring line it is extracted whether fluid is present in the grid cell where the point is located. This is done by finding all points where a pressure larger than zero is computed. These points are labeled 1, regardless the amount of fluid present in this cell, F(u11) in the figure. All points in empty cells are labeled NaN (not a number). Now it is known where fluid is present and where not, this can be translated to z- and x- coordinates. These 100 monitoring points are uniformly distributed and the distance between is therefore defined by the length of the monitoring line and is independent of the grid size:

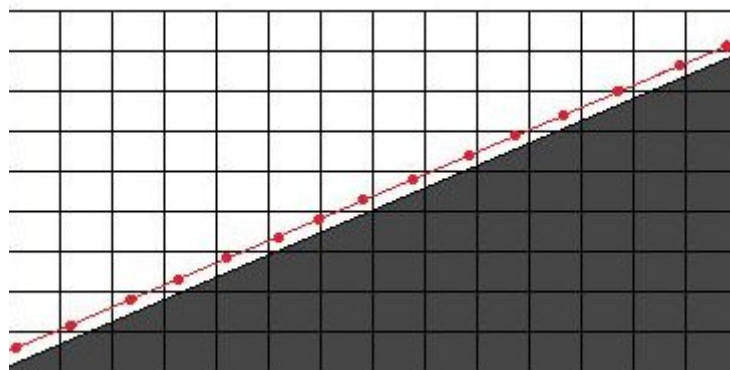
- $\Delta z = 0.0143$ for all grids and geometries
- $\Delta x = 0.0429, 0.057, 0.0857$ respectively depending of the geometry 1:3, 1:4, 1:6

Because Δz is smaller than the height of the grid cells and therefore in each consecutive row of grids cells a point will be present, the accuracy of the wave run-up results is determined by the Δz or the grid cells and the monitoring lines (see also section 5.4.2). In figure B-1c the wave run-up is overestimated, but it can also be overestimated with the applied procedure.

By plotting the extracted water heights on the z-axis in time, the wave signal along the slope of the geometry appears. It is checked if this procedure is correct, at the start of the simulation the waterline should be on $z=0$, the still water level.

In this report two different graphs are given, showing the wet values and wave signal along the slope. For the graph showing the wet values all points indicated by 1 are filled in (F in the figure), giving all points where water is present. To extract the wave signal from this along vertical lines the first point that is NaN (E in the figure) is searched for, giving the dry area.

The run-up height is determined from the created graphs, by reading the maximum height that is reached.



(a)

